NOTICE

The quality of this microform is heavily dependent upon the quality of the original thesis submitted for microfilming. Every effort has been made to ensure the highest quality of reproduction possible.

If pages are missing, contact the university which granted the degree.

Some pages may have indistinct print especially if the original pages were typed with a poor typewriter ribbon or if the university sent us an inferior photocopy.

Reproduction in full or in part of this microform is governed by the Canadian Copyright Act, R.S.C. 1970, c. C-30, and subsequent amendments.

AVIS

La qualité de cette microforme dépend grandement de la qualité de la thèse soumise au microfilmage. Nous avons tout fait pour assurer une qualité supérieure de reproduction.

S'il manque des pages, veuillez communiquer avec l'université qui a conféré le grade.

La qualité d'impression de certaines pages peut laisser à désirer, surtout si les pages originales ont été dactylographiées à l'aide d'un ruban usé ou si l'université nous a fait parvenir une photocopie de qualité inférieure.

La reproduction, même partielle, de cette microforme est soumise à la Loi canadienne sur le droit d'auteur, SRC 1970, c. C-30, et ses amendements subséquents.

ISBN 0-315-53861-9

BARITE BODIES WEST OF HEMLO, ONTARIO: PETROFABRIC AND GEOCHEMICAL STUDY

A Thesis

Presented to

the School of Graduate Studies

University of Ottawa

In Partial Fulfillment

of the Requirements for the

M.Sc. Degree in Geology

By

Dan Roach

1987

ABSTRACT

The western barite occurrences (WBO) are located within the Wawa Subprovince of the Superior Geological Province. The barite mineralization, located 25 km west of the Hemlo gold deposit, is in heterogeneous ductile shear zones within Archean metasedimentary rocks along the contact between mafic metavolcanic and metasedimentary rocks. Because of the lack of primary features, the precise nature and extent of the ductile deformation is uncertain.

The WBO contain interlayered barite-sulphide-quartz schist, pyrite-muscovite schist, chromium-muscovite schist, carbonaceous phyllite, biotitic metasedimentary units, amphibolitic mafic metavolcanic units and plagioclase -porphyritic felsic intrusions.

The WBO display a prominent mineral lineation which plunges moderately to the west, and a well-developed, east-west striking, steeply-dipping foliation. Ductile deformation involved a)pressure solution, as demonstrated for pyrite, quartz and ankerite, and b)crystal-plastic deformation, as observed in plagioclase, quartz, and probably barite. Barite and quartz display strong and consistent crystallographic preferred orientation with respect to the penetrative fabric.

Metamorphic microstructures indicate that ductile deformation occurred before and during peak amphibolite facies metamorphism. Fabrics in the barite-sulphide-quartz schist

indicate that barite-pyrite mineralization occurred before the end of ductile deformation. Microtextures in the plagioclase-porphyritic intrusion indicate emplacement prior to the end of ductile deformation. For the time period before the end of ductile deformation, the precise sequence involving barite-pyrite mineralization, intrusion, ductile deformation, and metamorphism is uncertain. Therefore, barite-pyrite mineralization may have occurred either before or during ductile shear. This uncertainty in the sequence may be due in part to the overprinting effects of progressive deformation and metamorphism. This uncertainty may also be due to a possible complex geological history, which may have involved overlapping and/or discontinuous geological events.

Evidence from the WBO is in accord with Hugons' (1986a) tectonic model of regional southeast-directed oblique thrusting coeval with the emplacement of the Cedar Lake Pluton (2690 Ma.). Under these conditions of regional thrusting, the contact between mafic metavolcanics and metasediments, hence the site of the WBO, are favourable zones for ductile shear. Mechanical properties of the barite-sulphide mineralization may have partially localized ductile shear within the WBO.

The WBO contain strongly isotopically-fractionated barite and pyrite. Sulphur isotopic values for pyrite from the baritic unit vary from -13 o/oo to -4 o/oo, whereas the isotopic composition of pyrite in the associated metasediments is close to 0 o/oo (ranging from -5 o/oo to +3 o/oo). $\Delta^{34}S_{barite\text{-}pyrite}$ range from 11.2 o/oo to 15 o/oo, with the

average being 13.4 o/oo. The consistent values of $\Delta^{34}S_{barite-pyrite}$ are attributed to either a)dynamic equilibrium during the primary mineralization, or b)re-equilibration during deformation and metamorphism. If the isotopic compositions are primary, then the values of $\Delta^{34}S_{barite-pyrite}$ are in accord with pyrite produced through hydrothermal reduction of sulphate.

The isotopic composition of barite and pyrite is generally proportional to the mole sulphur ratio of the barite-pyrite sample pairs. Considering the consistent difference in 34S between pyrite and barite, and the pressure solution during deformation, this proportionality suggests the possibility of isotopic exchange during metamorphism and deformation of the WBO.

CONTENTS Page

PLATES

FIGURES

ACKNOWLEDGEMENTS

I thank Eion Cameron and Keiko Hattori for their suggestion of this project, and for their guidance in the writing of this manuscript. I also thank Simon Hanmer for his valuable insight in the discussion of CPOs.

I also thank George Mzarek, John Loop, Paul Middlestead, and Mike Ouimet for expert assistance in their respective fields. Finally, I thank the Bunch of Guys hockey team for 2 years of great hockey.

CHAPTER 1. INTRODUCTION

1.1 ARCHEAN BARITE OCCURRENCES

Occurrences of barite are rare within Archean sedimentary rocks. Deposits have been reported from Western Australia (Barley et al.,1979), South Africa (Heinrichs and Reimer, 1977; Lowe and Knauth, 1977; Reimer, 1980), Zimbabwe (Morrison, 1968; Reimer, 1980), and India (Radhakrishna and Vasudev, 1977).

Some of these barite occurrences are sedimentary or sedimentary-exhalative in origin, as confirmed by preserved sedimentary and diagenetic features such as bedding, soft-sediment deformation and diagenetically recrystallized barite. Such features are only found in undeformed and slightly metamorphosed strata, as in sections of the Pilbara Block of Western Australia, and in the Barberton Mountain Lands of South Africa (Reimer, 1980; Barley et al., 1979; Heinrich and Reimer, 1977).

Intensely-deformed and highly-metamorphosed barite deposits, as in Zimbabwe and India, do not contain preserved primary features, and the exact nature of their origin is not known.

In Archean rocks of the Canadian Shield, barite is found almost exclusively in cross-cutting veins (Guillet, 1963). Stratiform barite is very rare, with reported possible occurrences at a) the Hemlo gold deposit (Cameron and

Hattori, 1985; Burk et al., 1986)), and b) the western barite occurrences (WBO) (Patterson, 1984). Separated by only 20 km, both Hemlo and the WBO are hosted in the Wawa Subprovince of the Superior Province (Fig. 1). The origin of these barite occurrences is uncertain, due predominately to intense deformation and amphibolite facies metamorphism of the Archean supracrustal host rocks.

The Archean rocks within the north-central region of the Wawa Subprovince contain an unusual abundance of sulphate (Cameron and Hattori, 1987). In addition to the aforementioned barite occurrences, there are notable sulphate occurrences (not neccessarily stratiform) at the Geco and Willroy massive sulphide deposits (Friesen et al., 1982; Bakker et al., 1985), and at Heron Bay (Cameron and Hattori, 1987) (Fig. 1). These rare sulphate occurrences, and the gold mineralization at Hemlo, have caused increased academic and economic interest in this region of the Wawa Subprovince. Of particular interest are the Hemlo deposit, and the host rocks of the Hemlo-Heron Bay area.

The geology of gold mineralization at Hemlo has been detailed by Valliant, et al., (1985), Quartermain (1985), Brown et al., (1985), and Burke et al., (1986). The deposit, with current reserves of 85 million tons at 0.23 oz/ton Au (Northern Miner, Jan. 17, 1985), is hosted in intensely deformed pyroclastic metavolcanics and metasediments of the Archean Heron Bay Group. Mineralization occurs within a sheared tuffaceous unit, near the contact between pyroclastic

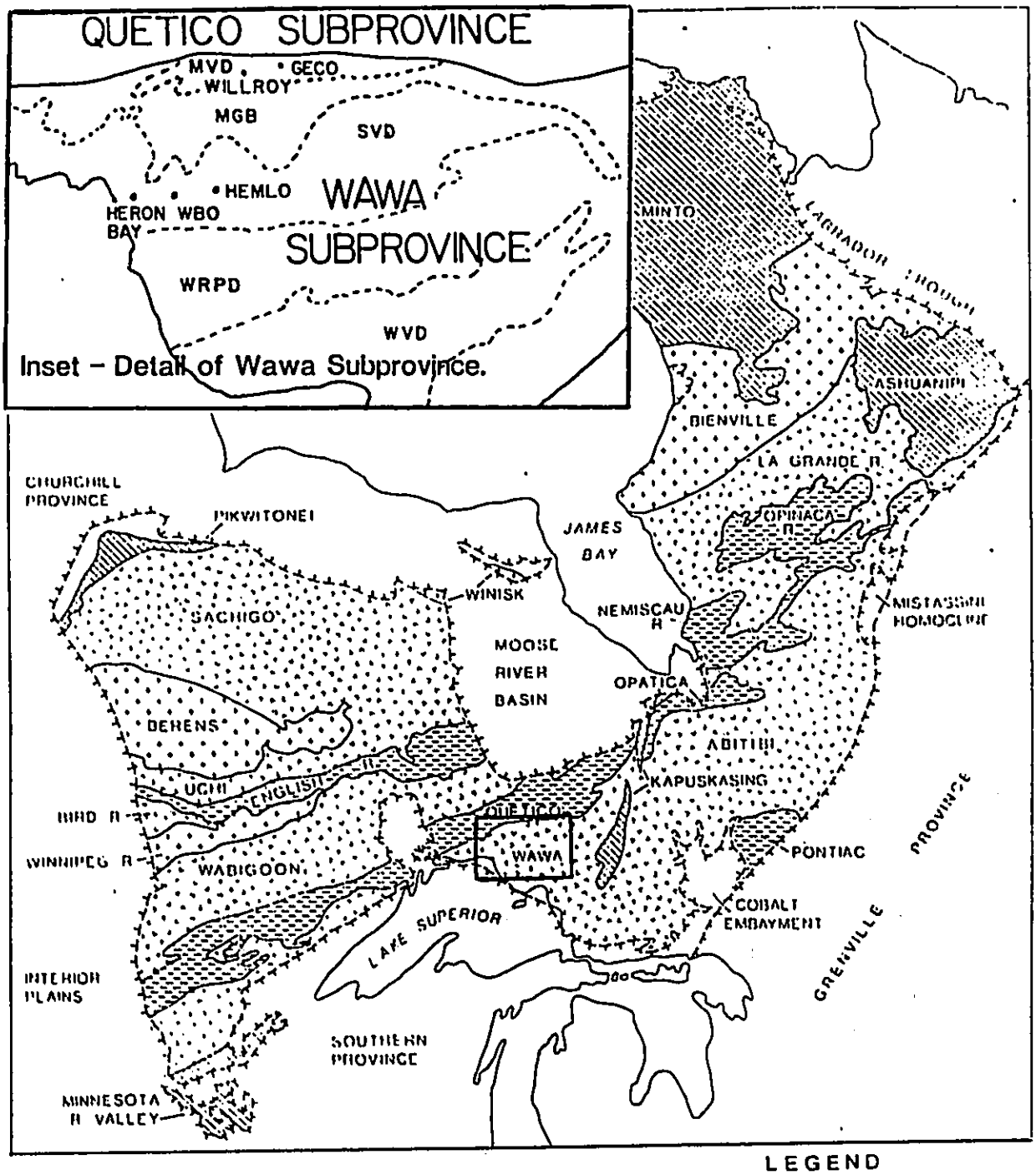

MVD—Manitouwadge Volcanic Domain

MGD—Manitouwadge Gneiss Domain

SVD—Schreiber Volcanic Domain

WRPD-White River Plutonic Domain

WVD—Wawa Volcanic Domain

Fig. 1 Geology of the Superior Province (after Card &Ciesielski, 1986)

metavolcanic rocks and metasiltstone (Fig. 2).

Harris (1984) identified a variety of minerals within the Hemlo deposit, including molybdenite, vanadium-rich green muscovite, cinnabar and sphalerite. Barite occurs interlayered with a pyritic-sericite schist in the thicker, central portion of the deposit. Barite also occurs within some thinner ore zones and within footwall rocks. A hydrothermal origin for barite and pyrite is suggested by their sulphur isotope composition (Cameron and Hattori, 1985). Hugon (1984,1986a,1986b) and Muir (1985) suggest that ductile deformation is important in the genesis of the Hemlo deposit.

The WBO were discovered during exploration of the Hemlo-Heron Bay area. Although not studied in detail, the WBO are described by Patterson (1984) as finely-bedded, with interfingering chert, carbonate, sericite schist, green-mica schist and graphitic schist. Patterson suggests that the WBO (which contain less than 400 parts per billion gold), are sedimentary in origin. Despite their lack of gold, the smaller WBO are similar in many respects to the larger Hemlo deposit. Both occur within the Heron Bay Group, near the contact between mafic metavolcanics and felsic metasediments. Both areas contain similar lithologies, including the baritic unit, pyritic-sericite schist, green-mica schist, and deformed porphyry. Furthermore, the Hemlo and WBO barite have essentially the same strontium isotopic composition, possibly indicating a similar origin for the 2 occurrences (Cameron and

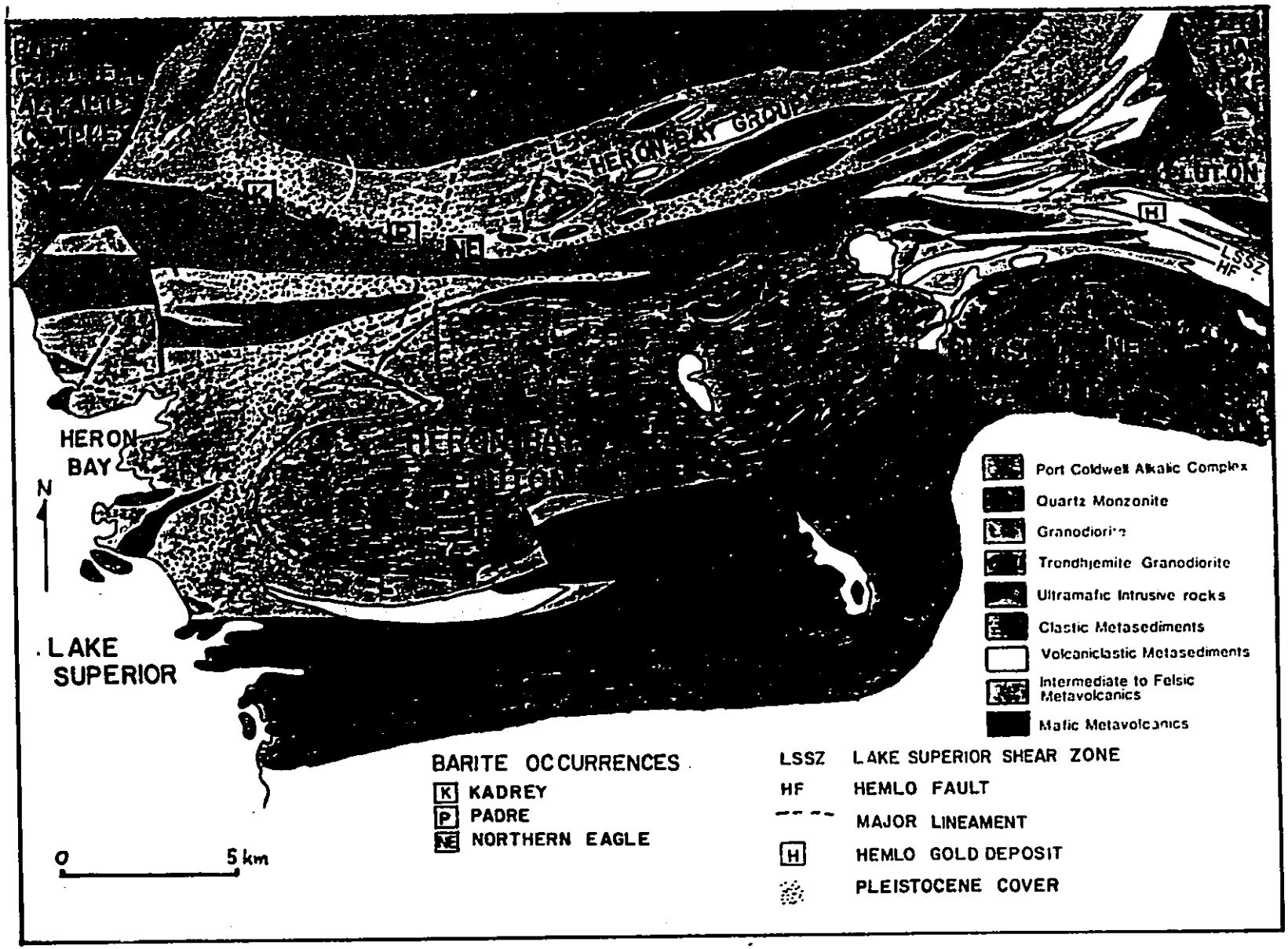

Fig. 2 Geology of the Hemlo–Heron Bay region. After Muir, 1985

Hattori, 1985). The above similarities suggest that an understanding of the origin of the WBO may be useful to the genetic interpretation of the Hemlo gold deposit. Furthermore, the WBO may reveal local geological factors responsible for the unusual abundance of sulphate in this region of the Superior Province. For these reasons, it is critical that the WBO are studied in detail.

1.2 PURPOSE

This study investigates in detail, the nature of the barite mineralization within the WBO. The obtained information is used in three ways:

a) to determine the possible origins for these rare concordant barite occurrences,

b) to relate these findings to the nearby Hemlo deposit, and

c) to reveal what was unique in the geological history of the region to form such rare Archean sulphate occurrences.

1.3 LOCATION

The thesis area is located approximately 25 km west of the Hemlo gold deposit (Fig. 3). The area is a 6 km strip parallel to Highway 17 from the Pic River to the Black River, containing the 3 main areas of study, located on mining claims held by Kadrey Energy Corporation, Padre Resources Limited and Northern Eagle Mines Limited.

1.4 SEQUENCE OF INVESTIGATION

Preliminary mapping and sampling were undertaken during the early portion of the 1984 field season. Thin sections were examined, and optical mineralogy was supplemented by microprobe identification. Preliminary isotopic and geochemical analyses were carried out on selected samples (these data guided further sampling and mapping).

Detailed mapping and sampling was undertaken in 1985. Selected samples from baritic units were then analysed for crystallographic preferred orientation (CPO) of barite and accompanying quartz. Detailed microstructure analyses were also made on various oriented samples. Additional barite and pyrite were analyzed for sulphur isotopes.

Two presentations summarizing the preliminary results have been made during the present investigation (Roach et al.,1985, 1986).

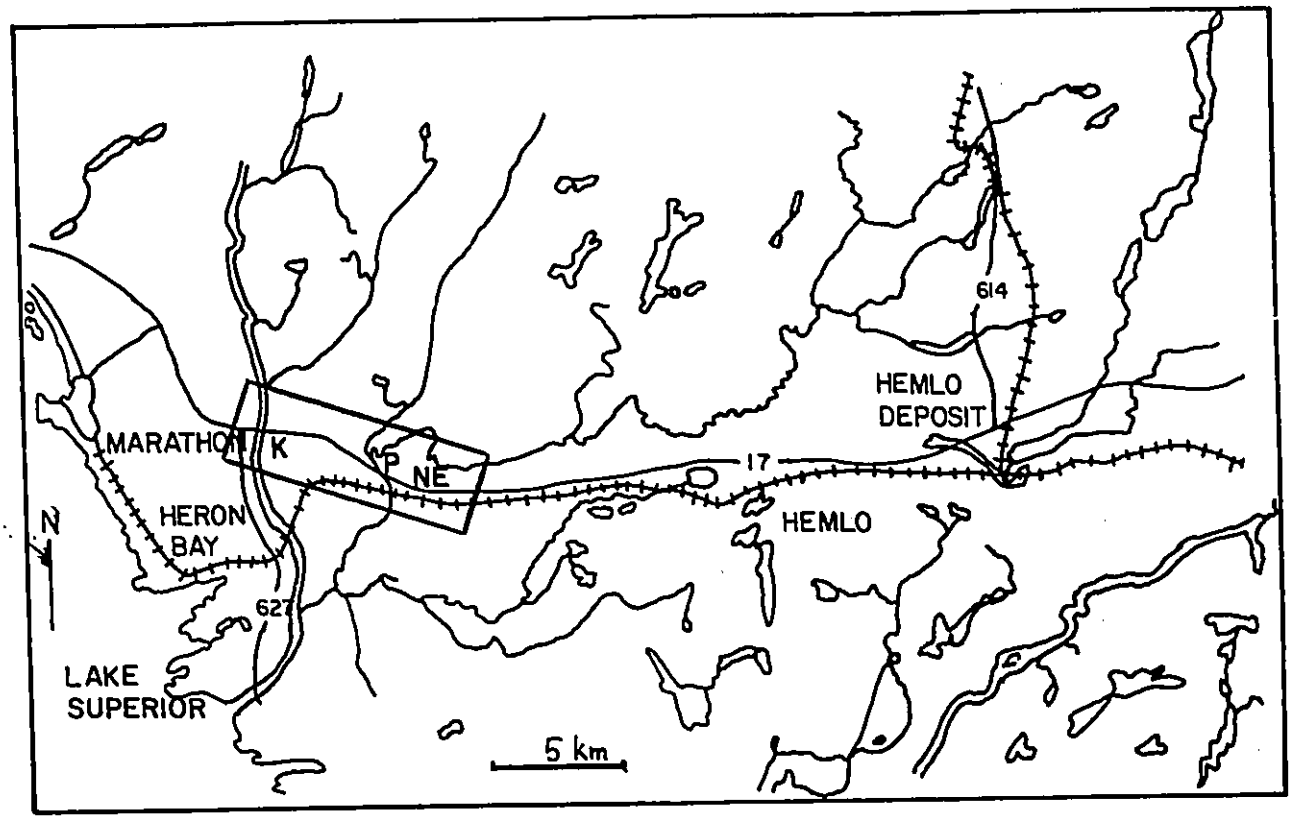

LOCATION MAP

Fig. 3

K—KADREY ENERGY CORP.
P—PADRE RESOURCES
NE-NORTHERN EAGLE MINES

CHAPTER 2. REGIONAL GEOLOGY

2.1 THE SUPERIOR PROVINCE

The Superior Geological Province is subdivided into 13 generally east-trending subprovinces (Fig. 1) defined by lithology, structural style, metamorphic grade, age of orogenic events, and geophysical characteristics (Stockwell et al., 1970; Goodwin, 1977, 1978; Card and Ciesielski, 1986). The subprovinces are classified into four types of litho-tectonic domains: (1) volcano-plutonic; (2) metasedimentary; (3) plutonic; and (4) high-grade gneiss (Card and Ciesielski, 1986). There is a spatial and possible genetic association between volcano-plutonic and metasedimentary domains (Fig. 1). These domains may represent accreted volcanic arc and associated sedimentary terrains (Card and Ciesielski, 1986).

The volcano-plutonic subprovinces are of economic importance, containing deposits of gold, copper, zinc and iron. These subprovinces contain metavolcanic sequences which are bordered and intruded by voluminous felsic plutonic rocks. These felsic plutonic rocks include early synvolcanic plutons and tonalitic gneiss, and younger foliated to massive plutons ranging from quartz diorite to granite and syenite (Card and Ciesielski, 1986).

The volcano-plutonic subprovinces commonly display irregular structural patterns, characterized by sinuous, bifurcating, commonly synformal metavolcanic belts with

upright folds and steep lineations, and intervening, commonly domal, gneissic-plutonic domains. Metamorphic grade generally increases from subgreenschist or greenschist in the central parts of the metavolcanic belts to low-pressure amphibolite facies at belt margins and within surrounding plutonic gneisses (Card and Ciesielski, 1986).

2.2 GEOLOGY OF THE WAWA SUBPROVINCE

The study area is located in the Wawa Subprovince. This volcano-plutonic subprovince is located between the Quetico Sedimentary Subprovince and the Southern Province (Fig. 1). The Wawa Subprovince is covered to the west by mainly Proterozoic platform sediments. To the east, the Wawa Subprovince displays a continuous transition from greenstone belts, through tonalitic gneiss and felsic plutons, into heterogeneous high-grade gneiss of the Kapuskasing Zone. This transition has recently been interpreted (Percival and Card, 1985) as an oblique cross section through a 20-km thick slab of Archean crust that was differentially uplifted along a major northwest-dipping thrust.

Zircon U-Pb geochronology suggests that major volcanism, deformation, metamorphism and plutonism in the Wawa Subprovince was mainly between 2750 to 2650 Ma ago (Prince and Hanson, 1972; Catanzero and Hanson, 1971; Krogh and Turek, 1982). Older dates (ca. 2900 Ma), have been reported for

plutonic rocks of the Wawa Subprovince (Turek et al., 1983).

2.3 GEOLOGY OF THE HEMLO-HERON BAY AREA

2.3.1 METAVOLCANIC SUPRACRUSTAL ROCKS

The Wawa Subprovince contains several economically-significant metavolcanic belts. One such belt, the Schreiber Volcanic Domain, hosts both the Hemlo gold deposit and the WBO (Fig. 1). This east-trending belt of metavolcanic supracrustal rocks forms a broad synform with granitic intrusions along its axis (Muir,1982a). Muir, (1982a) divided the supracrustal rocks into 2 main groups: the Heron Bay Group, and the Playter Harbour Group (Fig. 2).

HERON BAY GROUP

The northern Heron Bay Group, which bifurcates around the Cedar Lake Pluton, consists mainly of intermediate to felsic metavolcanics and metasediments (Muir, 1982b). Metavolcanic rocks include high-iron tholeiitic flows and calc-alkalic pyroclastic rocks of andesitic, dacitic, and rhyolitic composition. The coarsest pyroclastic rocks are found near a felsic volcanic center at Heron Bay. These rocks grade eastwardly into finer-grained pyroclastics that contain a

larger component of reworked material. Further east, near Hemlo, tuffs and tuffaceous metasediments begin to interfinger with argillacous metasediment. East of Hemlo, metasiltstones predominate. Within the Heron Bay Group there are additional felsic centres consisting of crystal tuffs and pyroclastic breccia, with locally derived conglomerates. The various lithologies of the Heron Bay Group, as described by Muir (1982b), are summarized below.

Mafic Metavolcanics

The mafic metavolcanics consist mainly of dark green, fine-grained, moderately-foliated, high-iron tholeiitic basalts. Pillows, where present, are generally moderately- to highly-stretched. Locally, amphibolitization obscures pillow selvages and varioles. The amphibolite is medium-grained, with alternating layers of anhedral to subhedral amphibole (45-55 vol%), and anhedral, equigranular plagioclase (40-45 vol%). Minor constituents include chlorite, epidote, carbonate, sericite, titanite, and pyrrhotite.

Fine-grained mafic metavolcanics are compositionally similar to the amphibolite, but with local, medium-grained (up to 3 mm diam.), anhedral garnet. Mafic tuff, lapilli tuff, and pyroclastic breccia are rare.

Minor amounts of foliated to lineated calc-alkalic andesite also occur. This rock typically consists of

anhedral, moderately-sericitized, very fine-grained to fine-grained plagioclase (up to 80 vol%), with fine-grained, subhedral to euhedral hornblende (up to 20 vol%), and minor biotite, chlorite, epidote, carbonate, and titanite.

Intermediate to Felsic Metavolcanics

Volumetrically significant, the intermediate and felsic metavolcanics grade laterally and imperceptibly into metasedimentary rocks of similar characteristics. Tuff and lapilli tuff predominate, whereas crystal tuffs are minor. The tuffaceous rock typically varies from medium to dark greenish-grey, to brownish-grey, with poorly-defined, discontinuous banding. This rock contains fine-grained, partly-sericitized plagioclase and quartz (up to 90 vol%), biotite or hornblende (up to 25 vol%), and minor amounts of chlorite, epidote, muscovite, titanite, and tourmaline.

Pyroclastic breccia and tuff breccia are uncommon, although minor amounts of highly-stretched felsic breccias are found locally within some volcanic-derived metasedimentary rocks.

Metasediments Derived from Unlithified Volcanic Sources

The intermediate to felsic metasedimentary rocks derived from unlithified volcanic sources are commonly well-banded with laminations resulting from varying proportions of biotite and opaque minerals. Banding, (most easily recognized on weathered surfaces), is typically less than 1 cm thick. Brown porphyroblast of garnet, and greenish porphyroblasts of poikiloblastic amphibole occur in the more felsic metasediments. The intermediate to felsic metasediments are composed of very fine-grained, anhedral plagioclase and quartz (60 to 90 vol%), muscovite (5 to 20 vol%), and minor chlorite, carbonate, epidote, garnet, amphibole, tourmaline, and microcline.

Metasediments Derived from Reworked Material

The reworked metasedimentary rocks are metamudstones and metawackes. The brown to black metamudstone typically forms relatively thin units (< 4m thick), containing very fine-grained quartz and plagioclase (.03 mm diameter), with varying amounts of biotite, muscovite, sulphides, and carbonacous matter. The metawacke which occurs predominately east of Hemlo is lithic arkosic in composition.

Locally, the pelitic metasediments are highly recrystallized and schistose. Porphyroblasts of garnet,

andalusite, staurolite, cordierite, and clumps of sillimanite are locally present (Muir, 1982a).

PLAYTER HARBOUR GROUP

The Playter Harbour Group (as described by Muir, 1982b), consists mainly of metamorphosed high-iron tholeiitic basalt flows. Near the granitic contacts, the mafic metavolcanics are amphibolitized, displaying significant recrystallization and moderate to strong lineation. The amphibolite often displays a metalayering defined by feldspar/amphibole segregations. Typically, the mafic metavolcanics consist of fine-grained, anhedral actinolite (45 to 50 vol%) and sericitized or saussuritized plagioclase (45 to 50 vol%), with epidote and minor carbonate and opaque minerals. The fine-grained mafic metavolcanics contain hornblende (55 to 60 vol%) and partly-sericitized, anhedral plagioclase (30 to 40 vol%), with minor chlorite, biotite, epidote, carbonate, quartz, and opaque minerals.

Well-foliated to schistose mafic tuff and lapilli tuff are locally present within the sequence. These dark green rocks contain stretched fragments of intermediate to felsic composition.

Intermediate to felsic metavolcanics are very minor within the Playter Harbour Group.

2.3.2 INTRUSIVE ROCKS

The intrusive rocks of the Hemlo-Heron Bay area, as described by Muir (1982b), are summarized below.

Mafic and Ultramafic Intrusive Rocks

Mafic and ultramafic intrusive rocks are predominately emplaced within the Playter Harbour Group. Muir (1982b) suggests that these intrusive rocks are comagmatic with the Playter Harbour Group. The predominate mafic intrusive is a medium- to coarse-grained gabbro consisting of twinned, anhedral plagioclase laths (10 to 60 vol%), euhedral hornblende (40 to 70 vol%), and minor epidote, chlorite, carbonate and biotite.

Also present are a few fine-grained, schistose mafic dykes, containing altered fragments of amphibole and biotite in a plagioclase, quartz, and hornblende matrix.

Massive peridotite and pyroxenite also intrude the Playter Harbour Sequence. The dark green peridotite consists of serpentine (up to 65 vol%), fine-grained tremolite and/or pyroxene, with minor magnetite, talc and chlorite. Pyroxenite is generally dark green, consisting almost entirely of medium-grained, subhedral crystals of pyroxene. The pyroxene displays minor to complete alteration to hornblende. Accessory minerals include chlorite, muscovite, talc, carbonate, and

epidote.

Intermediate to Felsic Intrusive Rocks

The supracrustal rocks of the Hemlo-Heron Bay area are intruded by Kenoran granitic bodies.

Pukaskwa Gneissic Complex

The Pukaskwa Gneissic Complex, located south of the supracrustal sequences, consists mainly of foliated and lineated trondhjemite with lesser amounts of granodiorite, and a border zone of plagioclase-porphyritic protomylonitic trondhjemite. The rock contains partly-sericitized plagioclase laths and minor recrystallized quartz phenocrysts, within a matrix of fine-grained, anhedral, granoblastic-polygonal plagioclase, quartz, and minor microcline. Green to olive-brown biotite and green hornblende occur as fine to very-fine, anhedral grains.

Cedar Lake Pluton

The Cedar Lake Pluton (2690 Ma; Corfu and Muir, 1986), is a massive hornblende-biotite granodiorite, located within the Heron Bay Group, east of Hemlo (Fig. 2). This intrusion

contains medium-grained, twinned, and weakly-zoned plagioclase laths; equant, anhedral, slightly-strained quartz, and anhedral microcline. Biotite and hornblende are typically anhedral and smaller (< 1 mm). Minor minerals include epidote, titanite, apatite, allanite, magnetite, and possibly zircon.

Heron Bay Pluton

The Heron Bay Pluton, located between the Heron Bay and Playter Harbour Groups (Fig. 2), is compositionally similar to the Cedar Lake Pluton. This hornblende-biotite granodiorite is plagioclase-porphyritic and weakly-foliated along its SE contact with mafic volcanics.

Gowan Lake Pluton

The northern Gowan Lake Pluton consists of at least two phases of quartz monzonite. One phase is a medium to coarse-grained, weakly-lineated, microcline porphyritic, biotite-hornblende quartz monzonite. This phase contains large (4 to 15mm), randomly-oriented, twinned, microcline phenocrysts, as well as subhedral to euhedral phenocrysts of fine- to coarse-grained hornblende. The groundmass contains fine-grained plagioclase, quartz, biotite, and microcline. Minor minerals include epidote, titanite, and allanite.

Another phase, which is non-porphyritic, consists of anhedral, relatively equigranular plagioclase, strained quartz and microcline, with hornblende, biotite and chlorite. Minor minerals include epidote, titanite, and apatite.

Late Felsic Dykes and Sills

The supracrustal rocks have also been intruded by numerous, concordant to slightly-discordant plagioclase- and quartz-plagioclase porphyritic dykes of various ages and composition (Muir, 1982b). Some dykes are believed to be marginal phases of the Cedar Lake Pluton, having U-Pb zircon ages of between 2690 to 2670 Ma (Corfu and Muir, 1986). Other porphyritic dykes are possibly related to volcanism (Muir, 1982b). The porphyritic dykes generally contain subhedral phenocrysts of plagioclase and less commonly quartz in an aphanitic to very fine-grained, slightly-foliated to well-foliated matrix.

PROTEROZOIC INTRUSIONS

Port Coldwell Alkalic Complex

The Proterozoic Port Coldwell Alkalic Complex, located NW of Heron Bay (Fig. 2), consists predominately of monzonite and gabbro. The complex has been studied in considerable detail (Currie, 1980; Lum, 1973; Milne, 1967; and Puskas, 1967a). This description is from the brief summary of Muir (1982b).

The predominate rock type of the Port Coldwell complex is a layered, coarse-grained monzonite, consisting of perthitic feldspar, olivine, augite, biotite, and magnetite.

Gabbro occurs predominately at the margin of the complex in contact with the country rock. The predominate gabbro is a biotite gabbro, consisting of biotite flakes (2 to 8 mm diameter), olivine, augite and plagioclase, with minor apatite and magnetite. Layered gabbro, of similar composition, displays a primary mineralogical banding due to alternating proportions of mafic and felsic minerals. The less common olivine gabbro contains significant fine-grained olivine and magnetite.

Mafic Dykes

Undeformed north- and northwest-trending subalkalic diabase dykes and later, less common, north-trending

pyroxene-magnetite and biotite lamprophyre dykes intrude all lithologies of the Hemlo-Heron Bay area. These undeformed dykes are of Proterozoic age, and many are related to the Port Coldwell Alkalic Complex. The fine- to coarse-grained dykes vary from 1 to 60 m in thickness. The diabase contains subhedral to euhedral plagioclase (45 vol%) and pyroxene (50 vol%), with minor uralite, biotite, quartz, and magnetite.

2.3.3 METAMORPHISM

Metamorphism in the Hemlo-Heron Bay area increases from low-grade, low-temperature greenschist facies in rocks significantly distant from intrusions, to amphibolite facies in rocks close to intrusive contacts (Muir, 1982b).

Burk et al., (1986) carried out detailed metamorphic studies of the host rocks at the Hemlo deposit. Metamorphic conditions were estimated using a geobarometer based on the reaction :

$$3 \text{ anorthite} \rightleftharpoons \text{grossular} + 2Al_2SiO_5 + \text{quartz}$$

(Ghent, 1976; Newton and Haselton, 1981), and a geothermometer based on Fe-Mg partitioning in garnet and biotite, assuming no other cations (Ferry and Spear, 1978).

Unfortunately, the samples Burke et al. (1986) used contain a significant amount of Mn and Ca. However, their gross pressure-temperature estimates range from bathozone 4 to bathozone 5 (as defined by Carmichael, 1978; modified by Archibald et al., 1983). This corresponds to temperatures of approximately 550°C, and pressures ranging from approximately 4 to 8 kb. The occurrence of a bathozone 5 assemblage at Hemlo is unique to Canadian Archean greenstone belts, which are generally characterized by bathozone 2 or 3 assemblages (Burk et al., 1986).

Burk et al., (1986) suggest that host rocks at Hemlo were initially metamorphosed to high-pressure, medium-grade, as evident from staurolite and kyanite. This event was followed by lower-pressure metamorphism marked by the generation of sillimanite and the development of a penetrative lepidoblastic schistosity. Burke et al., (1986), postulate that the early, high-pressure metamorphism occurred in response to tectonically-induced crustal thickening (DeWit, 1982; Poulsen et al., 1980; and Archibald et al., 1978). The subsequent lower-pressure metamorphism may have been due to rapid uplift and erosion, which caused significant lithostatic pressure decrease, and only minor temperature changes (Burk et al., 1986).

2.3.4 STRUCTURAL GEOLOGY

Geological structures in the Hemlo-Heron Bay area are complex. This is partly due to the weak to intense deformation which has obliterated many of the primary features. Structural complexity is also related to the inherent mechanical properties of the various lithologies, and the diversity of local deformation processes and events (Muir, 1985).

Recent investigations suggest that the large scale structure in the Hemlo-Heron Bay area was entirely formed during an event of heterogeneous dextral shearing (Hugon,1984,1986a,1986b). This implies that the diverse local structures, which include isoclinal folds, tectonometamorphic layering, and intense stretching lineation, are all related to a large zone of heterogeneous ductile shear. Hugon (1984) suggests that the entire 2 km wide domain between the Cedar Lake Pluton and the Pukaskwa Gneissic Complex (Fig. 2) has undergone dextral ductile shear with the most intense deformation occurring along the contact between metavolcanic and metasedimentary rocks. The entire deformed zone has been named the "Hemlo Shear Zone" (Hugon, 1984).

The Hemlo Shear Zone contains several zones of intense ductile deformation (Fig. 2). The Lake Superior Shear Zone, which hosts the ore at Hemlo, has an overall strike of 110° and can be traced on the surface for over 11 km (Muir, 1982b). This 5-40 m wide ductile shear zone occurs near the interface between felsic metavolcanic and metasedimentary

rocks (Hugon, 1984). The Hemlo Fault, which hosts the Muir Zone (Highway Zone), is another zone of intense deformation (Muir, 1982b; Hugon,1984). This 5-10 m wide zone roughly parallels the Trans-Canada Highway (17), and can be traced for over 10 km (Fig. 2). Another high-strain zone, up to 1.5 km wide and generally composed of plagioclase-porphyritic protomylonitic trondhjemite, occurs along the northern margin of the Pukaskwa Gneissic Complex (Muir, 1982b). These high-strain zones are commonly mylonitic with obvious indicators of dextral displacement (Hugon, 1984).

Hugon (1986a) suggests that the numerous WNW-ESE shear zones within the Hemlo Shear Zone are similar to C fabric (domains of simple shear) on a km scale. Hugon (1986a) also states that the general north- to northwest-plunging lineation plus the dextral component of relative displacement are indicative of regional, southeast-directed oblique thrusting. This thrusting is thought to have occurred along a 5-10 km wide, east-west trending zone that extends at least from Heron Bay to approximately 20 km east of Hemlo (Hugon, 1986a). Synkinematic metamorphic porphyroblasts within the thermal aureole of the Cedar Lake Pluton indicate that thrusting and peak metamorphism occurred during the emplacement of the Cedar Lake Pluton (Hugon, 1986b). Hugon, (1986b), suggests that the high pressure and temperature mineral assemblage at Hemlo supports the structural evidence of large-scale thrusting.

Preliminary zircon U-Pb dates from sheared, cross-cutting dykes (Corfu and Muir, 1986), confirm that shearing occurred

during the emplacement of the 2690 Ma Cedar Lake Pluton, and continued at least until the emplacement of 2670 Ma dykes (Hugon, 1986b).

CHAPTER 3. GEOLOGY OF THE WESTERN BARITE OCCURRENCES

3.1 GEOLOGICAL SETTING

The western barites occur within the Heron Bay Group as it narrows to a 4 km width between the northern Gowan Lake Pluton and the southern Heron Bay Pluton. The WBO are located on strike with possible western extensions of high-strain zones (Hugon, 1986b) and aerial photographic linaments (Muir, 1982a) observed in the Hemlo area (Fig. 2). Unfortunately, Pleistocene and Recent sediment (Fig. 2) cover large portions of the western Heron Bay Group, making extrapolation of structural and lithological trends difficult.

The WBO are located along the highly-deformed contact between southern mafic metavolcanics, and northern metasediments and felsic metavolcanics (Fig. 2). The main mineralized unit, a barite-sulphide-quartz schist, occurs as lenses which are interlayered with an enveloping pyrite-muscovite schist. North of the mineralization are biotitic metasediments. Thin lenses of carbonaceous phyllite occur within a few metres of the barite mineralization. Similarily, lenses of chromium-muscovite schist also occur within a few metres of the mineralization. Generally, thin layers of highly-deformed plagioclase porphyry are found south of the mineralization, but north of the amphibolitized mafic metavolcanics.

3.2 LOCAL ROCK TYPES

The rock types which typically comprise the WBO are briefly described in the following section. A microscopic description of most rocks is in the microtextures section.

Barite-Sulphide-Quartz Schist

The main baritic unit consists of up to 70 vol% barite, quartz (up to 30 vol%), sulphide (up to 10 vol%), and ankerite (up to 5 vol%), with minor celsian (see Appendix A for composition) and muscovite. Despite the lack of phyllosilicates, this light-grey rock is described as schistose due to a well-developed, planar-linear fabric defined by thin (1 to 50 mm wide), elongate, alternating zones of fine- to medium-grained barite, sulphide and quartz. Horizontal outcrop surfaces display thin, alternating lenses of sulphide, barite, and quartz. Foliation surfaces reveal a moderately-plunging lineation, defined by sulphide-rich elongate zones (aspect ratios > 10:1), which are typically less than 0.5 m in length. This rock grades both laterally, and across strike, into pyrite-muscovite schist.

Pyrite-Muscovite Schist

This buff to orange coloured, well-foliated, very fine- to fine-grained rock is predominately quartz and muscovite with minor sulphide (up to 10 vol%), tremolite (up to 10 vol%), ankerite (up to 5 vol%), and minor chlorite. Schistosity and colour banding are defined by thin (1 to 50 mm wide), alternating quartz-, muscovite-, and sulphide-rich layers. Sulphides occur as disseminated grains, and in thin (1 to 50 mm wide) elongate zones which define a lineation. Texturally, the rock varies from phyllite to schist.

Carbonacous Phyllite

This black, very-fine grained, well-foliated rock consists of carbonaceous matter and quartz, with minor pyrite, and muscovite. Elongate sulphide grains parallel a ridge lineation observed on foliation surfaces.

Chromium-Muscovite Schist

This green, fine-grained rock contains quartz and chromium-rich muscovite (up to 3 wt% Cr_2O_3), with minor chromite and pyrite. Schistosity is defined by thin (1 to 10 mm wide) lenses of alternating quartz-pyrite, and chromium-

muscovite. Locally, chromite grains (< 1 mm diameter) enveloped by lenses of chromium-muscovite, define a lineation observed on the foliation surface (see section 4.2.3 -microtextures).

Mafic MetaVolcanics

The mafic metavolcanics are commonly foliated to well-foliated with abundant hornblende and plagioclase, and minor biotite, quartz, titanite, and pyrrhotite. Hornblende and plagioclase are typically medium-grained, whereas biotite, titanite, quartz and pyrrhotite are fine-grained. Foliation is typically defined by alternating layers of plagioclase and oriented hornblende, with local concentrations of oriented, fine-grained biotite and pyrrhotite (see section 4.2 for microtextures). Mafic metavolcanics located closer to the barite-sulphide mineralization are generally more schistose, with increased concentrations of biotite, quartz, ankerite and pyrrhotite.

Biotitic Metasiltstone

The grey to dark-grey, phyllitic metasiltstone contains fine-grained quartz and biotite with minor fine-grained, subhedral almandine-spessartine garnet and elongate

pyrrhotite and pyrite (see section 4.1 for microtextures). Rootless isoclinal folds are occasionally displayed within this unit.

Plagioclase Porphyry

This intrusive rock contains medium-grained phenocrysts of plagioclase and minor quartz within a fine-grained matrix of plagioclase, quartz, carbonate, biotite, titanite and ilmenite. This rock displays a weak to very well-developed foliation defined primarily by oriented ilmenite and biotite (see section 4.2 regarding microtextures). Carbonate pressure shadows in the lineation direction often give the phenocrysts an elongated "quartz eye" appearance. The composition and texture of this intrusive rock are similar to the late felsic porphyry dykes described by Muir (1982b).

3.3 BARITE OCCURRENCES

3.3.1 NORTHERN EAGLE PROPERTY

Extensive trenching on property held by Northern Eagle Mines Ltd. has revealed a 75 m exposure of the previously described rock types (Fig. 4). Sulphide-sulphate mineralization occurs 10 m north of the contact between

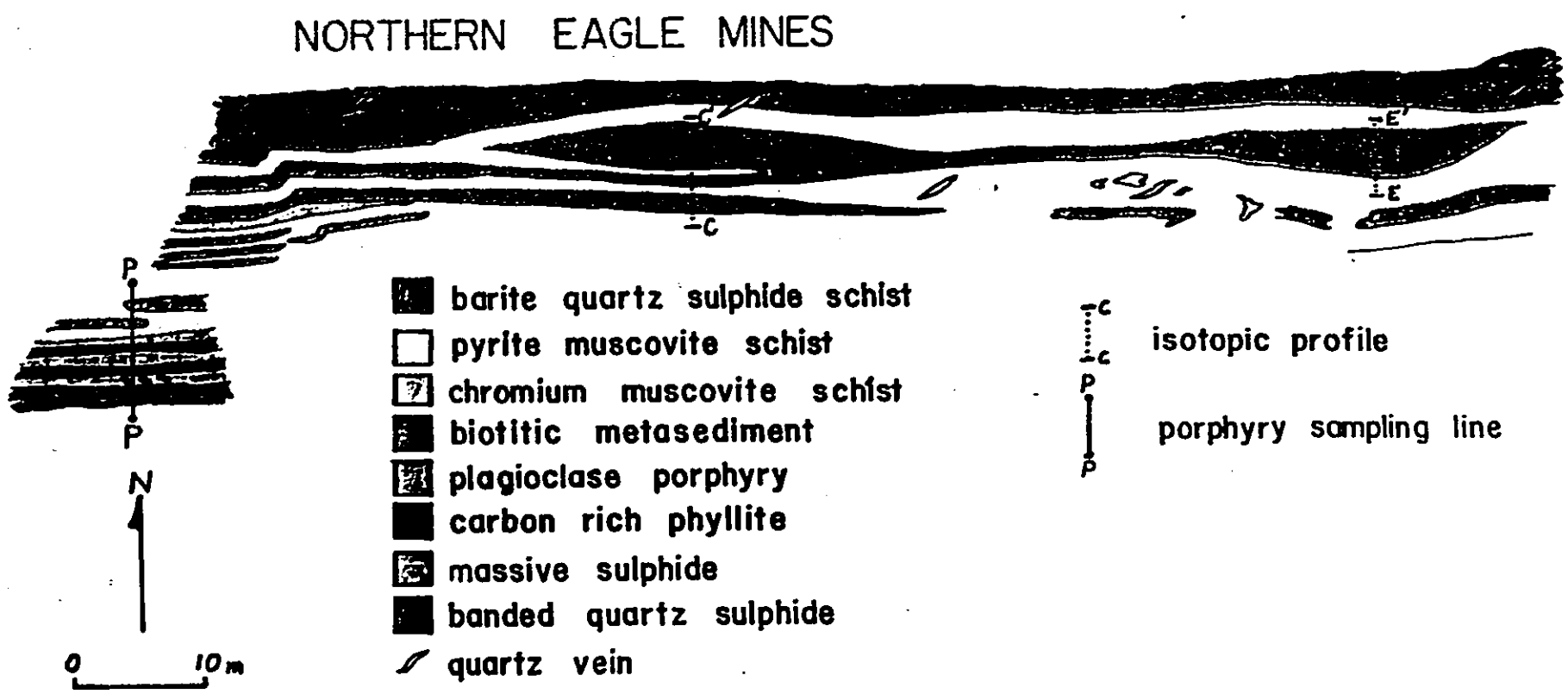

Fig. 4 Geology of Northern Eagle barite occurrence.

southern mafic metavolcanics and northern metasediments. Barite occurs within 3 thin (< 1 m wide) lenses of barite-sulphide-quartz schist, which interfinger with enveloping pyrite-muscovite schist. Immediately south of the mineralization, in the western section of the outcrop, are interlayered chromium-muscovite schist, carbonaceous phyllite and strongly-foliated plagioclase porphyry. A thin lens of massive pyrite, and several thin lenses of irregularly-banded pyrite and quartz occur just south of the chromium-muscovite schist.

The southeastern section of the outcrop contains thin, isoclinally folded lenses of biotitic metasiltstone which occur within pyrite-muscovite schist. The eastern section also displays a thinning baritic unit which terminates to the east into pyrite-muscovite schist. Biotitic metasiltstone occurs immediately north of the mineralization.

Just west of Northern Eagle, relatively undeformed plagioclase-porphyritic dykes cross-cut the foliation in biotitic metasiltstone.

3.3.2 PADRE RESOURCES PROPERTY

The poorly exposed Padre Resources occurrence is located 1 km west of Northern Eagle. This barite occurrence displays many similarities with Northern Eagle (Fig. 5). The mineralization occurs within felsic meatsediments, 10 m north of the

PADRE RESOURCES LIMITED

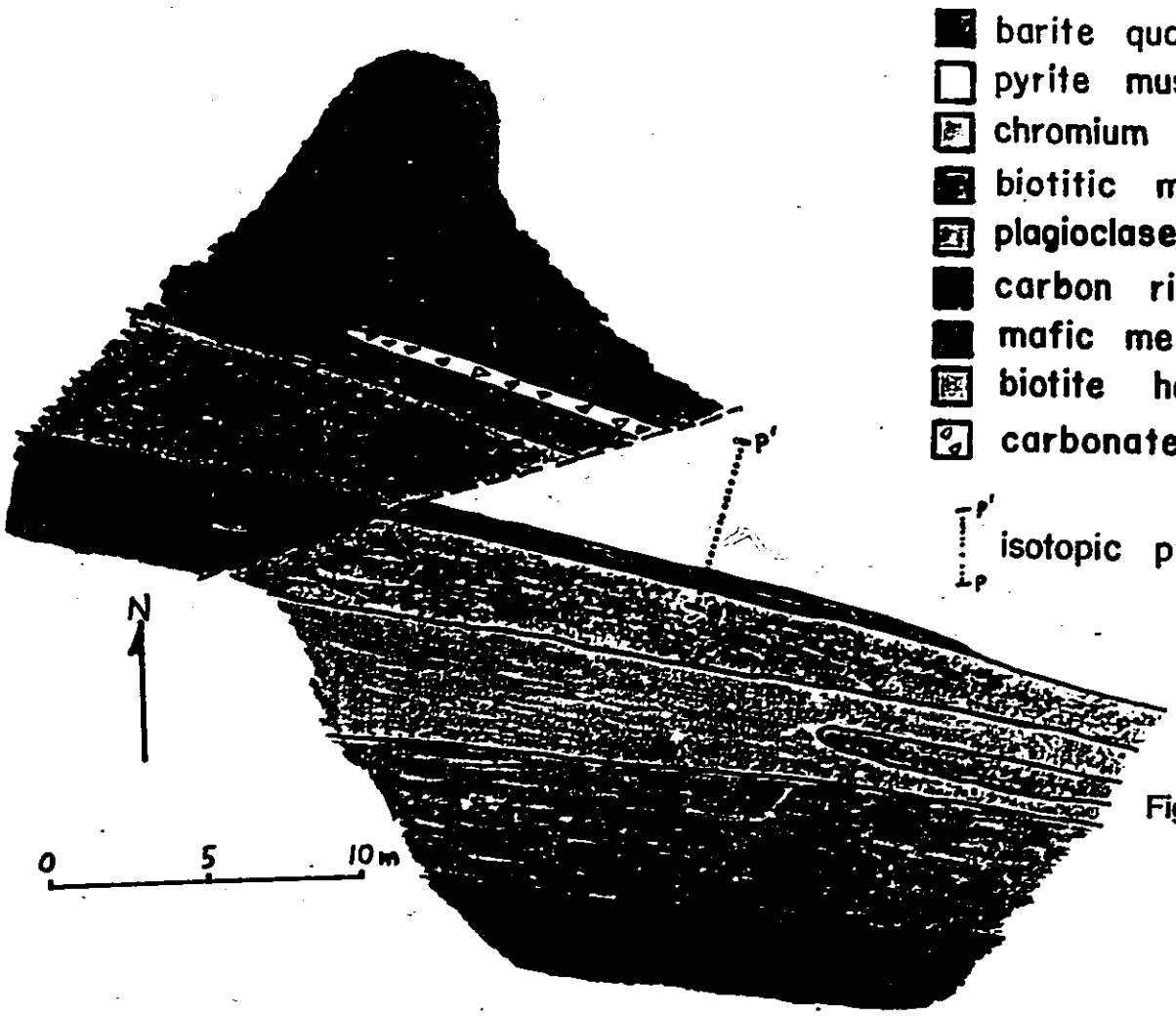

- barite quartz sulphide schist
- pyrite muscovite schist
- chromium muscovite schist
- biotitic metasediment
- plagioclase porphyry
- carbon rich phyllite
- mafic metavolcanics
- biotite hornblende schist
- carbonate fluorite breccia

P' isotopic profile P

Fig.5 Geology of Padre barite occurrence.

contact with mafic metavolcanics. Barite is found within a thin lens of barite-sulphide-quartz schist. Immediately south of the mineralization is carbonaceous phyllite and biotite-amphibole schist. Further south are interlayered chromium-muscovite schist and deformed plagioclase porphyry.

Immediately north of the barite mineralization is pyrite-muscovite schist, which grades northward into biotitic metasiltstone. Locally, the rocks are cut by a NE-striking fault, which has associated concordant, vuggy, cataclastic zones (< 20 cm wide) containing fragments of metasiltstone in a matrix of euhedral fluorite and ankerite.

3.3.3 KADREY ENERGY PROPERTY

The Kadrey barite occurrence, located 4 km west of Padre, is similar to the previously described occurrences. Surface mapping reveals a thin lens of barite-sulphide-quartz schist within a larger lenticular layer of pyrite-muscovite schist (Fig. 6). Lenses of carbonaceous phyllite and chromium-muscovite schist occur just north of the barite-sulphide-quartz schist. Further north are possible graded biotitic metasediments, with tops to the north (Plate 1). Amphibolitic mafic metavolcanics with interflow metasediments are south of the barite.

Patterson, (1984) states that drilling has revealed three parallel barite units, up to 3 m wide, with footwall

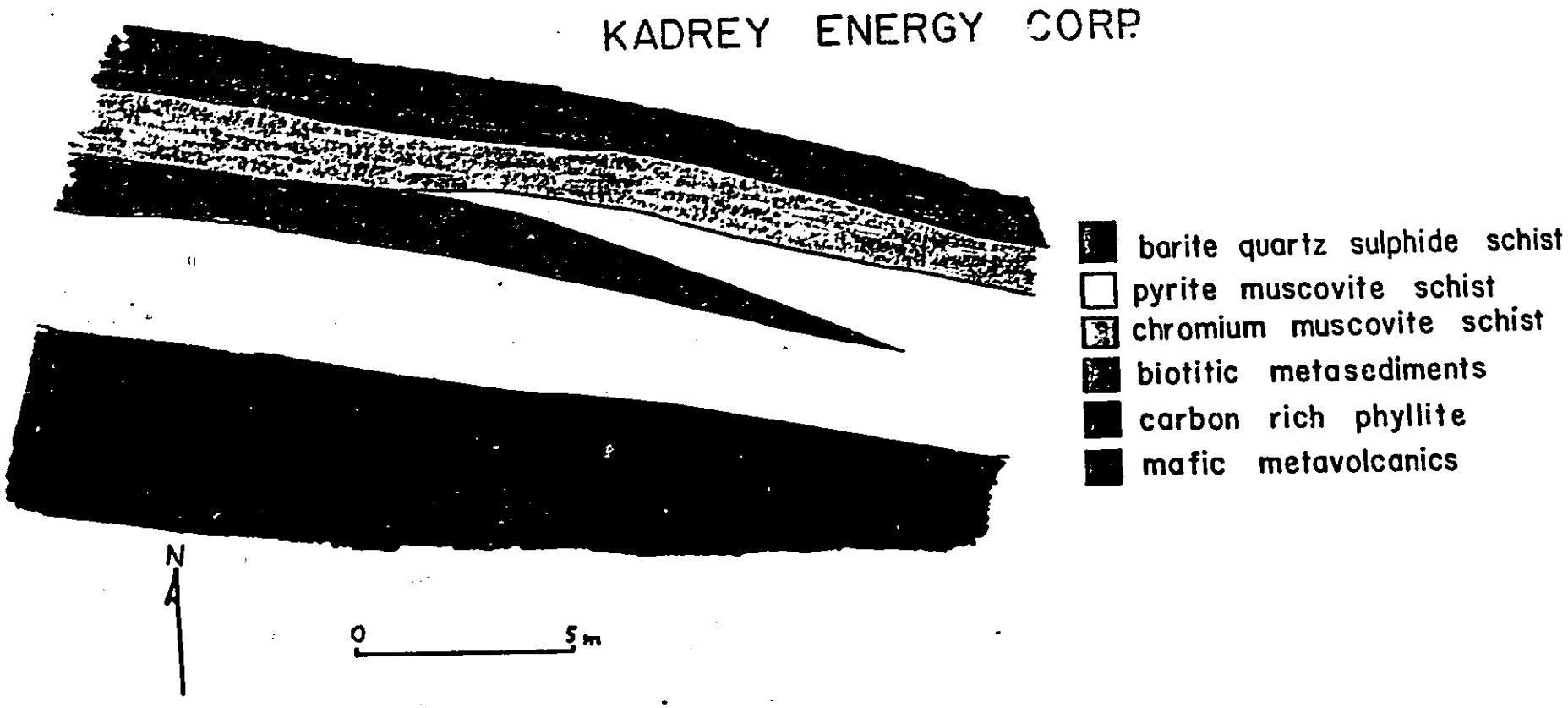

Fig. 6 Geology of Kadrey barite occurrence.

chromium-muscovite schist. Drilling has also revealed numerous breccias, and cross-cutting lamprophyre dykes.

3.4 LOCAL STRUCTURAL GEOLOGY

All rock types in the immediate vicinity of the WBO display evidence of moderate to very strong penetrative deformation (Plate 2). Primary features such as bedding are not preserved. Styles of deformation vary between, and within lithological units. Some of the various structures and their orientations are summarized in a structural sketch (Fig. 7).

3.4.1 FOLIATION AND MINERAL LINEATION

Banding and foliation within the WBO generally strike east-west, dipping steeply towards the south. Locally, the strike and dip of schistosity vary by as much as 30 (Fig. 8).

Mineral lineations occur within the foliation planes of all rock types. They are most easily observed on foliation surfaces of barite-sulphide-quartz schist (Plate 3). Mineral lineations generally have a moderate but variable western plunge. These lineations are steepest at Northern Eagle, becoming progressively less steep in the Padre and Kadrey occurrences (Fig. 8).

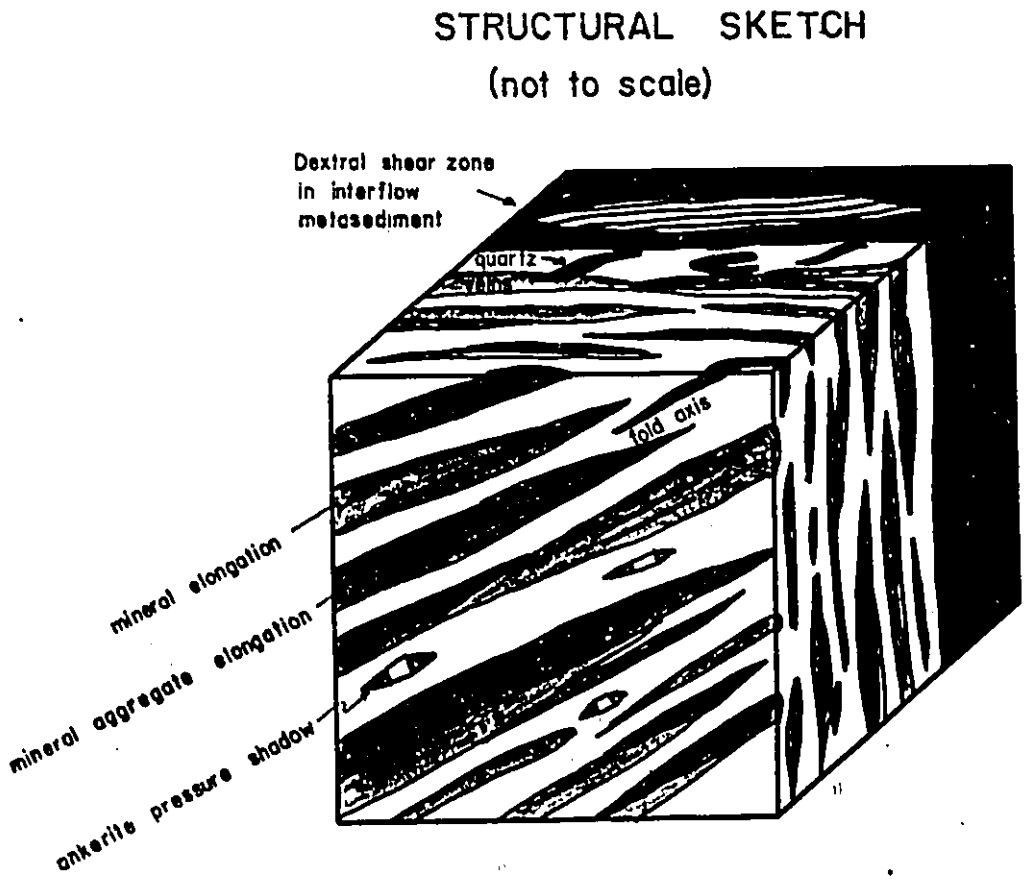

Fig. 7 Sketch of various structures within WBO.

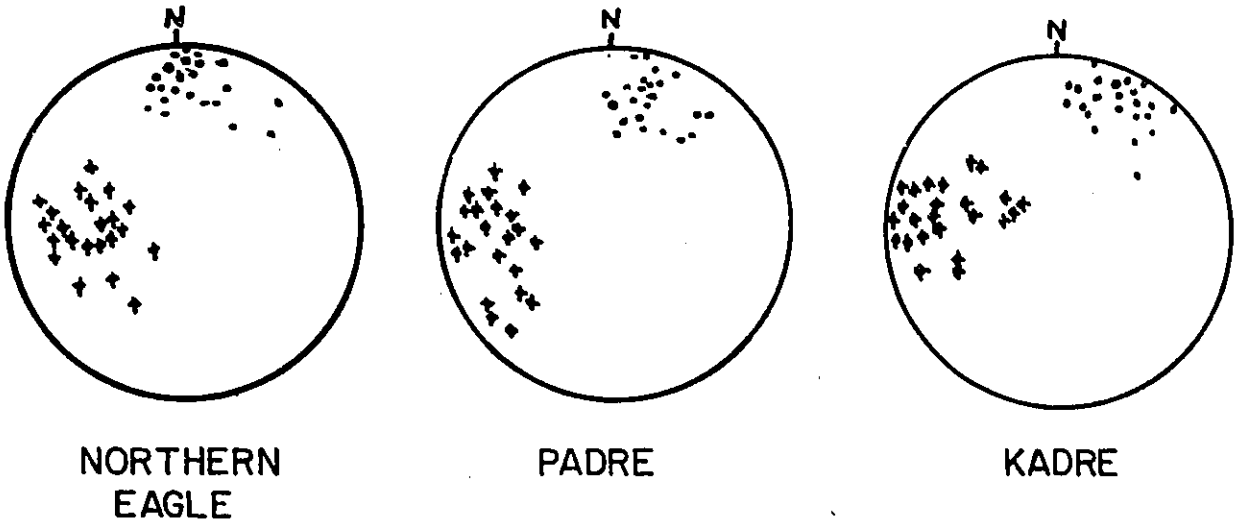

Fig. 8 Equal area projection of WBO structural data.

3.4.2 FOLDING

The few folds that are observed within the WBO can be divided into 2 types based on their orientation and shape. Most folds are rootless, isoclinal and axial planar to the well-developed foliation. These folds occur sporadically within schistose units, particularly in areas containing isolated layers of highly-contrasting composition. For example, the layering is tightly folded in the isolated pods of argillaceous metasediment which occur within pyrite-muscovite schist at Northern Eagle (Plate 4). At Padre, quartz-rich layers within chromium-muscovite schist are also isoclinally folded (Plate 5). These folded quartz layers have fold axes parallel to the mineral lineation.

Schistosity and banding are folded in the other observed fold type. These folds, typically chevron, are observed at microscopic and outcrop scale. For example, biotitic metasiltstone commonly displays well-developed kinking of phyllitic cleavage. At a larger scale, the pyrite-muscovite schist at Northern Eagle displays a chevron fold with an amplitude of approximately 0.5 m (Plate 6). The axial surfaces of these folds are generally steep and northwest-striking.

3.4.3 VEINS AND VEINLETS

Echelon quartz veins, up to 2 m in length and 10 cm in width, occur sporadically within biotitic metasiltstone and pyrite-muscovite schist at Northern Eagle (Plate 7). These undeformed sigmoidal veins have a NE strike and a moderate to steep southeastern dip, suggesting late sinistral offset.

En echelon sulphide veins, up to 10 cm in length and <0.5 cm in width, are oriented clockwise to the foliation in the pyrite-muscovite schist, suggesting a period of dextral displacement.

3.4.4 SHEAR ZONES

Penetrative foliation and lineation are common in zones of heterogeneous ductile simple shear (Ramsay, 1980). However, penetrative deformation does not confirm the presence of a ductile shear zone. Progressive shear deformation often results in very complex deformed rocks (Hugon, 1984). When protoliths are unknown and/or fine-grained, the rocks may not display recognizable effects of shear zone deformation. Since the WBO do not display undeformed protoliths, it is difficult to determine the precise nature of deformation at the WBO. However, it is possible to recognize structural features of ductile shear within the WBO.

One possible indicator of ductile shear is a small

dextral shear zone located within amphibolite, approximately 50 m south of the Padre barite mineralization (Plate 8). Its dextral sense of shear is suggested by the curvature of the foliation in the amphibolitized mafic metavolcanics (Ramsay, 1980).

At Northern Eagle, a local strain gradient is recognized in the medium-grained plagioclase-porphyritic intrusions which occur at various distances from the barite mineralization. From left to right, samples of porphyry in Plate 9, are collected closer to the barite mineralization (see Fig. 4 for sample locations). These samples demonstrate a progressive decrease in phenocryst size, and a decrease in the ratio of phenocryts to matrix, as a result of increased mylonitization towards the centre of the barite occurrence. Mafic metavolcanic rocks also display a local strain gradient, represented by stronger foliation in rocks closer to the barite. This local strain gradient is a common feature of non-coaxial deformation accompanying heterogeneous ductile shear (Ramsay, 1980).

There are several microscopic indicators of ductile shear. These structures are described in the microtextures section.

3.5 METAMORPHISM

The presence of hornblende within mafic metavolcanics suggests that the local rocks have been metamorphosed to amphibolite facies (Turner, 1981). There is little evidence of retrograde metamorphism. Microtextures relating metamorphism and deformation are described in the next section.

CHAPTER 4 MICROTEXTURES

The WBO lithologies were examined in thin and polished section. The observed microtextures are described in 2 sections. The first section describes microtextures associated with metamorphic garnet and hornblende. These microtextures demonstrate the timing of deformation relative to metamorphism. The second section describes the deformation microtextures of mineralized and important non-mineralized units, establishing a time relationship between sulphate-sulphide mineralization, intrusion, deformation, and metamorphism.

4.1 MICROTEXTURES OF METAMORPHIC MINERALS

4.1.1 HORNBLENDE

The occurrence of hornblende in the mafic metavolcanics south of the WBO suggests that the rocks have undergone amphibolite facies metamorphism (Turner, 1981). Hornblende typically occurs as large (up to 3 mm long), subhedral to euhedral grains which overprint a fine-grained, well-developed biotite-pyrrhotite foliation (Plate 10). This overprinted foliation is defined by the parallel alignment of elongated grains of pyrrhotite and fine-grained biotite. Within the hornblende, the overprinted foliation is defined predominately by elongated pyrrhotite grains (Plate 10). Hornblende grains are generally

randomly oriented, although some grains do display a preferred orientation of long axes parallel to the biotite-pyrrhotite foliation (Plate 11).

The signifance of the hornblende microstructures are listed below:

1) The preferred orientation of some hornblende grains may be due to a combination of a) deformation, b) grain rotation, and c) oriented crystal growth (Hobbs et al., 1976). These mechanism may have been activated in response to deviatoric stress which occurred during, or after amphibolite facies metamorphism (Kamb, 1959: Kumazawa,1963; Hartman and den Tex, 1964).

2) The biotite-pyrrhotite foliation, overprinted by hornblende, suggests that a foliation may have been developed before the onset of amphibolite facies metamorphism.

4.1.1 ALMANDINE-SPESSARTINE GARNET

Almandine-spessartine garnet containing 20.1 wt% FeO, 13.5 wt% MnO, 6.2 wt% CaO and 1.7 wt% MgO, occurs within the biotitic metasediments immediately north of the WBO. Due to the relatively high manganese concentration, the metamorphic grade at which these garnets grew is uncertain. Miyashiro (1965) suggests that almandine garnet enriched in manganese

can form in pelites during greenschist facies metamorphism, and this crystal growth can continue during amphibolite facies metamorphism. Almandine garnets similarily enriched in manganese also occur within the amphibolite-grade metasediments at Hemlo (Walford et al., 1986). Therefore, it is possible that the garnets within the WBO formed during greenschist metamorphism, and crystal growth may have continued during amphibolite facies metamorphism.

The typically fine-grained (< 1 mm diameter), subhedral to euhedral garnet contains abundant inclusions of elongate pyrite and pyrrhotite (sulphide inclusions are generally more elongate than sulphide grains occurring outside of garnet) (Plate 12). Despite a lack of retrograde alteration, most garnet crystals have at least 1 irregular grain boundary, usually subparallel to the foliation (Plate 13). Crystal boundaries at high angles to the foliation are generally sharp Plate 13). Smaller garnet grains, which typically do not deflect the biotite foliation, are often longer in directions subparallel to the foliation (Plate 13).

The small size and irregular crystal boundaries suggest that garnet growth was limited. The extension of smaller garnets parallel to the foliation may be a result of impeded crystal growth perpendicular to the biotite foliation. This has been demonstrated for garnet in the pelitic schists of the Sanbagawa metamorphic terrain of Japan (Sakai et al.,1985). Alternatively, the inequant garnet shapes may be due to garnet pressure solution (Bell et al., 1986).

Despite the uncertainty in the grade at which the garnets grew (greenschist to amphibolite facies), the microstructures of garnet still reveal the following timing aspects of deformation:

1) Elongate sulphide inclusions suggest that non-hydrostatic stress was present before and/or during garnet growth.

2) Impeded garnet growth perpendicular to the biotite foliation suggests that a biotite foliation was developed prior to garnet growth.

4.1.3 METAMORPHIC MICROTEXTURES-SUMMARY

Microtextures associated with hornblende suggest that deviatoric stress was present during amphibolite facies metamorphism. A biotite-pyrrhotite foliation, which is overprinted by hornblende and possibly garnet, was probably developed before amphibolite facies metamorphism.

4.2 DEFORMATION MICROTEXTURES OF WBO LITHOLOGIES

4.2.1 BARITE-SULPHIDE-QUARTZ SCHIST

4.2.1.1 SCHISTOSITY AND LINEATION

The baritic unit consist predominantly of barite, quartz, ankerite, and pyrite with minor celsian (up to 37 wt% BaO), tremolite, sphalerite and galena. The intense planar-linear deformation displayed in hand sample is less obvious in thin section due to the absence of both brittle and ductile strain-features. Typical amphibolite facies mylonite microstructures, such as undulose extinction, deformation bands, polygonization and subgrain formation (Bell and Etheridge, 1973), are only rarely observed within the baritic unit. Instead, the constituent minerals form compositional layers of interlocking, strain-free grains. This crystalloblastic fabric, with its abundant 120 triple junctions, is similar to the fabric described by Hugon (1984) for rocks hosting the gold mineralization at Hemlo.

The penetrative planar-linear fabric is also defined by the parallel alignment of elongated mineral grains. Barite grains, elongated approximately 2:1, define the foliation and lineation. The barite is typically lenticular in shape, and its grain boundaries with quartz are usually concave on the barite side (Plate 14).

The penetrative fabric is also defined by sulphide lenses

consisting of euhedral pyrite within elongate aggregates of anhedral sphalerite and galena (Plate 15). Sulphide occasionally occurs in small (< 1 cm amplitude), rootless, tight folds, axial planar to the foliation. The sulphide lenses (which define a planar-linear fabric), suggest either a) sulphide mineralization during ductile deformation, or b) remobilization of sulphides during ductile deformation. The latter possibility can occur through any combination of a) partial melting, b) pressure solution, and c) crystal plastic deformation. For the WBO, partial melting is unlikely, since the lowest melting temperature in the Pb-Fe-S system is 723° C (Craig and Kullerud, 1968). A limited amount of remobilization may have occurred through crystal-plastic deformation, as suggested by the observed order of relative plasticity: galena >= sphalerite > pyrite (Pederson, 1980). Pressure solution may have also occurred, as indicated by a few small sulphide veins (<10 cm long and <3 mm wide) in the pyrite-muscovite schist (Plate 16). During deformation of the WBO, dislocation creep was probably predominant at higher metamorphic grades (amphibolite facies), whereas pressure solution probably prevailed at lower temperatures (Kerrich et al., 1977).

Tremolite and celsian also define the penetrative fabric of the baritic unit. The long axis of tremolite grains are generally subparallel to the foliation and lineation (Plate 17). Celsian grains display 3 modes of occurrence. Most celsian occurs as small (< 1 mm long) lenticular grains parallel to the foliation (Plate 18). Celsian also occurs concentrated

in the nose of the small rootless, sulphide-rich folds. (Plate 19). Celsian occurs least frequently as larger (up to 3 mm diameter), euhedral crystals, which overprint the foliation (Plate 20).

The tectonometamorphic fabric within the baritic unit is best demonstrated where the barite foliation is deflected around larger inclusions. In Plate 21, the barite foliation is deflected around a 5 mm lens of ankerite. Smaller lenses of ankerite (<1 mm wide), displaying deformation twinning, also define the penetrative foliation.

The deformation microstructures of the WBO baritic units differ significantly from sedimentary and diagenetic microstructures preserved in the relatively undeformed Archean barite deposits of the Fig Tree Group of South Africa. The slightly metamorphosed South African deposits contain barite beds which have been largely recrystallized during diagenesis (Heinrichs and Reimer, 1977). This diagenetic recrystallization has resulted in large (2 to 10 cm long) bladed barite grains oriented perpendicular to bedding (Fig. 9). These individual barite blades are often accompanied by diagenetic bundles of barite blades that diverge slightly upward (Fig. 9). These diagenetic features reach lengths of up to 0.5 m. In the Fig Tree deposits, the few barite beds that have survived diagenetic recrystallization consist predominately of very fine-grained laths of barite (< 1 mm long) oriented parallel to bedding.

The WBO do not contain primary or diagenetic microstructures. Instead, the WBO contain small, lensoidal barite grains which define a strong foliation. This suggests that the WBO barite has been deformed. Deformation microstructures of barite are presently undocumented. For this reason, samples of highly-deformed Paleozoic stratiform barite from the Selwyn Basin were briefly examined for deformation microstructures (samples obtained from W.D. Goodfellow, Geological Survey of Canada). These samples (Plate 22) display bundles of barite blades similar to the diagenetic clusters described by Heinrichs and Reimer (1977) for the South African deposits (Fig. 9). The perimeter zones of these larger grains are dominated by small, optically misoriented, lensoidal barite grains which are elongated parallel to the axial planar foliation (Plate 23). Small misoriented grains are often indicative of dynamic recrystallization for minerals such as quartz and plagioclase (e.g. Bell and Etheridge, 1973; Marshall and Wilson, 1976; White, 1975; and White, 1977). Similarily, these small, misoriented, lensoidal barite grains may indicate dynamic recrystallization in barite. The small, (possibly recrystallized), lensoidal barite grains from the Paleozoic deposits, are remarkably similar to WBO barite (Plate 15). However, the large remnant barite blades are absent in the WBO. This may indicate that deformation has resulted in complete recrystallization of the WBO barite.

The possibility of dynamic recrystallization during barite deformation is tested by a study of barite crystallo-

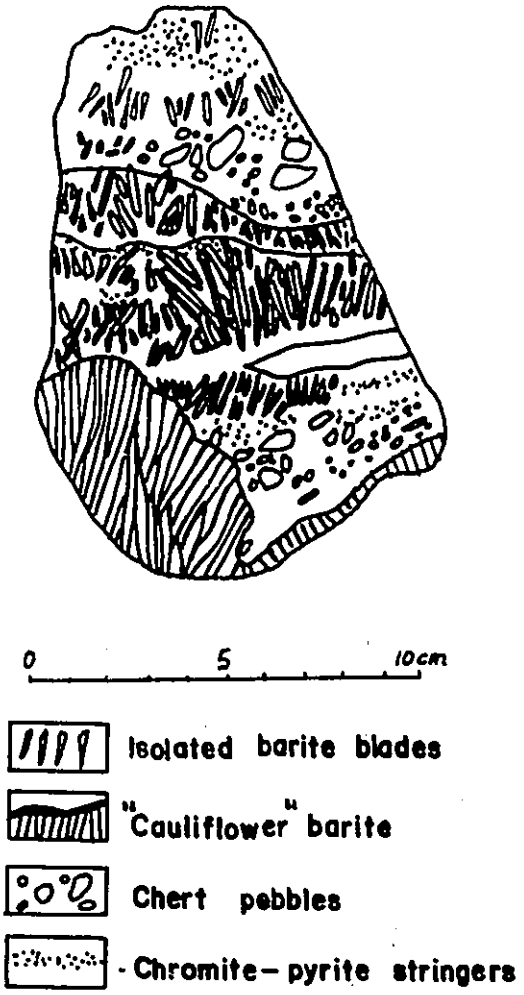

Fig. 9 Diagenetic recrystallization textures of Fig Tree Group barite (after Heinrichs and Reimer, 1977)

graphic preferred orientation (CPO). The results are described in the following section.

4.2.1.2 CRYSTALLOGRAPHIC PREFERRED ORIENTATON (CPO)

A universal stage analysis was carried out on barite and quartz to determine if the grains were crystallographically oriented with respect to the penetrative fabric. The samples were selected from various baritic units at Northern Eagle. The principal vibration axes, X,Y, and Z were measured for barite, and the C-axes were measured for quartz. Each analysis entailed the measurement of approximately 250 grains.

BARITE CPO

A strong and consistent CPO is observed for barite grains in the 3 thin sections analyzed (Plates 24,25,26). The most obvious features of the projected contours are the X and Y point maxima which occur in the foliation plane at right angles to the lineation. This feature is demonstrated in all 3 oriented thin sections. At right angles to these point maxima are great circle concentrations which appear as peripheral rings in all of the X and Y axes projections. Also immediately noticeable is the apparent lack of discrete elements within the CPO for Z axes in any of the thin sec-

tions. Two weaker patterns have also been identified for the X and Y axes: 1) a weak great circle, perpendicular to the lineation, and 2) a weak great circle distribution, parallel to foliation. These weak great circles are best displayed in sample 43B (see Plate 24).

The pattern elements of the barite CPO, particularly the parallel point maxima for X and Y, seem at odds with the orthorhombic crystal structure of barite. This apparent discrepancy is explained if more than 1 crystal axis is preferentially oriented in the same external direction. For the WBC barite, both the X and Y axes are preferentially oriented in a direction perpendicular to lineation and parallel to foliation. In orthorhombic minerals, geometry dictates that the 2 axes perpendicular to the axes of point maximum must be concentrated in a plane perpendicular to that point maximum. Since there are 2 parallel point maxima in the barites measured, all of the axes patterns should display great circle concentrations perpendicular to the point maxima. These great circle concentrations are observed in the X and Y axes patterns, but apparently not in the Z axes patterns. This discrepancy is resolved by plotting only the grains contributing to the point maxima for the X and Y axes (Fig. 10a). Fig. 10a demonstrates that there are corresponding great circle concentrations for the X, Y and Z optical directions, and these great circle concentrations have less angular variability in the X and Y axes patterns, relative to the Z axis.

SAMPLE: B43BL

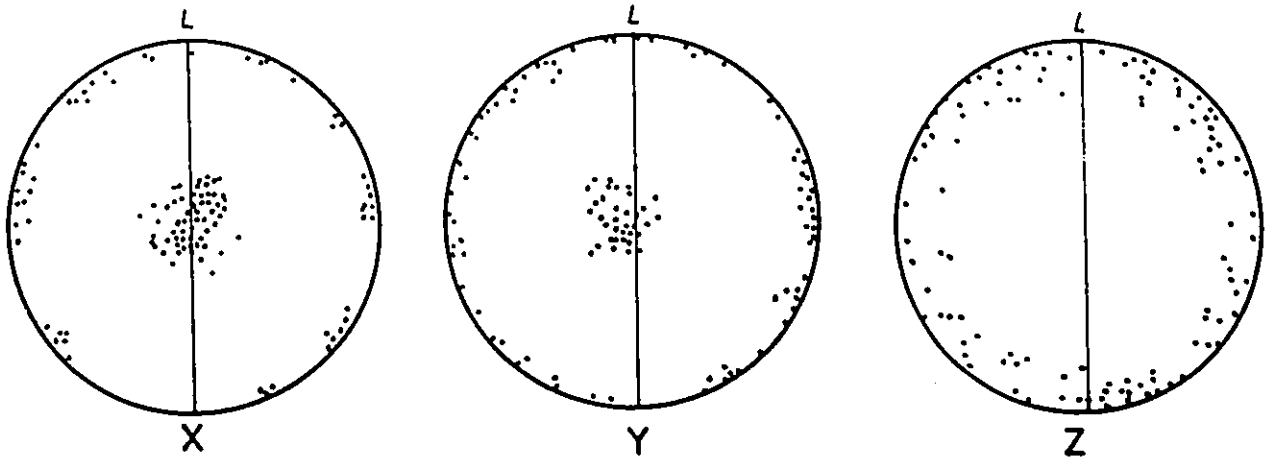

Fig. 10a Equal area projection of X, Y &Z axes of barite crystals in sample B43BL. Only those crystals with X or Y axes within 30° from the vertical point max. are plotted. See text for discussion.

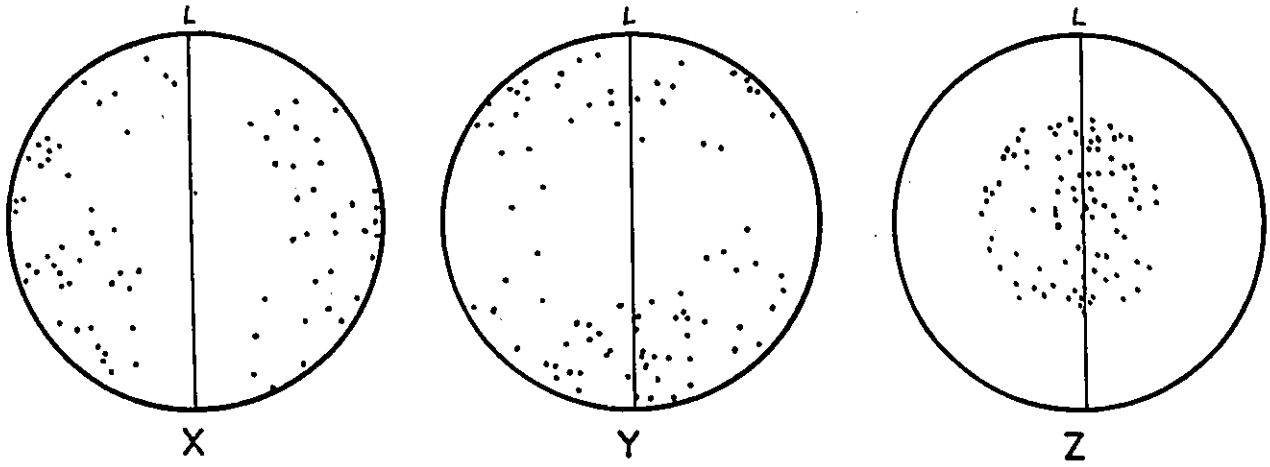

Fig. 10b Equal area projection of X, Y &Z axes of barite crystals in sample B43BL. Those crystals with X or Y axes within 30° from the vertical are not plotted. See text for discussion.

L – lineation Vertical line – foliation

It can also be demonstrated that the minor great circle concentrations for the X and Y axes are independent of the point maxima for X and Y. This is demonstrated in Fig. 10b where barite grains displaying point maxima for the X and Y axes are not plotted. This diagram cannot show the weak great circle concentrations since all of the points within 30° of the X and Y point maxima have been removed. However, this diagram does display point depletions which are orthoginal for the X and Y axes, suggesting that this weaker CPO is independent of the strong point maxima for X and Y. The CPO of barite demonstrates that the mineral axes are preferrentially oriented with respect to the penetrative foliation and lineation. This relationship may be due to any combination of:

a) crystal-plastic deformation of barite during the event which produced the penetrative foliation and lineation, or

b) oriented crystal growth during ductile deformation.

Perhaps the somewhat complex nature of the barite CPO is due to a combination of these crystal orienting processes.

QUARTZ CPO

Quartz also displays a strong and consistent CPO (Plate 27). Quartz C-axis point maxima from all measured sections

display a monoclinic symmetry with respect to the foliation. These maxima are rotated clockwise 35°-45° from the foliation. Samples Q39 and Q44EPL, taken from different baritic units, display additional point maxima located perpendicular to lineation and parallel to foliation. Sample Q23, taken from the deformed porphyry, also displays slightly monoclinic point maxima located at a high angle to lineation and approximately 15° from the foliation plane. Sample Q44EPL also displays a weak great circle concentration located at between 35° to 45° from the foliation.

The quartz C-axis fabrics from the baritic and porphyritic units are only marginally similar to fabrics observed in well documented shear zones (Lister and Williams, 1980). The measured C-axis fabric is distinctly different from the fabric predicted by Lister and Hobbs (1980) for ductile shear zones. The predicted fabric contains a major girdle orthogonal to the flow plane of the kinetic framework of the deformation, and a minor girdle perpendicular to the long axis of the finite strain ellipsoid (Fig. 10c). In most shear zones, this model is represented by an inclined single girdle or point maxima oriented at a steep angle (>75°) to the foliation (Fig. 10c) (Passchier,1983). The C-axis point maxima from the WBO is only inclined by 35° to 45° from the foliation plane. This anomalous orientation suggests that either: a) the conditions during shear were unlike those required by the Lister and Hobbs model, or b) the deformation history is more complex and involves more than just a single episode of

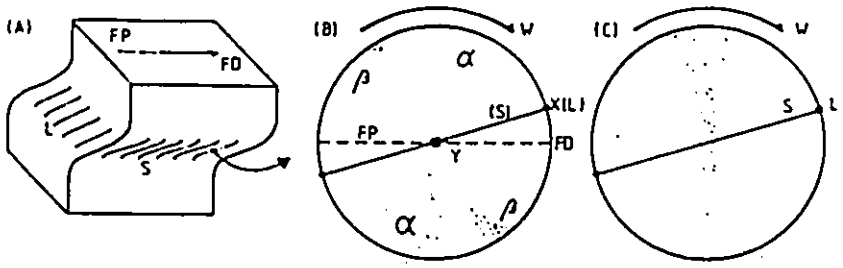

Fig. 10c. Schematic diagram of the geometric relationship of the foliation (S) and lineation (L) developed in a ductile shear zone, and the shape of asymmetric quartz c-axis fabrics from the zone. A. Model of the shear zone. FD = flow direction; FP = flow plane. B. Model c-axis fabric of Lister and Hobbs (1980) possessing internal asymmetry. X and Y represent long and intermediate axes of the finite strain ellipsoid. α = main girdle; β = minor girdles. C. c-axis fabric as usually described from ductile shear zones, with a righthanded external asymmetry with respect to S and L, (after Passchier, 1983).

ductile shear. The failure of the measured C-axis fabric to match the Lister and Hobbs model also precludes a determination of shear sense (Lister and Williams,1980; Paschier,1983). However, the presence of a quartz CPO does suggest that quartz has been deformed, at least partially through crystal-plastic deformation.

4.2.2 DEFORMATION MICROTEXTURES OF PLAGIOCLASE PORPHYRY

The porphyritic unit consists predominately of oligoclase and quartz phenocryts within a highly-foliated matrix of fine-grained quartz, oligoclase, ankerite, biotite, and ilmenite. The relatively large phenocrysts of oligoclase and quartz make the porphyritic unit particularily well suited for microtextural analysis.

4.2.2.1 PENETRATIVE DEFORMATION

The fine-grained matrix of the porphyry has a well-developed foliation and lineation defined primarily by the parallel alignment of biotite and ilmenite grains, and by the elongation of fine-grained quartz (Plates 28 and 29). This foliation anastomoses around the larger phenocrysts of oligoclase and quartz (Plates 28, 29 and 30). The generally euhedral and twinned oligoclase phenocrysts often diplay very fine

oscillatory zoning (Plate 30). Oligoclase phenocrysts commonly appear elongated due to an alignment of long crystal faces (Plate 31), and the preferred orientation of adjacent ankerite and quartz pressure shadows (Plate 32). These pressure shadows indicate that quartz and ankerite were probably precipitated via pressure solution.

The smaller and less common quartz phenocrysts are not single euhedral crystals, as are oligoclase phenocrysts. Instead, the quartz phenocrysts are elongate aggregates of fine-grained interlocking quartz (Plate 33). These elongate aggregates are often deflected around the larger oligoclase phenocrysts (Plate 33).

4.2.2.2 STRAIN GRADIENT AND DYNAMIC RECRYSTALLIZATION

Small (<50 um), polygonal grains of oligoclase commonly cccur along the rim of oligoclase phenocrysts (Plate 34). These small grains display a variable amount of crystallographic misorientation from the host oligoclase grains. Phenocryst boundaries are typically bulging or serrated, with incomplete or attached polygons (Plate 35). In deformed metamorphic rocks of upper-greenschist facies to granulite facies, these small grains are indicative of dynamic recovery and recrystallization (Marshall and Wilson, 1976; Vernon, 1975; White, 1975: Hanmer, 1982). The polygonal grains with small relative misorientations and less distinct boundaries are con-

sidered subgrains, a product of dynamic recovery. Polygonal grains with distinct grain boundaries and relatively large misorientations are considered to be new, dynamically recrystallized grains (Vernon, 1975).

In deformed oligoclase phenocrysts, the subgrains and recrystallized grains are concentrated along grain boundaries subparallel to the foliation (Plate 34). Grain boundaries in pressure shadows generally lack both subgrains and recrystallized grains. Some oligoclase phenocrysts have been partially or totally recrystallized. These totally recrystallized grains are recognized by a preserved deflection in the biotite-ilmenite foliation (Plates 36 and 37). Recrystallized grains are also distinguished from relic grains by their lack of minute inclusions (Plate 37) (Vernon, 1975).

Quartz phenocrysts also contain polygonal grains of variable misorientation. These equally-distributed polygonal grains are an order of magnitude larger than the subgrains and recrystallized grains of oligoclase (Plate 38). Subgrains and new grains of quartz in mylonitic rocks of amphibolite facies metamorphic grade have been attributed to dynamic recovery and recrystallization, respectively (e.g. Bell and Etheridge, 1973; Kerrich et al., 1980).

The extent of recrystallization of both oligoclase and quartz demonstrates a strain gradient at Northern Eagle (see Section 3.4-Shear Zones). Extensive recrystallization has reduced the number and size of phenocrysts in porphyritic units closest to the barite (Plate 9). Porphyrytic units far-

ther from the barite (>15 m) display more, and relatively larger phenocrysts (Plate 9). This strain gradient is also demonstrated by an intensity increase in the biotite and ilmenite foliation, and by the restricted occurrence of ankerite and quartz pressure shadows in porphyritic units closest to the barite. The described microstructures suggests that the porphytitic units within the WBO have been extensively recrystallized, largely through dynamic recrystallization and recovery. The extent of recrystallization demonstrates that a strain gradient, centered on the baritic units exists within the WBO.

4.2.3 CHROMITE AND CHROMIUM-MUSCOVITE

Chromium-muscovite (up to 3.7 Wt% Cr_2O_3) is found within all WBO. At Padre, small chromite grains (< 1mm diameter) are enveloped by lensoidal aggregates of chromium-muscovite (Plate 39). Along the edge of these lenses, the chromium-muscovite is aligned parallel to the foliation. The chromite grains (up to 50 Wt % Cr_2O_3;see Appendix A) have an unusual deep red colour in transmitted light. The edges of the chromite grains are partially replaced by chromium-muscovite grains, (Plate 39). The chromite grains of Plates 39 and 40 demonstrate the various extent of the chromite to chromium-muscovite reaction. In some cases, only remnants of chromite attest to the former presence of a larger chromite grain.

The occurrence of chromite and chromium-muscovite is not unusual in Archean barite deposits. The undeformed and slightly metamorphosed Archean barites from the Fig Tree Group of South Africa contain both chromite and chromium-muscovite (Heinrichs and Reimer, 1977). The chromite grains in these deposits are surrounded by a rim of dark green, fine-grained fuchsite, and a further rim of large fuchsite sheaves. The chromite and chromium-muscovite textures at Padre differ only in the amount of flattening of the chromium-muscovite envelope. This remarkable similarity suggests that chromite and chromium-muscovite mineralization occurred before the end of ductile deformation. Furthermore, the chromite to chromium-muscovite reaction, which involves the addition of Si, K, Al, and OH-, may also have occurred before the end of deformation.

4.2.4 SUMMARY OF DEFORMATION MICROTEXTURES

Deformation microtextures indicate that barite-sulphide mineralization, chromite and chromium-muscovite mineralization, and porphyritic intrusion occurred before the end of ductile deformation. Deformation probably involved a) pressure solution, as demonstrated for pyrite, quartz and ankerite, and b) dynamic recrystallization, as observed in plagioclase, quartz, and possibly barite. Both barite and quartz are crystallographically oriented with respect to the penetrative foliation and lineation.

CHAPTER 5 SULPHUR ISOTOPES

5.1 RESULTS

Barite and pyrite samples from sections across Northern Eagle, Padre, and Kadrey (Figs. 4, 5 and 6), were analysed for their sulphur isotopic composition. The four isotopic profiles of the WBO display some common characteristics (Fig. 12).

In the pyritic-muscovite-schists immediately north and south of the the baritic unit, pyrite typically has an isotopic composition close to 0 o/oo, with values ranging from -5 o/oo to +4o/oo. Within the baritic-unit, pyrite values range from -15 o/oo to -5 o/oo. At Kadrey and Northern Eagle central, the pyrite in the baritic-unit is progressively enriched in 34S towards the northern margin of the baritic unit.

Isotopic profiles for barite generally parallel the pyrite isotopic profiles. The $\Delta^{34}S_{barite-pyrite}$ ranges from 11.5 o/oo to 15.5 o/oo, with the average being 13.4 o/oo, (13 barite-pyrite pairs ananlyzed).

At the sample scale (5 cm^3), the barite concentration is generally more variable than the pyrite concentration (see Fig. 12). The breaks in the isotopic sections of Fig. 12 generally represent a highly-weathered pyrite-muscovite schist, which is unsuitable for sampling.

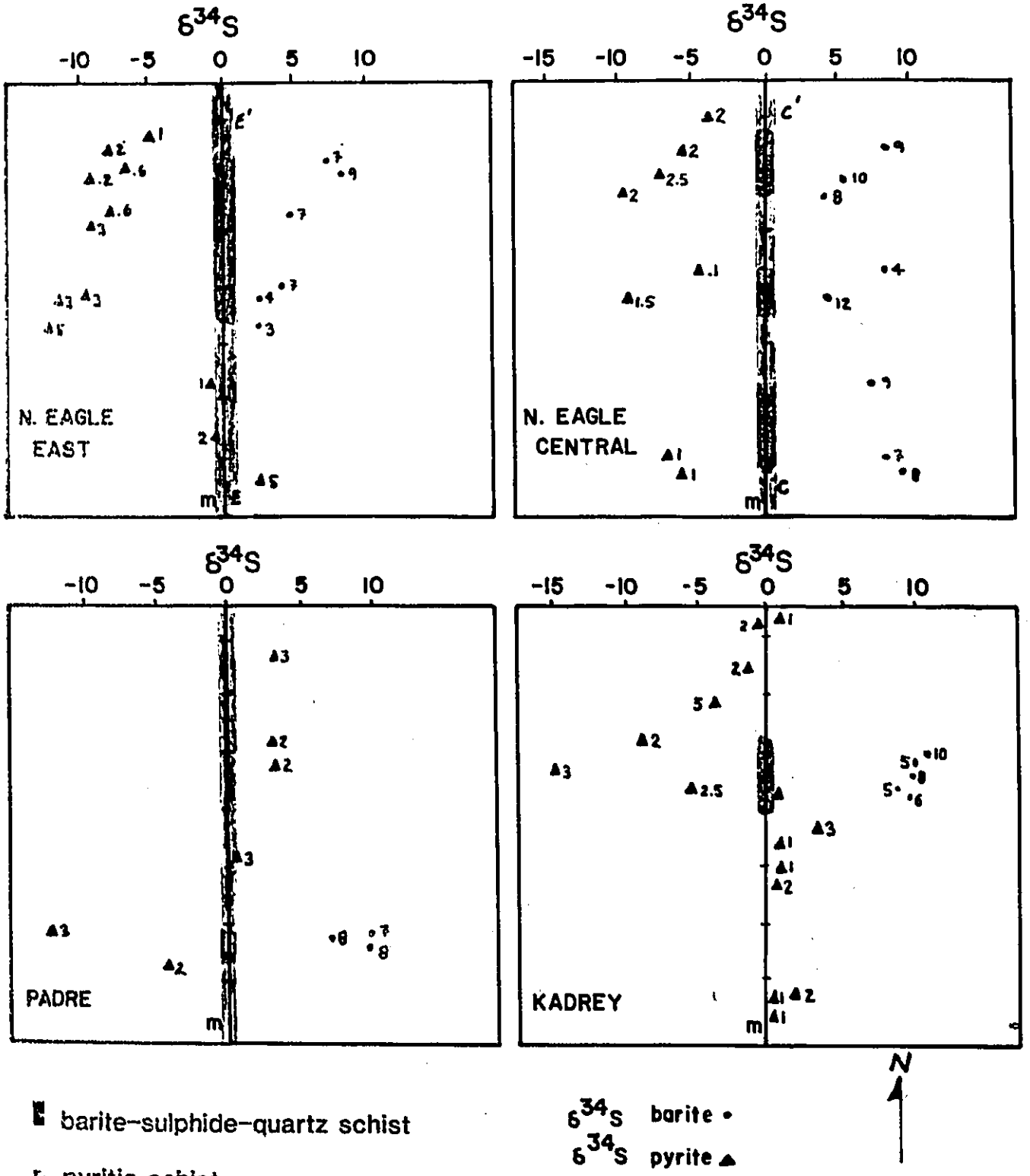

Fig. 12 Isotopic profiles across the WBO. See Fig. 4 & 5 for profile locations. Number beside point is % sulphur from barite or pyrite in sample.

5.2 INTERPRETATION

Sulphur isotopes are often determined in the study of sulphide-sulphate deposits. Useful information can be obtained from: a) the isotopic composition of mineral species, and b) the distribution of these isotopic values within a deposit. If both of these characteristics are primary, then the isotopic data may be used to determine certain physiochemical conditions of mineralization. If either characteristic is not primary, then it is difficult to interpret conditions at the time of mineralization.

The WBO are zones of intense heterogeneous ductile shear. Both the extent, and the precise nature of the deformation are uncertain. Therefore, it is not known if the barite-pyrite sample pairs are in their primary position. The complex structures often associated with ductile shear zones (for example see Hugon, 1984), suggest that the position of the barite-pyrite samples were likely changed during deformation. Therefore, for isotopic interpretation, the position of the sample pairs should not be considered primary.

5.3 INTERPRETATION ASSUMING ISOTOPIC COMPOSITONS ARE PRIMARY

Despite recrystallization and transposition of barite and sulphide during deformation, it is possible that the isotopic compositions of barite and pyrite are primary. If this is the case, the isotopic data might be compared with isotopic data from known barite-sulphide deposits.

The $\Delta^{34}S_{barite-pyrite}$ from the WBO is in general agreement with several known barite-sulphide occurrences of probable hydrothermal origin. These include the Aberfeldy deposit ($\Delta^{34}S_{barite-pyrite}$ = 12 o/oo; Willan and Coleman, 1983), the Big Stubby deposit ($\Delta^{34}S_{barite-pyrite}$ = 15 o/oo; Lambert et al., 1978), and the Kuroko deposits studied by Kajiwara, 1971 ($\Delta^{34}S_{barite-pyrite}$ = 17 o/oo). The mode of formation suggested for some of these hydrothermal stratiform barite-sulphide occurrences involves the mixing of Ba^{2+}-bearing hydrothermal solutions with sulphate-bearing surface waters (e.g. Aberfeldy deposit; Willan and Coleman,1983). This mixing and the resulting sulphate-sulphide mineralization can be complex, particularily if the physical and chemical conditions of the hydrothermal system are temporally or spatially varied (Lusk, 1972).

In some hydrothermal deposits sulphides are thought to be produced through either bacterial or hydrothermal reduction of seawater sulphate. Biogenically produced sulphides can be quite variable in isotopic composition, as

demonstrated for Phanerozoic sulphides (Garrels and Lerman, 1984). This variation is largely dependent on the physical and chemical conditions of the coeval seawater system (Ohmoto and Rye, 1972). It is not known whether a similar biogenic reduction was operating in the Archean. This uncertainty makes it difficult to determine if biogenic reduction was involved in the formation of the WBO. However, the carbonaceous phyllite within the WBO, which is a likely site for biogenically produced sulphides, contains pyrite with isotopic compositions consistently near 0 $^{o}/_{oo}$. This suggests a lack of biogenic sulphate reduction in the formation of the WBO.

The WBO sulphide may have been produced through the high-temperature reduction of seawater sulphate (e.g. Kajiwara, 1971). This process might produce at least a partial isotopic equilibrium between seawater sulphate and hydrothermal sulphides, possibly explaining the relatively constant $^{34}S_{barite-pyrite}$ from the WBO. Furthermore, the variation in isotopic composition of the WBO barite and pyrite is also reasonable under conditions of hydrothermal reduction. Isotopic variation in hydrothermal sulphides and sulphates can be due a) mixing of sulphur species from different sources, b) changing chemical conditions (e.g. pH, fO_2, etc. ; Ohmoto, 1972), and c) partial reduction in a closed sulphate reservoir (Ohmoto and Rye, 1972).

Within the WBO, the isotopic composition of barite and pyrite varies, whereas the $\Delta^{34}S_{barite-pyrite}$ is relatively

constant. This may indicate that the bulk isotopic composition of the mineralizing hydrothermal solution was spatially or temporally varied, assuming that the isotopic values are primary.

5.4 INTERPRETATION ASSUMING ISOTOPIC COMPOSITIONS ARE NOT PRIMARY

It is possible that the isotopic composition of WBO barite and pyrite represents isotopic exchange which occurred subsequent to mineralization. For the WBO, this exchange may have occurred as a result of: a) metamorphism, (up to amphibolite-facies), and/or b) hydrothermal fluid flow related to heterogeneous ductile shear.

The possibility of metamorphic isotopic exchange within barite-sulphide deposits has been investigated at the Asen (Rickard et al., 1979) and Aberfeldy (Willan and Coleman, 1983) deposits. At Asen, Rickard et al. (1979), ruled out the possibility of sulphur isotopic exchange between barite and sulphide during greenschist facies metamorphism. At Aberfeldy, no isotopic exchange occurred between barite-pyrite and sulphide-sulphide pairs (at a <1cm scale) during greenschist to lower-amphibolite facies metamorphism (Willan and Coleman, 1983). In the studies at Asen and Aberfeldy, the possibility of metamorphic reequilibration is tested by plotting the mole sulphur ratios of pyrite-barite pairs against

the sulphur isotopic composition of barite and pyrite. If local re-equilibration occurred during metamorphism, then barite and pyrite from barite-rich samples is expected to be isotopically heavier than barite and pyrite from pyrite-rich samples. More precisely, the isotopic composition of barite and pyrite is expected to be proportional to the mole sulphur ratio of the barite-pyrite sample pair. No such relationship was observed at either Asen or Aberfeldy.

A similar test was carried out on the isotopic data from the WBO. Fig. 13 illustrates the relationship between the isotopic compositon of the WBO barite and pyrite, and the mole sulphur ratio of the barite-pyrite pairs. Isotopically heavier barite and pyrite generally correlate with sample pairs containing a greater fraction of barite sulphur. However, this trend is somewhat uncertain due to: a) the variation in isotopic compositions observed at similar mole sulphur ratios, and b) the obvious exceptions to the observed trend, most notably the pyrite-only values clustered around 0 o/oo.

The general correlation observed in the data of Fig. 13 is consistent with an isotopic model suggesting local isotopic exchange subsequent to mineralization. However, for this model to be valid, it must also be consistent with the aforementioned variance and exceptions.

The observed variance may be just a reflection of the primary variation in isotopic values. Under conditions of the model, (local isotopic exchange subsequent to mineraliza-

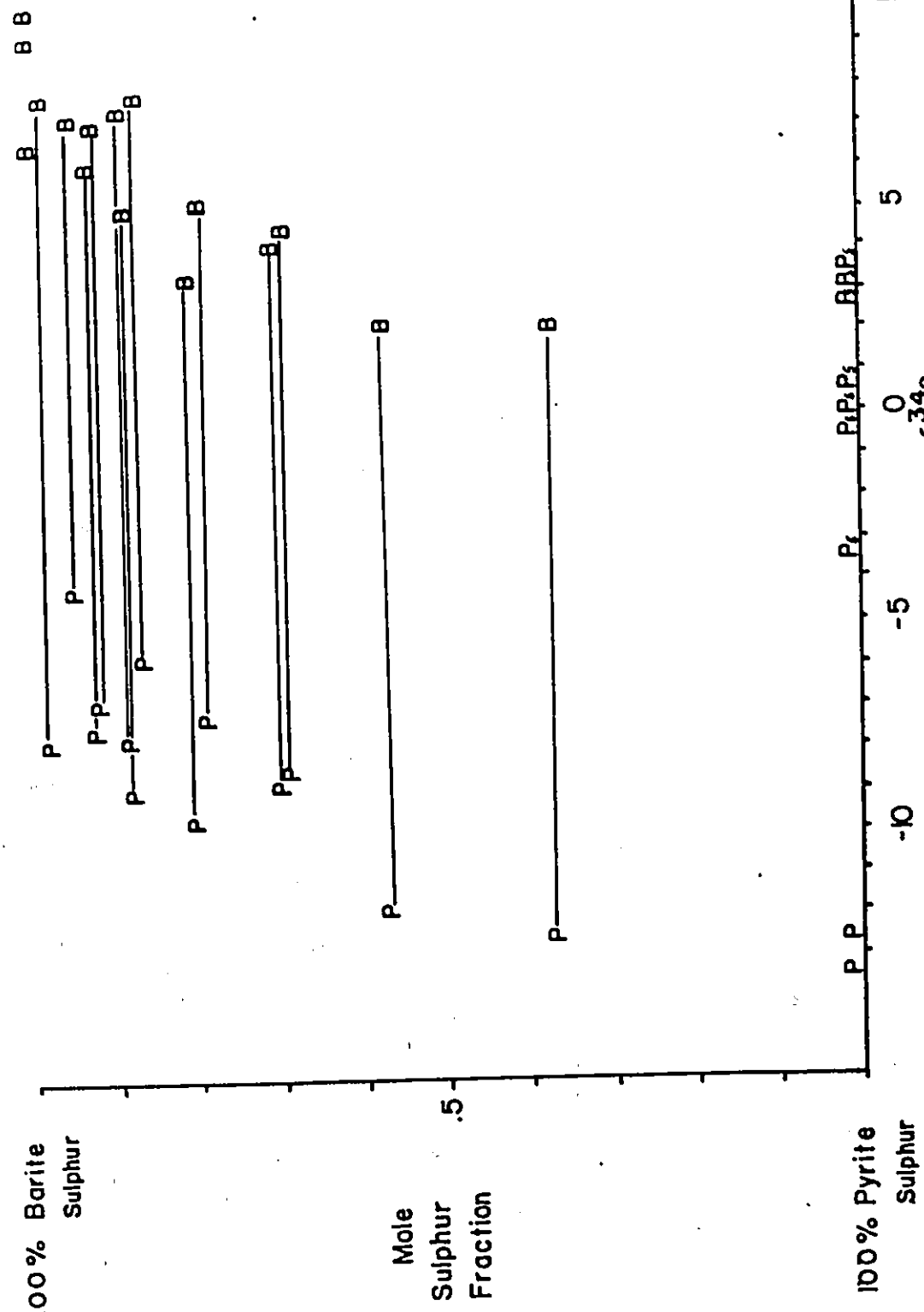

Fig. 13 Plot of isotopic values vs. mole sulphur ratio of sample. Analyses of barite & pyrite from the same sample are joined by a line. (See text for discussion.)

tion), the local primary bulk isotopic compositions would be preserved. Therefore, samples of identical mole sulphur ratios could have different values depending on the original isotopic composition of barite and pyrite.

Furthermore, under conditions of the model, the isotopic variation in samples containing only one sulphur species must be due to differences in primary isotopic composition. This might explain the pyrite isotopic values which are exceptions to the the trend in Fig. 13. Interestingly, all of these pyrite-only samples which have isotopic compositions close to 0 o/oo, occur outside of the baritic unit. Pyrite-only samples from within the baritic unit have isotopic compositions close to -13 o/oo.

Isotopic variance within samples of similar mole sulphur ratios may also be a result of the sample size. Inconsistent isotopic values would result from sample sizes that are larger or smaller than the scale of isotopic exchange. This can be illustrated by a 5 cm^3 sample which contains a layer of pure barite, and a layer of mixed barite and pyrite. If isotopic exchange occurred at a scale smaller than the layering (say 0.5 cm), then the barite and pyrite within the mixed layer would be isotopically altered, whereas the pure barite layer would remain largely unchanged (since it contains no pyrite). An analysis of this sample would produce an average pyrite isotopic composition equal to the pyrite value from the mixed layer. The barite isotopic composition of the sample would be equal to the weighted average of the altered

barite plus the unchanged barite. Consequently, the $\Delta^{34}S_{barite-pyrite}$ would not represent the isotopic exchange present at the smaller scale. For the WBO, the small range of $\Delta^{34}S_{barite-pyrite}$, from 11.2 o/oo to 15 o/oo, suggests that the sample size might be slightly larger than the scale of isotopic exchange (if it occured).

The possibility of metamorphic reequillibration is further tested by a determination of metamorphic temperature based on the isotopic fractionation between barite and pyrite. The average $\Delta^{34}S_{barite-pyrite}$ of 13.4 o/oo indicates an equilibrium temperature of approximately 475° C (Ohmoto and Rye, 1979). This hypothetical temperature is within the limits of amphibolite facies metamorphism (Turner, 1980), and therefore reasonable for the WBO.

Since ductile deformation occurred before and during amphibolite facies metamorphism (see chapter 4-microtextures), it is reasonable to suggest that any changes which might have occurred in isotopic composition are probably due to the simultaneous effects of metamorphism and ductile deformation.

Chemical transformations have been noted in several ductile shear zones (for a review see Beach, 1976). Therefore, it is possible that sulphur isotopic exchange may also occur in ductile shear zones, particularily if sulphur species are put into solution. One means of putting minerals into solution during ductile deformation is pressure solution. This process, which is more likely at lower metamorphic grades

(Kerrich et al., 1977), involves the dissolution of minerals in regions of high stress, and the later redeposition of minerals in regions of stress relief (Pederson, 1980). The en echelon pyrite veins which occur at Northern Eagle (see microtextures section), suggest that pyrite was possibly put into solution via pressure solution during deformation. For isotopic exchange, it is advantageous for another sulphur species, such as sulphate, to be in solution with the aqueous sulphide. Because of the unknown nature of barite deformation mechanisms, it is not clear if barite sulphur was put into solution during deformation. However, isotopic exchange may occur between minerals and hydrothermal solutions, particularily if the minerals are not in chemical equilibrium with the fluid (Cole et al., 1983). Therefore, it is possible that isotopic exchange occurred during metamorphism and ductile deformation.

5.5 Isotopic Summary

Due to heterogeneous ductile shear, the observed positions of barite and pyrite through sections of the WBO are unlikely to be primary. Therefore, only the isotopic compositions are used in interpretation. If the isotopic composition of WBO barite and pyrite is primary, then the relatively constant $\Delta^{34}S_{barite-pyrite}$ (average = 13.4 o/oo), and the low values for pyrite suggest that

sulphide might have been formed by the hydrothermal reduction of sulphate.

The observed isotopic values of barite and pyrite may also represent isotopic exchange which occurred subsequent to mineralization. This exchange may have occurred during deformation and metamorphism.

CHAPTER 6 DISCUSSION AND CONCLUSIONS

6.1 REVIEW OF GEOLOGY AND ISOTOPIC DATA

The WBO are located in dextral heterogeneous ductile shear zones, which occur within metasediments, along the contact between mafic metavolcanics and metasediments. The WBO contain interlayered barite-sulphide-quartz schist, pyrite-muscovite schist, chromium-muscovite schist, carbonaceous phyllite, biotitic metasediment, amphibolitic mafic metavolcanics, and plagioclase-porphyry intrusions. The WBO display a prominent mineral lineation which plunges moderately to the west, and a well-developed, east-west striking, steeply-dipping foliation. En echelon pyrite veins, and quartz-ankerite pressure shadows suggest that strain was partly accomodated by the introduction of pressure solution. The strong CPO of barite and quartz, and the dynamically recrystallized grains of plagioclase, quartz and possibly barite, suggest that strain may have also been accomodated by dislocation creep mechanisms. The metamorphic microtextures of almandine-spessartine garnet and hornblende suggest that ductile deformation occurred before and during peak amphibolite facies metamorphism.

Within the WBO, strain increases towards the barite-sulphide-quartz schist, suggesting that this unit may be central within the shear zones. This may suggest that deformation provided a dilatant zone for barite-pyrite

mineralization. It may also be possible that this unit was a favourable site for ductile deformation, due to the possible ductile nature of barite.

The relationship between the individual barite occurrences is uncertain. The WBO may be sheared fragments of a single larger occurrence, or sheared independent occurrences. Lack of outcrop, and the uncertain extent of ductile deformation preclude this distinction.

The WBO contain strongly isotopically-fractionated barite and pyrite. Pyrite sulphur isotopic values from the barite-sulphide-quartz schist vary from -13 $^{o}/_{oo}$ to -4 $^{o}/_{oo}$, whereas the isotopic composition of pyrite in the associated metasediment is close to 0 $^{o}/_{oo}$, (ranging from -5 $^{o}/_{oo}$ to +3 $^{o}/_{oo}$). $\Delta^{34}S_{barite-pyrite}$ range from 11.2 $^{o}/_{oo}$ to 15 $^{o}/_{oo}$, with the average being 13.4 $^{o}/_{oo}$.

The isotopic composition of barite and pyrite is generally proportional to the mole sulphur ratio of the barite-pyrite sample pair. This relationship, and the pressure solution of pyrite, suggest that isotopic exchange may have occurred during metamorphism and ductile deformation.

6.2 GEOLOGICAL SEQUENCE

From the geology, it is evident that the site of the WBO was the focus of several major geological events. These events probably include barite-sulphide mineralization (in this discussion sulphide refers to pyrite, galena, and sphalerite), porphyritic intrusion, heterogeneous ductile shear, and metamorphism (up to amphibolite facies). A time relationship between these events is discussed below (see also Fig. 11):

a) Plagioclase-porphyritic intrusions are deformed within the WBO, indicating that intrusion occurred before the end of ductile shear.

b) The penetrative fabric in the barite-sulphide-quartz schist, defined by the elongate aggregates of sulphides and lensoidal grains of barite, indicate that barite-sulphide mineralization occurred before the end of ductile shear.

c) The metamorphic microtextures of garnet and hornblende suggest that ductile deformation occurred before and during peak amphibolite facies metamorphism.

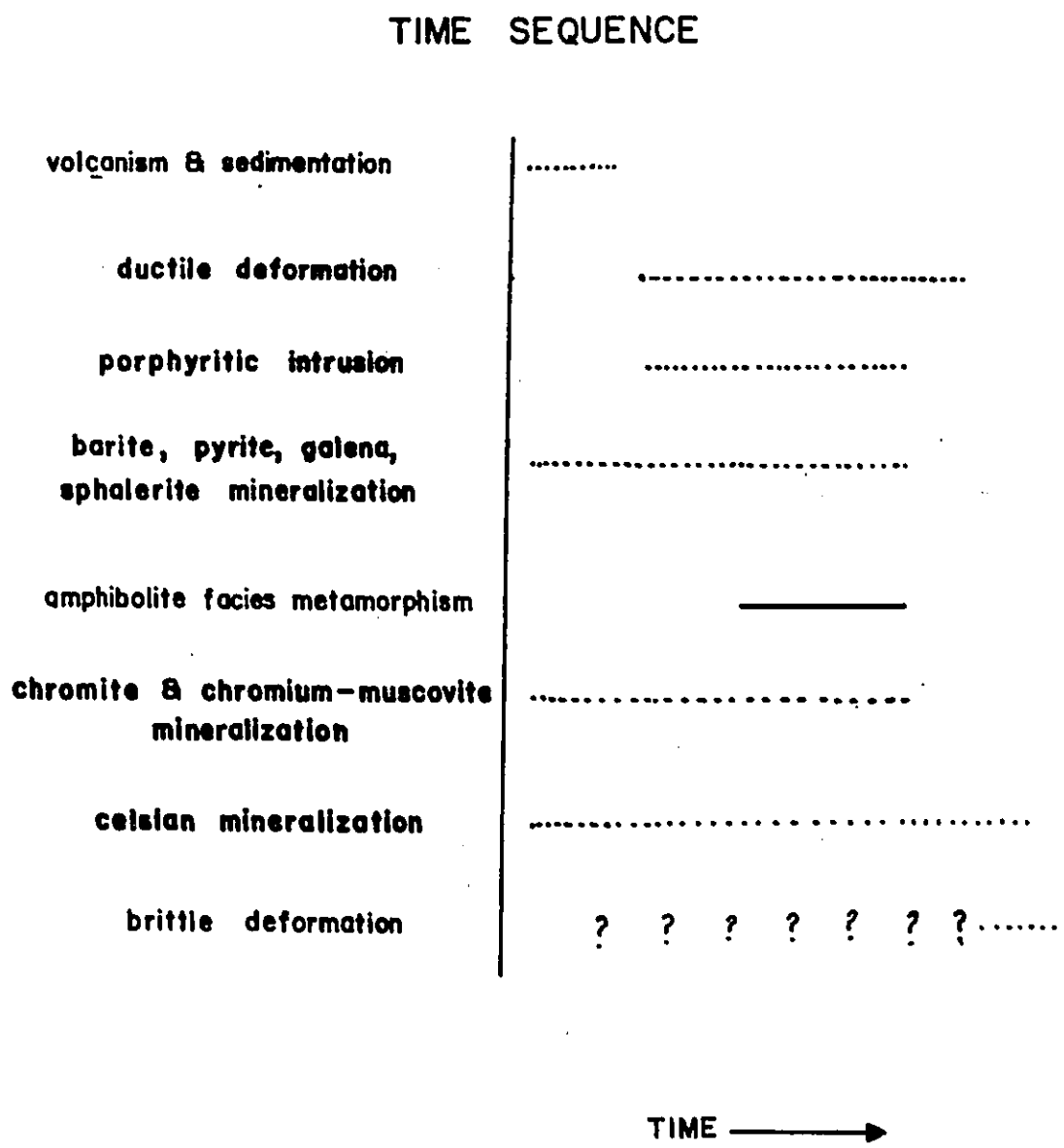

Fig. 11 Proposed timing of geological events for the WBO.

As illustrated in Fig. 11, barite-sulphide mineralization and porphyritic intrusion occurred before the end of ductile shear. Ductile shear at Hemlo was thought to have continued until at least 2670 Ma (Hugon, 1986b). If the timing of deformation at the WBO was similar, then this would suggest that the barite-sulphide mineralization within the WBO is Archean. This is in accord with the Sr isotopic data which suggests an Archean origin for the barite from Hemlo and the WBO (Cameron and Hattori,1985).

For the time period prior to the end of ductile deformation, there is no clear evidence, either geological or isotopic, that indicates any specific sequence involving barite-sulphide mineralization, porphyritic intrusion, and ductile shear. Therefore, it may be possible that barite-sulphide mineralization and porphyritic intrusion occurred before and/or during ductile deformation (see Fig. 11).

This uncertainty in the geological sequence may be due in part to the overprinting effects of progressive deformation and metamorphism. Overprinting may have obscured earlier formed structural, metamorphic and isotopic features. Furthermore, the observed geological and isotopic characteristics may reflect only the most recent significant geological event. Specifically, it is possible that the observed structural fabric is due mainly to the later stages of deformation. Earlier structural fabrics may have been overprinted. Similarily, it is possible that primary isotopic

characteristics were changed during metamorphism and/or deformation.

The uncertainty might also be expected if barite-sulphide mineralization, intrusion and ductile deformation occurred episodically over a protracted period. This idea is partly supported by the protracted period suggested for ductile shear (Hugon, 1986b), and felsic intrusion (Corfu and Muir, 1986), at the Hemlo deposit. Zircon U-Pb ages of deformed felsic dykes at Hemlo (Corfu and Muir, 1986), indicate that shearing was active at least at 2690 Ma, and continued during the emplacement of the 2690 to 2670 Ma felsic dykes (Hugon, 1986). Therefore, it may be possible that at least ductile shear and felsic intrusion also occurred over a protracted period within the WBO.

6.3 POSSIBLE ORIGINS FOR BARITE-SULPHIDE MINERALIZATION

As indicated in the above discussion, it is difficult to determine whether barite-sulphide mineralization is pre- or synkinematic, with respect to the ductile shear. This determination is further hampered by the lack of documented shear zones which contain a similar barite and sulphide mineralogy. Furthermore, there is an uncertainty as to the structural, mineralogical, and isotopic characteristics that might distinguish between pre- and synkinematic barite-sulphide mineralization.

Since the WBO were possibly formed prior to ductile shear, it is possible that the WBO are sheared equivalents of a known barite-sulphide deposit type. The known deposit types include epigenetic vein and replacement deposits (for examples see Guillet, 1963), syngentic deposits formed through hydrothermal-exhalative processes (eg. Fig Tree Group, South Africa; Heinrichs and Reimer, 1977), and deposits created through the baritization of evaporitic gypsum (eg. North Pole Group, Western Australia; Barley et al., 1978). If the the WBO did form prior to deformation, then certain characteristics, in addition to the isotopic data (see Chapter 5), favour a possible hydrothermal-exhalative origin. One important characteristic is the consistent association between carbonaceous phyllite and the WBO. A similar association between carbonaceous matter and barite has been noted in other barite-sulphide deposits of probable exhalative origin (for example see TEA deposit, Selwyn Basin; Lydon et al., 1985). This association may suggest the presence of bacteria during barite-sulphide mineralization.

Carbonaceous matter has also been reported in deposits which are thought to have formed through baritization of evaporitic gypsum (Barley et al., 1978). However, these deposits contain only minor sulphide. Therefore, the significant sulphide content of the WBO does not support an evaporitic origin.

Carbonaceous material has not been reported in vein barite deposits (Guillet, 1963). Furthermore, the gradational barite contacts, and high quartz content of the WBO contrast with the sharp barite contacts, and low quartz content reported in vein barite occurrences (Guillet, 1963).

If barite-sulphide mineralization occurred prior to deformation, then a hydrothermal-exhalative origin would be a strong possibility. However, as indicated previously, the timing of barite-sulphide mineralization relative to ductile shear is uncertain. Furthermore, some of the above characteristics may not be exclusive to hydrothermal-exhalative barite-sulphide deposits. It is possible that some of these characteristics might be found in barite- and sulphide-mineralizing shear zones, particularily if carbonaceous metasediment occurs in the deformed sequence. Therefore, the precise origin of the WBO barite and pyrite is uncertain. Furthermore, geological and isotopic evidence does not unequivocally indicate whether barite-pyrite mineralization occurred before or during ductile shear.

6.4 REGIONAL CONTEXT - DISCUSSION

Geological evidence from the WBO is very much in accord with the tectonic history described by Hugon (1986a,1986b). Hugon suggests that southeast-directed oblique thrusting occurred along a 5 - 10 km wide, east-west trending zone that

extended at least from Heron Bay to approximately 20 km east of Hemlo. Hugon suggests that this regional thrusting created a swarm of discrete shear zones that are akin to C-fabric (domains of simple shear) on a km scale. In such a model, the most intense ductile deformation is expected along the contact between metavolcanics and metasediments (Hugon, 1984). Therefore, the WBO are located in sites which are structurally favourable for ductile deformation. Furthermore, within the WBO, the strain increases towards the baritic units. These factors suggest 2 possibilities: a) shear zone deformation facilitated movement of hydrothermal fluids, producing the barite-sulphide mineralization, or b) deformation occurred subsequent to mineralization and was centered on the site of the WBO because of the possible ductile nature of the barite-sulphide mineralization.

Hugon (1986a, 1986b), suggests that shearing occurred during peak amphibolite facies metamorphism, coeval with the emplacement of the Cedar Lake Pluton. The metamorphic microtextures of the WBO suggest ductile deformation before and during peak amphibolite facies metamortphism.

6.5 HEMLO AND THE WBO - A COMPARISON

The WBO and the Hemlo gold deposit have many similarities. Both occur within the Heron Bay Sequence, near the contact between mafic metavolcanics and felsic metasediments. Similar litholgies include amphibolite, biotite schist, pyrite-sericite schist and barite-sulphide schist. The schistose rocks from the Hemlo deposit contain a more diverse mineral assemblage, which includes microcline, staurolite, kyanite, sillimanite plus numerous ore minerals (Burk et al., 1986; Harris, 1986). The carbonaceous phyllite from the WBO has not been reported at the Hemlo deposit.

Structurally, both occurrences display extensive deformation and recrystallization associated with dextral heterogeneous ductile shear. Furthermore, both occurrences have been metamorphosed to amphibolite facies.

As with the WBO, it is not clear at Hemlo whether barite-sulphide mineralization occurred before or during ductile shear (Burk et al., 1986).

Both Hemlo and the WBO contain highly-fractionated barite and pyrite. Furthermore, the $\Delta^{34}S_{barite-pyrite}$ of 13.4 $^{o}/_{oo}$ determined for the WBO is similar to the values of 12.6 $^{o}/_{oo}$ and 13.2 $^{o}/_{oo}$ reported for the Hemlo deposit (Cameron and Hattori, 1985). This may suggest a) a common mode of origin for these 2 occurrences of barite, or b) similar conditions of metamorphic isotopic exchange.

CONCLUSIONS

The WBO are located in zones of heterogeneous ductile shear. Because of the lack of primary features, the extent of this deformation is uncertain.

The WBO display a prominent mineral lineation which plunges moderately to the west, and a well-developed, east-west striking, steeply-dipping foliation. Deformation probably involved a)pressure solution, as demonstrated for pyrite, quartz and ankerite, and b)dynamic recrystallization, as observed in plagioclase, quartz, and possibly barite. Barite and quartz are crystallographically oriented with respect to the penetrative fabric.

Metamorphic microtextures indicate that ductile deformation occurred before and during peak amphibolite facies metamorphism. Fabrics in the barite-sulphide-quartz schist indicate that barite-pyrite mineralization occurred before the end of ductile deformation. Microtextures in the plagioclase-porphyritic intrusion indicate emplacement prior to the end of ductile deformation. For the time period before the end of ductile deformation, the precise sequence involving barite-pyrite mineralization, intrusion, ductile deformation, and metamorphism is uncertain. Therefore, barite-sulphide mineralization may have occurred either before or during ductile shear. This uncertainty in the sequence may be due in part to the overprinting effects of progressive deformation and metamorphism. This sequential uncertainty may also be due to a

possible complex geological history, which may have involved overlapping and/or discontinuous geological events.

Evidence from the WBO is in accord with Hugons (1986a) tectonic model of regional southeast-directed oblique thrusting, coeval with the emplacement of the Cedar Lake Pluton (2690 Ma.). The WBO are located along a metavolcanic-metasedimentary contact, which is a favourable site for dextral ductile shear under conditions of regional thrusting. Mechanical properties of the barite-pyrite mineralization may have localized ductile shear within the WBO.

The WBO contain strongly isotopically-fractionated barite and pyrite. Pyrite sulphur isotopic values from the baritic unit vary from $-13^{0}/_{00}$ to $-4^{0}/_{00}$, whereas the isotopic composition of pyrite in the associated metasediment is close to $0^{0}/_{00}$ (ranging from $-5^{0}/_{00}$ to $+3^{0}/_{00}$). $\Delta^{34}S_{barite-pyrite}$ range from $11.2^{0}/_{00}$ to $15^{0}/_{00}$, with the average being $13.4^{0}/_{00}$. If the isotopic compositions are primary, then the consistent $\Delta^{34}S_{barite-pyrite}$ suggests at least partial equilibrium between sulphate and sulphide during mineralization. Furthermore, the values of $^{34}S_{barite-pyrite}$, if primary, are in accord with sulphides produced through hydrothermal reduction of sulphate.

The isotopic composition of barite and pyrite is generally proportional to the mole sulphur ratio of the barite-pyrite sample pair. Considering the pressure solution of pyrite and the consistent $\Delta^{34}S_{barite-pyrite}$, this proportionality suggests that isotopic exchange possibly occurred during

metamorphism and deformation of the WBO.

REFERENCES

Archibald, D.A., Glover, J.K., Price, R.A., Farrar, E., and Carmichael, D.M., 1983. Geochronology and tectonic implications of magmatism and metamorphism, southern Kootenay Arc and neighbouring regions, southeastern British Columbia. Part 1: Jurassic to mid-Cretaceous. Can. Jour. Earth Sci., v. 20, 12: 491-504.

Archibald, N.J., Bettenay, L.F., Binns, R.A., Grove, D.I., and Gunthorpe, R.J., 1978. The evolution of Archean greenstone terrains, Eastern Goldfields Province, Western Australia: Precambrian Res., 6: 103-131.

Ashendorf, D., 1980. Are sulphur isotope ratios sufficient to determine the antiquity of sulphate reduction. Origins Life, 10: 325-333.

Barley, M.E., Dunlop, J.S.R, Glover, J.E. and Groves, D.I., 1979. Sedimentary evidence for an Archean shallow-water volcanic-sedimentary facies, Eastern Pilbara Block, Western Australia. Earth and Planet. Sci. Letters, 43: 74-84.

Barnes, H.L., 1979. The solubility and occurrence of non-ore minerals, in Geochemistry of Hydrothermal Ore Deposits, ed. H.L. Barnes, John Wiley and Sons, New York: 461-508.

Bartley, M.W. and Page, T.W., 1957. Unpublished Geological Report on the Hemlo Area, Thunder Bay District, Ontario, for Canadian Pacific Railway Limited; Resident Geologist's Files, Ontario Ministry of Natural Resources, Thunder Bay, Ontario: 17p.

Beach, A., 1976. The interrelations of fluid transport, deformation, geochemistry and heat flow in early Proterozoic shear zones in the Lewissian complex. Philos. Trans. R. Soc. London, A280:569-604.

Bell, T.H. and Etheridge, M.A. 1973: Microstructures of mylonites and their descriptive terminology. Lithos 6 : 337-348.

Bell, T.H., Rubenach, M.J. and Fleming, P.D., 1986. Porphyroblast nucleation, growth and dissolution in regional metamorphic rocks as a function of deformation partitioning during foliation development. J. Metamorphic Geology, 4: 37-67.

Brown, P., Carson, D., Cooper, P., Farr, E., Gibson, J., Harvey, J., Hogg, W. MacIsaac, N., Mackie, B., Nash, W., and Pierce, G., 1985. Golden Giant Joint Venture Properties - Hemlo: p. 58-65 in Gold and Copper-Zinc Metallogeny: Hemlo-Manitouwadge-Winston Lake, Ontario, Canada; A Compendium edited by R.H. McMillan and D.J. Robinson, A Joint Publication of Mineral Deposits Division, Geological Association of Canada, and Geology Division, The Canadian Institute of Mining and Metallurgy, 91p.

Burk, R., Hodgson, C.J., and Quartermain,R.A., 1986. The geological setting of the Teck-Corona Au-Mo-Ba Deposit, Hemlo, Ontario, Canada. Proceedings of Gold 86 Symposium, Toronto, 1986. Editor A.J. Macdonald, Toronto, Canada:311-326.

Carmichael, D.M., 1978. Metamorphic bathozones and bathograds: A measure of the depth of post-metamorphic uplift and erosion on the regional scale. Amer. Jour. Sci., 278:769-797.

Cameron, E.M., 1982. Sulphate and sulphate reduction in early Precambrian oceans. Nature, 296:145-148

Cameron, E.M. and Hattori, K., 1985. The Hemlo gold deposit, Ontario: a geochemical and isotopic study. Geochim. Cosmochim. Acta, 49:2041-2050.

Cameron, E.M., and Hattori, K., 1987. Archean sulphur cycle:evidence from sulphate minerals and isotopically fractionated sulphides in the Superior Province.Isotope Geoscience (In press).

Card, K.D., 1979. Regional geological synthesis, central Superior Province. Geol. Surv. Can. Paper 79-1A:87-90.

Card, K.C. and Ciesielski, A., 1986. Subdivisions of the Superior Province of the Canadian Shield. Geoscience Canada, V13, 1: 5-13.

Catanzero, E.J. and Hanson, G.N., 1971. U-Pb ages for sphene from early Precambrian igneous rocks in Northeastern Minnesota - Northwestern Ontario. Can. Jour. Earth Sci. 8: 1319-1324.

Cole, D.R., Ohmoto, H. and Lasaga, A.C., 1983. Isotopic exchange in mineral-fluid sysytems. 1. Theoretical evaluation of oxygen isotopic exchange accompanying surface reactions and diffusion. Geochimica. Acta., 47: 1681-1693.

Corfu, E. and Muir, T.L., 1986. Preliminary U-Pb ages from the Hemlo area, Northwestern Ontario. Geol. Assoc. Can., Mineral. Assoc. Can., Can. Geophy. Un., Joint Ann. Meet. Abst. Vol.: 59.

Craig J.R., and Kullerud, G., 1968. Sulphide melts in the Cu-Fe-Pb-S system (Abs.). Geol. Soc. America, Spec. Paper 115:39-40.

Currie, K.L., 1980. A contribution to the petrology of the Coldwell Alkaline Complex, Northern Ontario. Geol. Surv. Canada, Bull. 287: 42p.

DeWit, M.J., 1982. Gliding and overthrust nappe tectonics in Barberton Greenstone Belt: J. Struct. Geol., v.4, 2:117-136.

Donelly, T.H., Lambert, I.B., Oehler, D.Z., Hallberg, J.A., Hudson, D.R., Smith, J.W., Bavinton, O.A. and Golding, L., 1977. A reconnaissance study of stable isotope ratios in Archean rocks from the Yilgarn Block, Western Australia. J. Geol. Soc. Aust., 24: 409-420.

Ferry, J.M., and Spear, F.S., 1978. Experimental calibration of the partitioning of Fe and Mg between biotite and garnet. Contrib. Mineral. Petrol., 66:113-117.

Fripp, R.E.P., Donelly, T.H. and Lambert, I.B., 1979. Sulphur isotope results. Geol. Soc. S. Afr. Spec. Publ. 6: 205-208.

Garrels, R.M. and Lerman, A., 1984. Coupling of the sedimentary sulphur and carbon cycles- an improved model. Am. J. Sci., 284: 989-1007.

Ghent, E.D., 1976. Plagioclase-garnet-Al_2SiO_5-quartz: a potential geobarometer-geothermometer. American Mineral., 61:710-714.

Goodwin, A.M., 1977. Archean volcanism in Superior Province, Canadian Shield. Geol. Assoc. Can. Spec. Paper 11.

Guillet, G.R., 1963. Barite in Ontario. Ontario Dept. of Mines, Industrial Mineral Report No. 10: 42 pg.

Hanmer, S.K., 1982. Microstructure and geochemistry of plagioclase and microcline in naturally deformed granites. J. Struct. Geol., 4:197-213.

Hannington, M.D., Scott, S.D., Jonasson, I.R. and Hall, G.E.M., 1986. Sulfur isotopic evidence for local, non-equilibrium mixing during formation of a seafloor polymetallic sulfide deposit: Axial seamount. 1986. Geol. Assoc. Can., Mineral. Assoc. Can., Can. Geophy. Un., Joint Ann. Meet. Abst. Vol. : 77.

Harris, D.C., 1984. Mineralogy of the international Corona and Golden Giant Gold Deposits, Hemlo Area, Ontario. Geol. Assoc. Canada, Prog. with Abst. 9: 71.

Hartman, P., and E. den Tex, 1964. Piezocrystalline fabrics of olivine in theory and nature. in Rock Deformation and Tectonics, Int. Geol. Cong., 22nd., India, 1964. Proc. Sec. 4.: 54-114.

Hattori, K. and Cameron, E.M., 1986. Archean magmatic sulphate. Nature, 319:45-47.

Hattori, K. and Cameron, E.M., 1986. Geochemistry of gold mineralization at Hemlo, 1986. Geol. Assoc. Can., Mineral. Assoc. Can., Can. Geophy. Un., Joint Ann. Meet. Abst. Vol. : 78.

Heinrichs, T.K. and Reimer, T.O., 1977. A sedimentary barite deposit from the Archean Fig Tree Group of the Barberton Mountain Land (South Africa), Econ. Geol., 72: 1426-1421.

Hobbs, B.E., Means, W.D., Williams, P.F., 1976. An Outline of Structural Geology. John Wiley and Sons, New York: 571p.

Holland, H.D., 1984. The Chemical Evolution of the Atmosphere and Oceans, Princeton Univ. Press, Princeton, New Jersey: 582 p.

Hugon, H., 1984. The Hemlo deposit; gold mineralization within a dextral shear zone. Ont. Geol. Surv. Misc. Paper 119:212-216.

Hugon, H., 1986a. The Hemlo ore zone: a highly strained central portion of a large-scale zone of heterogeneous ductile shear. Geol. Assoc. Can., Mineral. Assoc. Can., Can. Geophy. Un., Joint Ann. Meet. Abst. Vol. : 83.

Hugon, H., 1986b. The Hemlo Gold Deposit, Ontario, Canada: A central portion of a large scale, wide zone of Heterogeneous ductile shear.Proceedings of Gold 86 Symposium, Toronto, 1986. Editor A. James Macdonald, Toronto, Canada:379-387.

Ingerson, E., 1938. Summary of an article by Bruno Sander: "Uber Zusammwngange zwischen Teilbewegung und Gefuge in Gesteinen." Rpe. Comm. Structural Petrology, Bull. Nat. Res. Coun.: 23-31.

Kajiwara, Y., 1971. Sulfur isotope study of the Kuroko-ores of the Shakanai No.1 deposits, Akita Prefecture, Japan. Geochemical Journal, 4: 157-181.

Kamb, W.B., 1959b. Theory of preferred orientation developed by crystallization under stress. J. Geology, 67: 153-170.

Kerr, P.F., 1977. Optical Mineralogy. McGraw-Hill Book COmpany, New York.

Kerrich, R., Allison, I., Barnett, R.L., Moss, S. and Starkey, J., 1980. Microstructural and chemical transformations accompanying deformation of granite in a shear zone at Mieville, Switzerland; with implications for stress corrosion cracking and superplastic flow.Contrib. Mineral. Petrol. 73: 221-242.

Kerrich, R., Fyfe, W.S., Gorman,B.E., and Allison, I., 1977. Local modification of rock chemistry by deformation. Contrib. Mineral. Petrol., 65:183-190.

Kiyosu, Y., 1980. Chemical reduction and sulfur-isotope effects of sulfate by organic matter under hydrothermal conditions. Chemical Geology, 30: 47-56.

Knopf, E.B. and Ingerson, E., 1938. Structural Petrology. Geol. Soc. Am. Memoir, 6: 270.

Krogh, T.E. and Turek, A., 1982. Precise U-Pb zircon ages from the Gamitaigama greenstone belt, southern Superior Province. Can. Jour. Earth Sci., 19: 859-867.

Kumazawa, M., 1963. A fundamental thermodynamic theory on non-hydrostatic field and on the stability of mineral orientation and phase equilibrium. Nagoya Univ., J. Earth Sci., 11: 145-217.

Lambert, I.B., Donelly, T.H., Dunlop, J.S.R. and Groves, D.I., 1978. Stable isotopic compositions of early Archean sulphate deposits of probable evaporitic and volcanogenic origins. Nature, 276: 808-810.

Lister, G.S. and Hobbs, B.E., 1980. The simulation of fabric development during plastic deformation, and its application to quartzite: The influence of deformation history. J. Struct. Geol., 2:355-371.

Lister, G.S. and Williams, P.F., 1980. Fabric development in shear zones: Theoretical controls and observed phenomena. J. Struct. Geol., 1: 283-297.

Lowe, D.R. and Knauth, L.P., 1977. Sedimentology of the Onverwacht Group (3.4 billion years), Transvaal, South Africa, and its bearing on the characteristics and evolution of the early earth. Jour. Geology, 85: 699-723.

Lum, H.K., 1973. Petrology of the Eastern Gabbro and associated sulphide mineralization of the Coldwell Alkalic Complex; Ontario. unpublished B. Sc. Thesis, Carleton University, Ottawa Ontario: 69 p.

Lusk, J., 1972. Examination of volcanic-exhalative and biogenic origins for sulfur in the stratiform massive sulfide deposits of New Brunswick. Econ. Geol., 67: 169-183.

Lydon, J.W., Goodfellow, W.D. and Jonasson, I.R., 1985. A general genetic model for stratiform baritic deposits of the Selwyn Basin, Yukon Territory and District of Mackenzie. Geol. Surv. Can. Paper 85-1A: 651-660.

Lydon, J.W., Jonasson, I.R., and Hudson, K.A., 1985. The distribution of gold in the TEA barite deposit, Yukon Territory; in Current Research, Part A, Geol. Surv. Can. Paper 85-1A: 661-667.

Marshall, D.B. and Wilson, C.J.L., 1976. Recrystallization and peristerite formation in albite. Contrib. Mineral. Petrol. 57: 55-69.

Milne, V.G., 1967. Geology of Cirrus Lake-Bamoos Lake area. Ontario Div. Mines, Geol. Rept. 43: 61 p.

Monster, J., Appel, P.W.U., Thode, H.G., Schidlowski, M., Carmichael, C.M. and Bridgwater, D., 1979. Sulphur isotope studies in early Archean sediments from Isua, West Greenland: implications for the antiquity of bacterial sulphate reduction. Geochim. Cosmochim. Acta, 43: 405-413.

Morrison, E.R., 1970. Barium minerals in Rhodesia: Rhodesia Geol. Survey, Min. Resources Ser. 15: 16 p.

Muir, T.L., 1982a. Geology of the Hemlo area, District of Thunder Bay. Ont. Geol. Surv. Rept. 217: 65 p.

Muir, T.L., 1982b. Geology of the Heron Bay area, District of Thunder Bay. Ont. Geol. Surv. Rept. 218: 80 p.

Muir, T.L., 1983. Geology of the Hemlo-Heron Bay Area; p. 230-239 in The Geology of Gold in Ontario, edited by A.C. Colvine, Ontario Geological Survey, Miscellaneous Paper 110: 278 p.

Muir, T.L., 1984. Hemlo Stratigraphic Study; p. 49-52 in Summary of Field Work, 1984, Ontario Geological Survey, edited by John Wood, Owen L. White, R.B. Barlow, and A.C. Colvine, Ont. Geol. Surv. Misc. Paper 119: 309p.

Muir, T.L., 1985. Geology of the Hemlo-Heron Bay Area: p. 30-38 in Gold and Copper-Zinc Metallogeny: Hemlo-Manitouwadge-Winston Lake, Ontario, Canada; A Compendium edited by R.H. McMillan and D.J. Robinson, A Joint Publication of Mineral Deposits Division, Geological Association of Canada, and Geology Division, The Canadian Institute of Mining and Metallurgy: 91p.

Miyashiro, A., 1965. Metamorphism and metamorphic belts. George Allen and Unwin Ltd., London: 492 p.

Newton, R.C., and Haselton, H.T., 1981. Thermodynamics of the garnet-plagioclase-Al_2SiO_5-quartz geobarometer. in Newton, R.C., et al., eds., Thermodynamics of minerals and melts:New York, Springer-Verlag:131-147.

Ohmoto, H., 1972. Systematics of sulfur and carbon isotopes in hydrothermal ore deposits. Econ. Geol., 67:551-578.

Ohmoto, H. and Lasaga, A.C., 1982. Kinetics of reactions between aqueous sulfates and sulfides in hydrothermal systems. Geochim. Cosmochim. Acta, 46: 1727-1745.

Ohmoto, H. and Rye, R.O., 1979. Isotopes of sulfur and carbon. In Geochemistry of Hydrothermal Ore Deposits (ed. H.L. Barnes), pp. 509-567. John Wiley and Sons, New York.

Passchier, C.W., 1983. The reliability of asymmetric c-axis fabrics of quartz to determine sense of vorticity. Tectonophysics, 99: T9-T18.

Patterson, G.C., 1983. Current Activities in the Hemlo Area: p. 237-240 in Summary of Field Work, 1983, by the Ontario Geological Survey, edited by John Wood, Owen L. White, R.B. Barlow, and A.C. Colvine, Ont. Geol. Surv. Misc. Paper 116: 313 p.

Patterson, G.C., 1984. Field Trip Guidebook to the Hemlo Area; Ont. Geol. Surv., Misc. Paper 118: 33p.

Patterson, G.C., 1985. Exploration history and field stop descriptions of the Hemlo area. In: R.H. McMillan and D.J. Robinson (editors), Gold and Copper-Zinc Metallogeny, Hemlo-Manitouwadge-Winston Lake, Ontario, Canada, Geol. Assoc. Can. and Can. Inst. Min. Metall.: 66-86.

Pedersen, F.D., 1980. Remobilization of the massive sulfide ore of the Black Angle MIne, Central West Greenland, Econ. Geol., 73: 1022-1041.

Percival, J.A. and Card, K.D., 1985. Archean crust as revealed in the Kapuskasing uplift, Superior province, Canada. Geology, 11:323-326.

Perry, E.C. Jr, Monster, J. and Reimer, T., 1971. Sulfur isotopes in Swaziland system barites and the evolution of the earth's atmosphere. Science, 171: 1015-1016.

Poulsen, K.H., Borradaile, G.J., and Kehlenbeck,M.M., 1980. An inverted Archean succession at Rainy Lake, Ontario: Can. Jour. Earth Sci., 17:1358-1369.

Prince, I.A. and Hanson, G.N., 1972. Rb-Sr isochron ages for the Giants Range Granite, Northeastern Minnesota, IN: Studies in Mineralogy and Precambrian geology. Geol. Soc. Amer. Mem. 135: 217-224.

Puskas, F.P., 1967a. Geology of the Port Coldwell Area. Ontario Dept. Mines, Open File Report 5014.

Quartermain, R., 1985. road guide to the geology of the Teck-Corona mine at Hemlo, Ontario. In: R.H. McMillan and D.J. Robinson (editors), Gold and Copper-Zinc Metallogeny, Hemlo-Manitouwadge-Winston Lake, Ontario, Canada, Geol. Assoc. Can. and Can. Inst. Min. Metall.: 39-46.

Radhakrishna, B.P., and Vasudev, V.N., 1977. The Early Precambrian of the Southern Indian Shield. Geol. Soc. India, vol. 18, no. 10: 525-541.

Ramsay, J.G., 1980. Shear zone geometry: a review. J. Struct. Geol., 4:69-79.

Rickard, D.T., Zweifel, H. and Donelly, T.H., 1979. Sulphur isotope systematics in the Asen pyrite-barite deposits, Skellefte district, Sweden. Econ. Geol., 74: 1060-1068.

Reimer, T.O., 1980. Archean sedimentary baryte deposits of the Swaziland supergroup (Barberton Mountain Land, South Africa). Precambrian Res., 12: 393-410.

Roach, D.E., Cameron, E.M., Hattori, K., 1985. Banded barite occurences west of Hemlo. Current Activities Forum, 1985, Program with abstracts; Geol. Surv. Canada Paper 85-8.

Roach, D.E., Cameron, E.M., Hattori, K., 1986. Geology and geochemistry of baritic bodies west of Hemlo. Geol. Assoc. Can., Mineral. Assoc. Can., Can. Geophy. Un., Joint Ann. Meet. Abst. Vol.: 119-120.

Russel, M.J., Hall, A.J., Willan, R.C.R., Allison, I., Anderton, R., Bowes, G., 1984. On the origin of the Aberfeldy celsian +baryte+base-metal deposits, Scotland; in Prospecting in areas of glaciated terrains; for 6th. international symposium organized by the Institue of Mining and Metallurgy, Glasgow, Scotland, 1984: 159-170.

Sakai, C., Banno, S., Toriumi, M. and Higashino, T., 1985. Growth history of garnet in pelitic schists of the Sanbagawa metamorphic terrain in central Shikoku. Lithos, 18: 81-95.

Sakai, H., Osaki, S. and Tsukagishi, 1970. Sulfur and oxygen isotopic geochemistry of sulfate in the black ore deposits of Japan. Geochemical Journal, 4: 27-39.

Sander, B., 1911. Uber Zusammenhange Zwischen Teilbewegung und Gefuge in Gesteinen. Tschermaks Mineral. Petrogr. Mitt., 30: 381-384.

Sangster, D.F., 1968. Relative sulphur isotope abundances of ancient sea and stratabound deposits. Geol. Assoc. Can. Proc., 19: 79-91.

Sasaki, A. and Kajiwara, Y. 1971. Evidence of isotopic exchange between seawater sulfate and some syngenetic sulfide ores. Soc. Mining Geol. Japan, Spec. Issue 3: 289-294.

Schidlowski, M., 1979. Antiquity and evolutionary status of bacterial sulfate reduction: sulfur isotope evidence. Origins Life, 9: 299-311.

Skyring, G.W. and Donelly, T.H., 1982. Precambrian sulfur isotopes and a possible role for sulfite in the evolution of biological sulfate reduction. Precambrian Res., 17: 41-61.

Smith, J.W., Young, N.B., and Lawlor, D.L., 1964. Direct determination of sulphur forms in Green Riveroil shale. Anal. Chem., 36:618-622.

Starkey, J., 1977. The contouring of orientation data represented in spherical projection. Can. J. Earth Sci. , 14: 268-277.

Stockwell, C.H., McGlynn, J.C., Emslie, R.F., Sanford, B.V., Norris, A.W., Donaldson, J.a., Fahrig, W.f. and Currie, K.L. (1970). Geology of the Canadian shield. In Geology and Economic Minerals of Canada, ed. R.J.W. Douglas, Geol. Surv. Canada, Rept. 1:43-150.

Thompson, J.E., 1931. Geology of the Heron Bay Area, District of Thunder Bay; Ontario Department of Mines, V40, Part 2,43p. Accompanied by Map Number 40d, scale 1 inch to 1.5 mile.

Thorpe, R.I., 1979. A sedimentary barite deposit from the the Archean Fig Tree group of the Barberton Mountain Land (South Africa)-a discussion. Econ. Geol. 74: 700-702.

Turek, A., Smith, P.E. and Van Schmus, W.R., 1982. Rb-Sr and U-Pb ages of volcanism and granite emplacement in the Michipicoten belt- Wawa, Ontario. Can. J. Earth Sci., 19: 1608-1626.

Turner, F.J., 1981. Metamorphic petrology:mineralogical, field, and tectonic aspects. McGraw-Hill International Series in the Earth and Planetary Sciences, Hemisphere Publishing Corporation: 524 p.

Valliant, R., Guthrie, A., Bradbrook, C., Motzok, A., McIlveen, D., Kent, J., MacMillan, G., Skrecky, G., Wingfield, T., and Sheehan, D.G.. 1985. Field Guide to Geological Setting of Lac Minerals Limited Pyritic Gold Oredbodies, Hemlo, Ontario: p. 47-57 in Gold and Copper-Zinc Metallogeny: Hemlo-Manitouwadge-Winston Lake, Ontario, Canada; A Compendium edited by R.H. McMillan and D.J. Robinson, A Joint Publication of Mineral Deposits Division, Geological Association of Canada, and Geology Division, The Canadian Institute of Mining and Metallurgy, 91p.

Vernon, R.H., 1975. Deformation and recrystallization of a plagioclase grain. American Mineral., 60: 884-888.

Vinogradov. V.I., Reimer, T.O., Leites, A.M. and Smelov, S.B., 1976. The oldest sulfates in the Archean formations of the South African and the Aldan Shields, and the evolution of the earth's oxygen atmosphere. Translated from Litologiya i Poleznye Iskopaemye, 4 : 12-27.

Walford, P., Stephens, J., Skrecky, G., and Barnett, R., 1986. The geology of the "A" zone, Page-Williams Mine, Hemlo, Ontario Canada. Proceedings of Gold 86 Symposium, Toronto, 1986. Editor A. James Macdonald:p.362-378.

Westgate, L.M. and Anderson, T.F., 1982. Extraction of various forms of sulfur from coal and shale for stable sulfur isotope analysis. Anal. Chem., 54: 2136-2139.

White, S., 1975. Tectonic deformation and recrystallization of oligoclase. Contrib. Mineral. Petrol., 50: 287-304.

White, S., 1977. Geological significance of recovery and recrystallization processes in quartz. Tectonophysics, 39:143-170.

Willan, R.C.R. and Coleman, M.L., 1983. Sulphur isotope study of the Aberfeldy barite, zinc, lead deposit and minor sulfide mineralization in the Dalradian metamorphic terrain, Scotland. Econ. Geol., 78: 1619-1656.

Williams, P.J., Tomkinson, M.J. and Cattell, A.C., 1985. Petrology and deformation of metamorphosed volcanic-exhalative sediments in the Gairloch Schist Belt, N.W. Scotland. Minerala. Deposita 20: 320-308.

PLATE 1 Biotitic metasiltstone with possible graded beds (gb) indicating stratigraphic tops to the north. Note the boudinaged quartz-rich unit. End of pen for scale. (From metasediments north of Kadrey barite occurrence.)

PLATE 2 Strongly-foliated quartz-pyrite-muscovite schist (QPMS), and barite-sulphide-quartz schist (BSQS) from Northern Eagle barite occurrence.


plate
1


plate
2

PLATE 3 Pyrite-sphalerite-galena (PSGL) aggregates defining a lineation on the foliation surface of barite-sulphide-quartz schist at Northern Eagle.

PLATE 4 Rootless, isoclinal folds of argillaceous metasediment (A) within pyrite-muscovite schist at Padre barite occurrence.

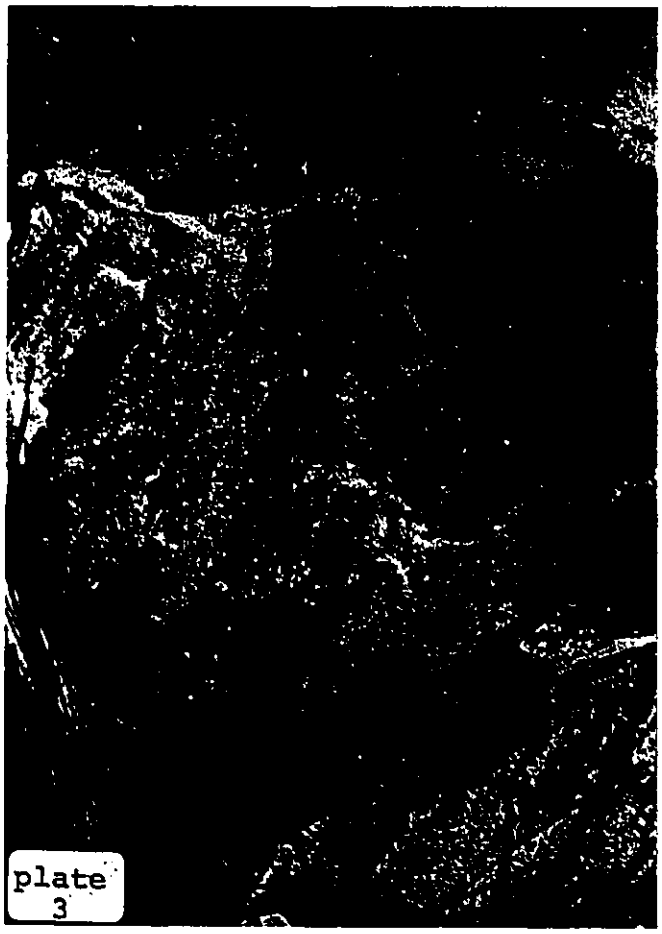
plate
3

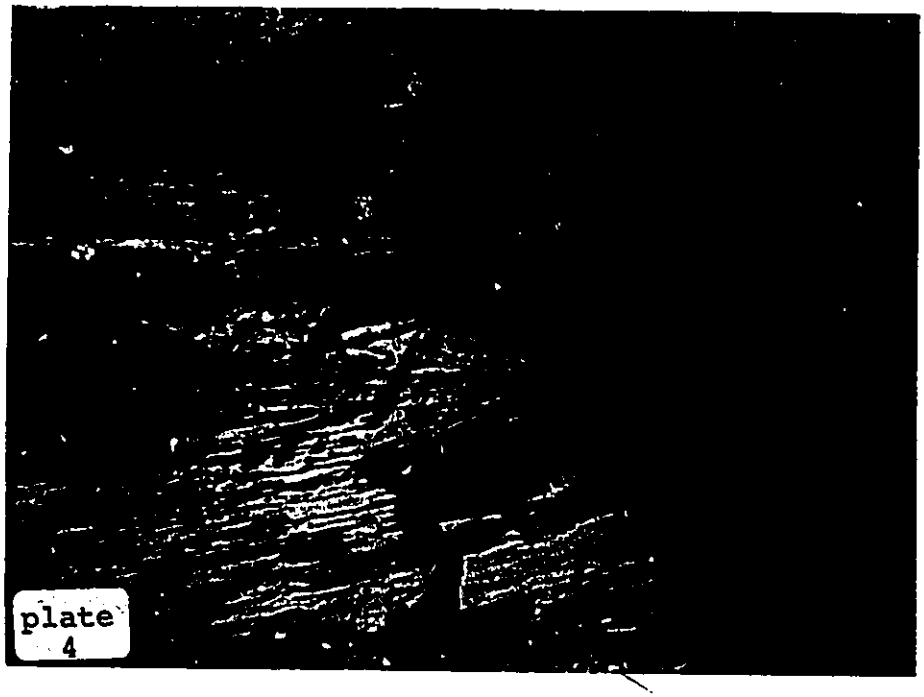
plate
4

PLATE 5 Folded quartz-rich layers (QL) within chromium-muscovite schist at Padre.

PLATE 6 Chevron folding in quartz-pyrite-muscovite schist from just north of the barite mineralization at Northern Eagle. Pencil in center of photo points north.

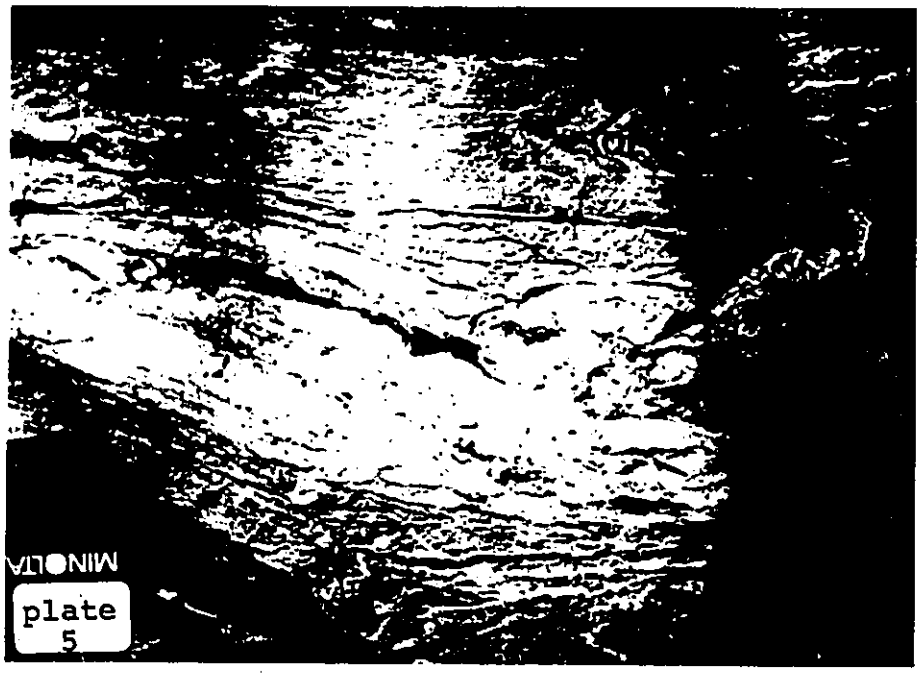
MINOLTA
plate
5

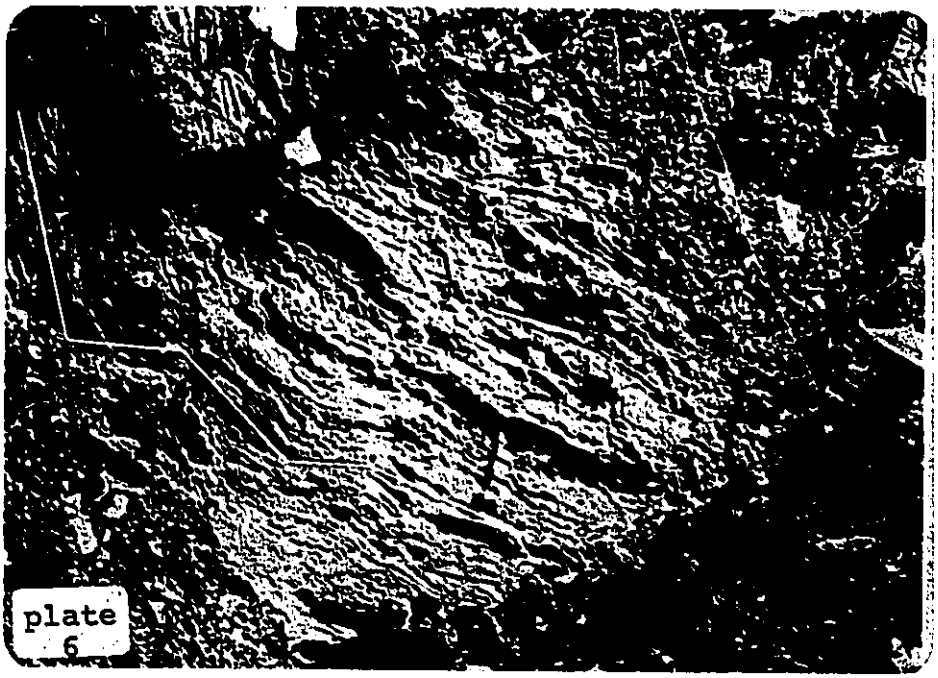
plate
6

PLATE 7 Quartz-vein (q) from echelon set within biotitic metasiltstone north of barite mineralization at Northern Eagle. (North is top of photo). Note the rotated foliation adjacent to the quartz vein.

PLATE 8 Curved foliation in amphibolite (AM), approximately 50 m south of Padre barite mineralization. This may represent a fabric associated with dextral shear.


plate
7

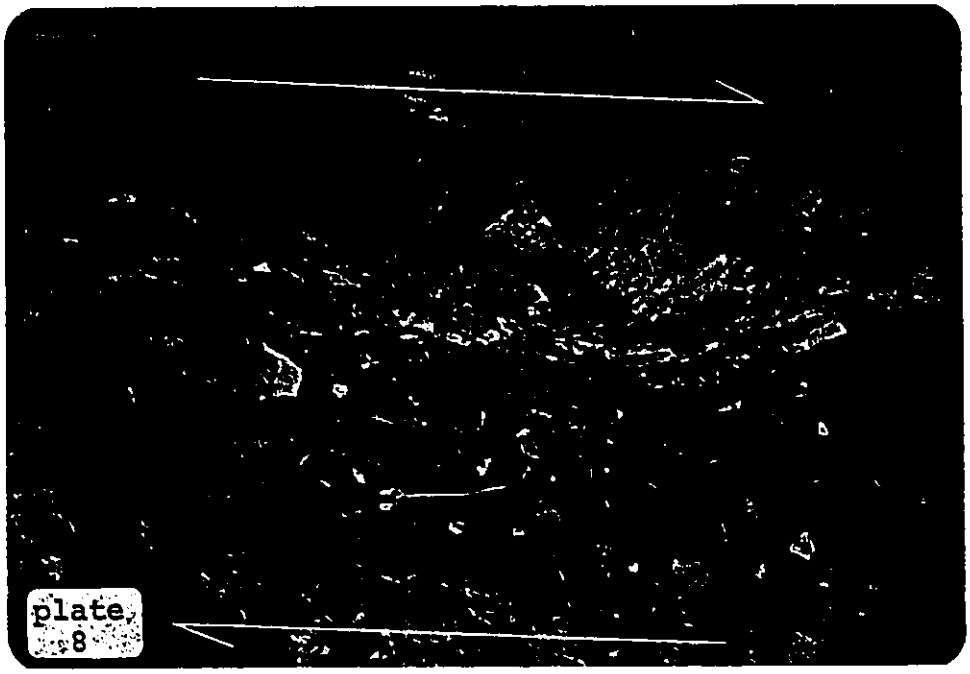
plate
8

PLATE 9 Samples of plagioclase-porphyrytic intrusion demonstrating strain gradient at Northern Eagle. Numbers above each sample are distance (in metres) from the barite-sulphide-quartz schist. Note the decreased volume ratio of phenocrysts/matrix, and the smaller phenocryst size in units closest to the barite mineralization.

PLATE 10 Photomicrograph of hornblende (H) overgrowing a foliation defined by elongate pyrrhotite (opaque) and biotite (B). Sample from just south of barite mineralization at Northern Eagle. Note the random orientation of hornblende crystals. (Single polarizer, width of photo is 6 mm).

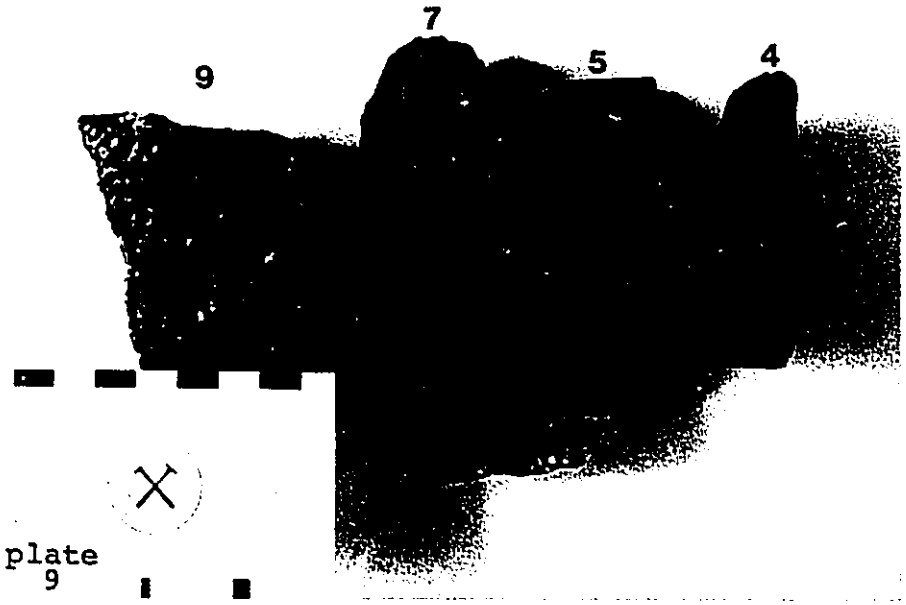
9
7
5
4
plate
9

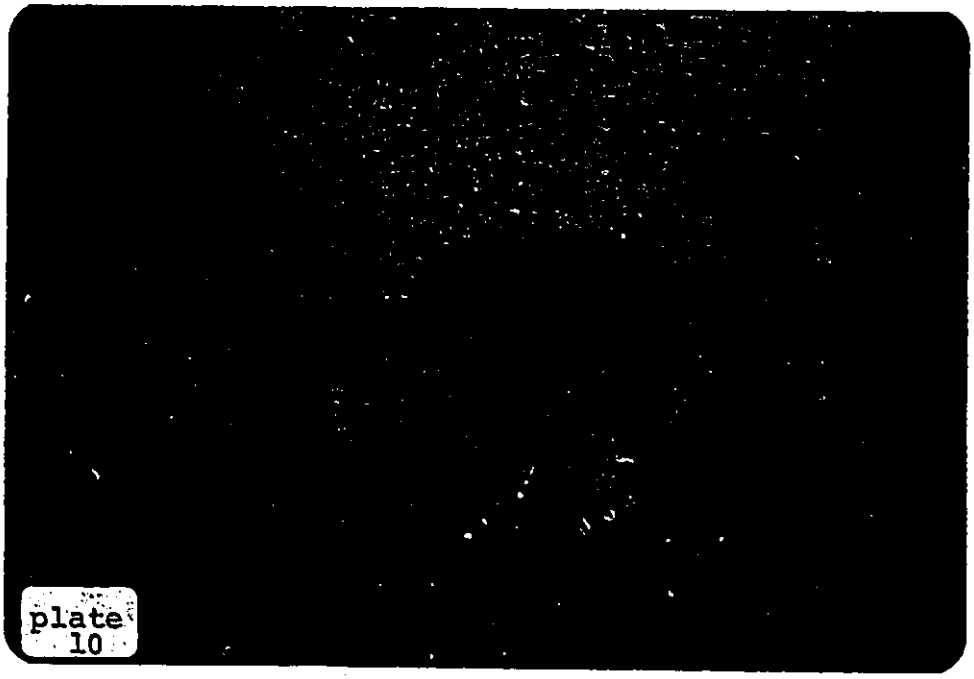
plate
10

PLATE 11 Photomicrograph of hornblende (H) in amphibolite from Northern Eagle. Note the dual mode of occurrence. Some hornblende crystals are randomly oriented, whereas others parallel the pyrrhotite (opaque) foliation. (Single polarizer, plane light, width of photo is 3 mm.)

PLATE 12 Photomicrograph of garnet (G) with pyrite (P) and elongate pyrrhotite (Po) inclusions. Note that sulphide inclusions are more elongate than independent sulphide grains. (Sample from biotitic metasiltstone north of Northern Eagle.) (Reflected light, single polarizer, width of photograph is 6 mm).

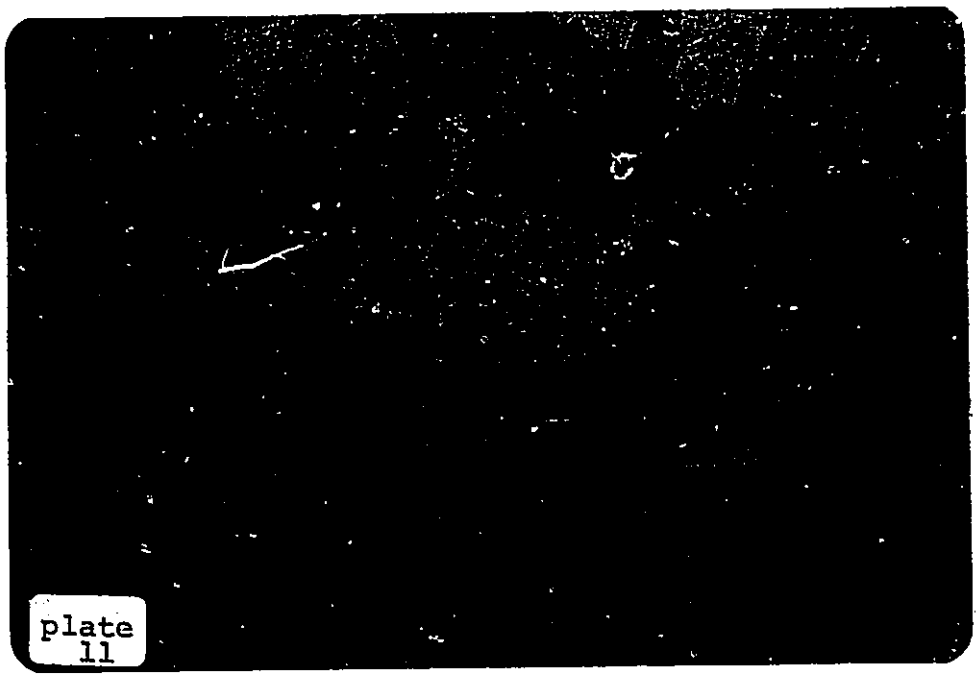
plate
11

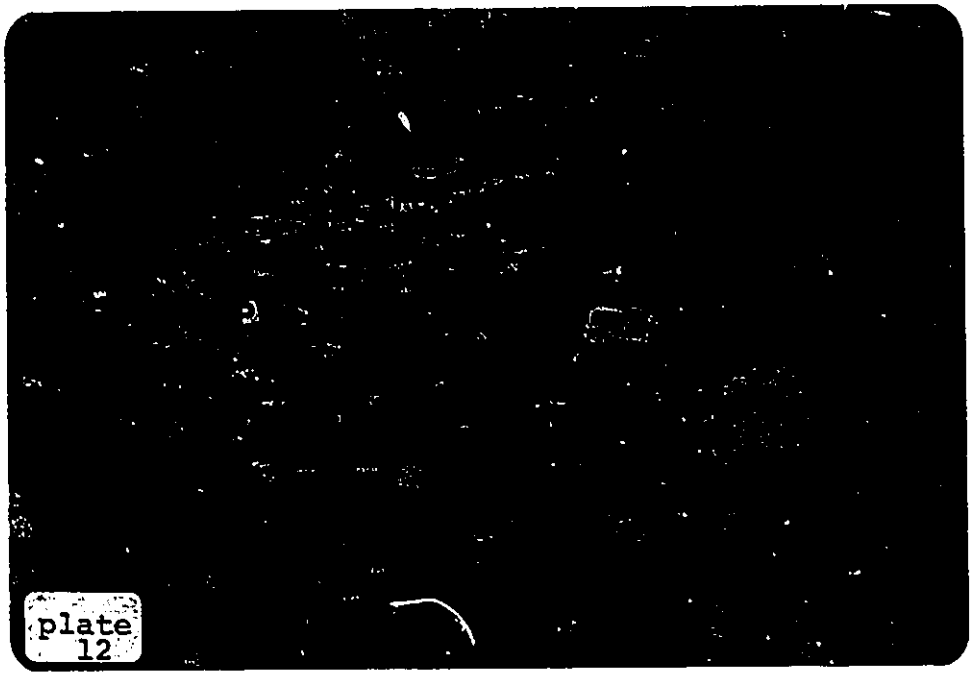
plate
12

PLATE 13 Photomicrograph of garnet (G) within biotitic metasiltstone. Note the irregular crystal boundaries at high angles to the foliation. (single polarizer, width of photo is 3 mm).

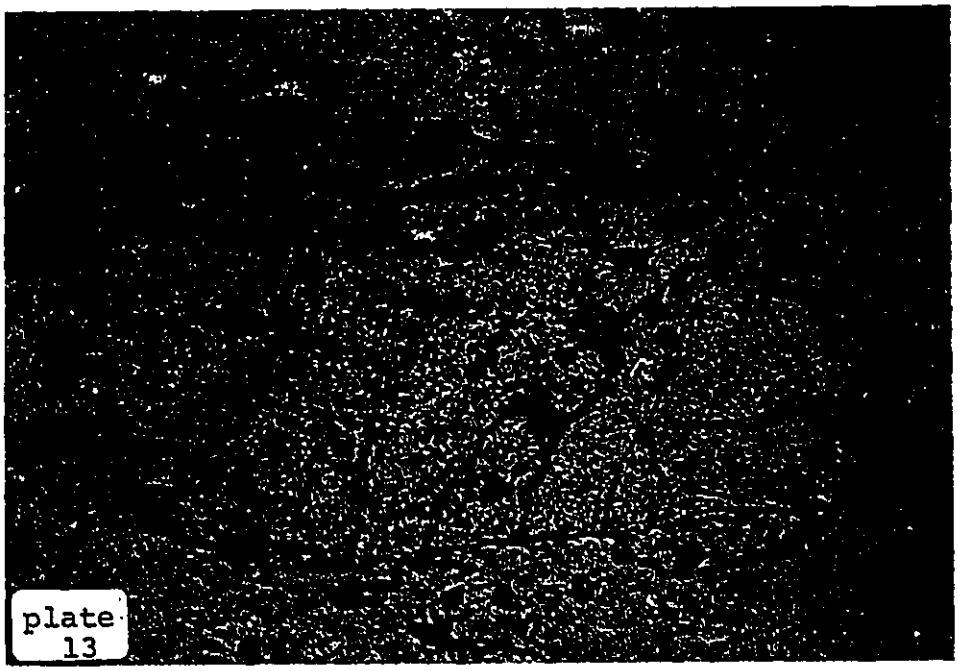
plate
13

PLATE 14 Photomicrograph of elongate barite (B) and quartz (Q) from barite-sulphide-quartz schist at Northern Eagle. Note the concave boundaries in barite, and the triple junctions between quartz grains. (Crossed polars, width of photo is 3 mm).

PLATE 15 Photomicrograph of sulphide aggregate from barite-sulphide-quartz schist at Northern Eagle. Note the euhedral pyrite (P), and anhedral galena (G) and sphalerite (S). (Reflected light, width of photo is 3 mm).


plate
14


plate
15

PLATE 16 En echelon sulphide veins in pyrite-muscovite schist at Northern Eagle. Note the wide, possibly folded termination of the rightmost vien.

PLATE 17 Photomicrograph of tremolite (Tr) oriented subparallel to the barite-sulphide foliation. Sample from barite-sulphide-quartz schist at Padre. (Crossed polars, width of photo is 3 mm).

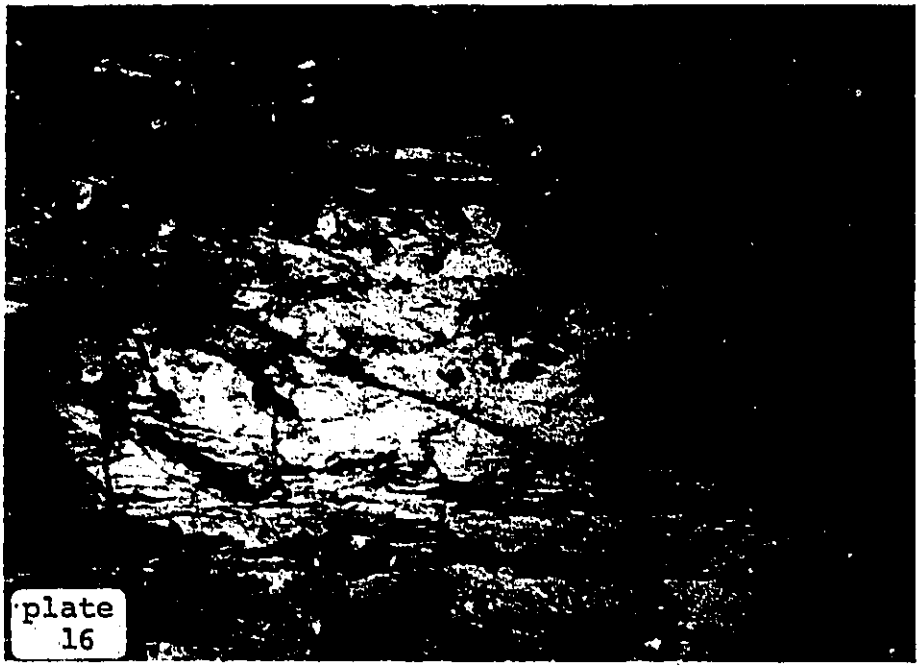
plate
16

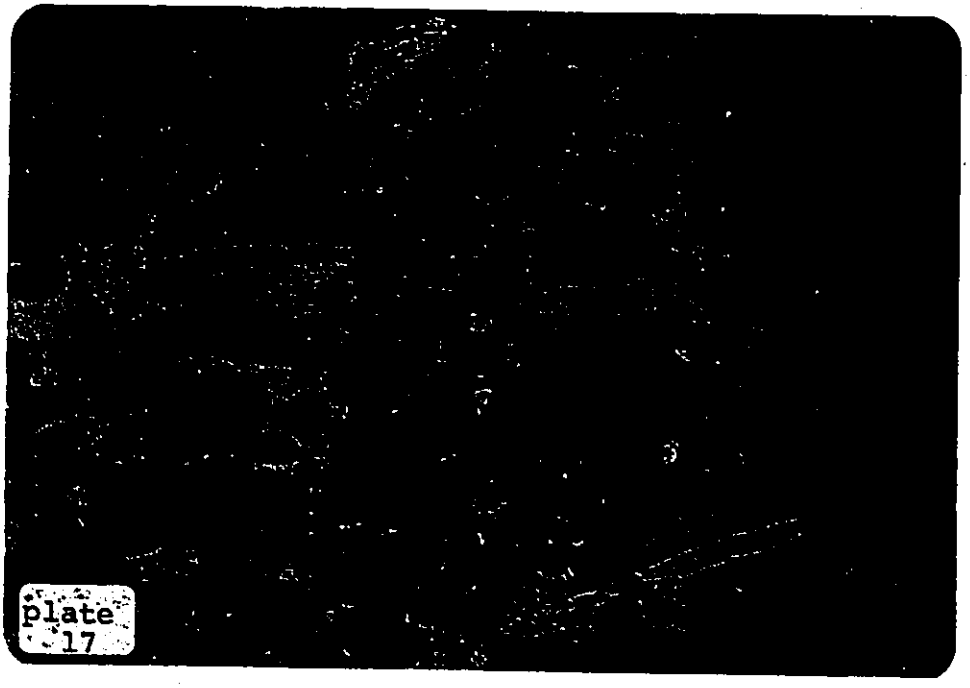
plate
17

PLATE 18 Photomicrograph of lensoidal celsian (C), oriented parallel to elongate barite foliation. (Crossed polars, width of photo is 3 mm).

PLATE 19 Photomicrograph of folded sulphide aggregate within barite-sulphide-quartz schist at Northern Eagle. (Crossed polars, width of photo is 3 mm).

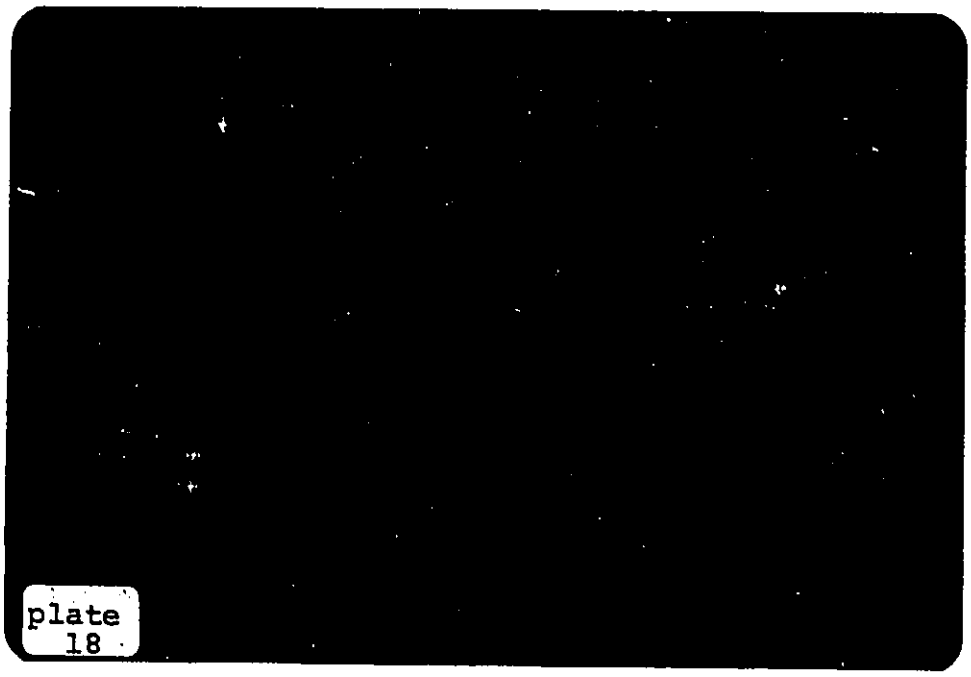
plate
18

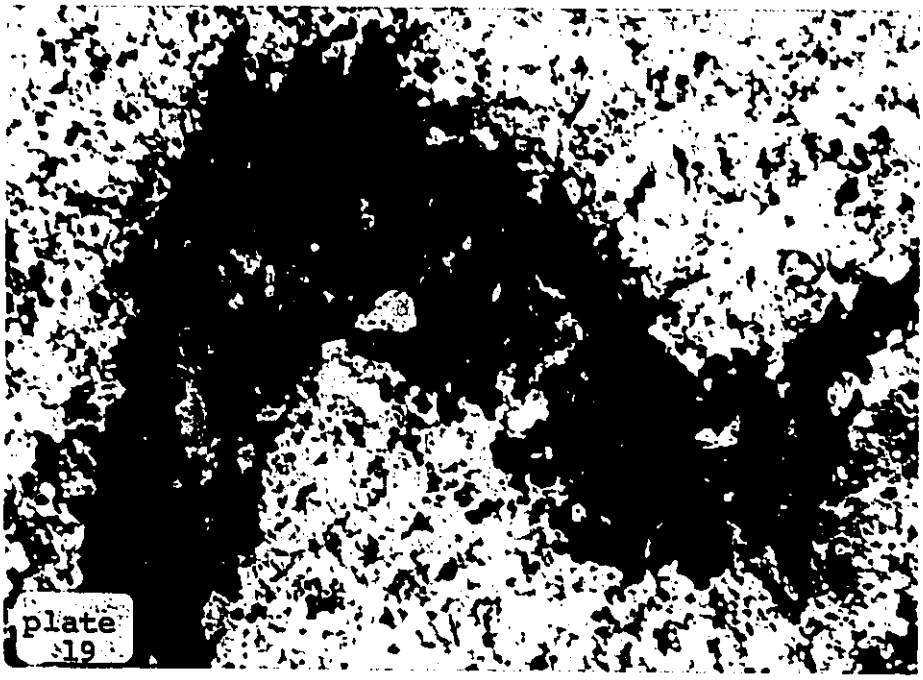
plate
19

PLATE 20 Photomicrograph of celsian (C), overgrowing foliation in barite-sulphide-quartz schist at Northern Eagle. (Crossed polars, width of photo is 6 mm).

PLATE 21 Photomicrograph of barite-quartz foliation (bq) deflected around ankerite (A) inclusion. Sample from barite-sulphide-quartz schist at Northern Eagle. (Crossed polars, width of photo is 6 mm).

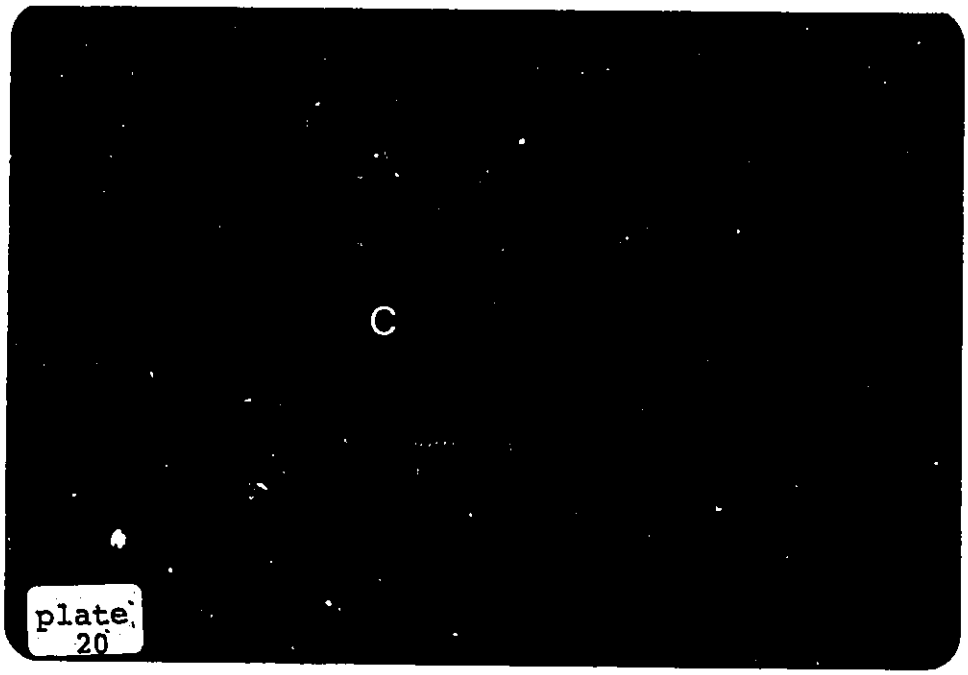
C
plate
20


plate
21

PLATE 22 Photomicrograph of bladed barite from Moose barite occurrence in the Selwyn Basin. Note the small lensoidal barite grains around the perimeter of the larger grain. (Crossed polars, width of photo is 6 mm).

PLATE 23 Photomicrograph of elongate barite grains (B), which define the foliation in a deformed Moose barite occurrence from the Selwyn Basin. (Crossed polars, width of photo is 2 mm).


plate
22


plate
23

PLATE 24 X, Y, and Z axes preferred orientation patterns for barite from barite-sulphide-quartz schist sample 43B. (vertical line-foliation, L-lineation, Contouring based on Starkey, 1977.

PLATE 25 X, Y and Z axes preferred orientation patterns for barite from barite-sulphide-quartz schist sample 38. (vertical line-foliation, L-lineation) Contouring based on Starkey, 1977.

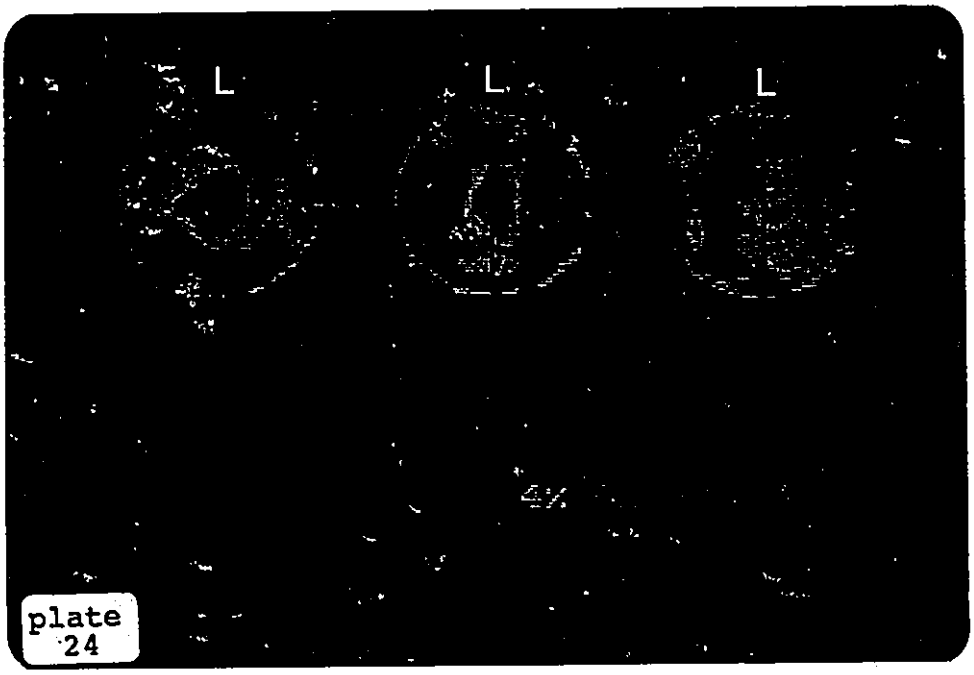
L
L
L
plate
24

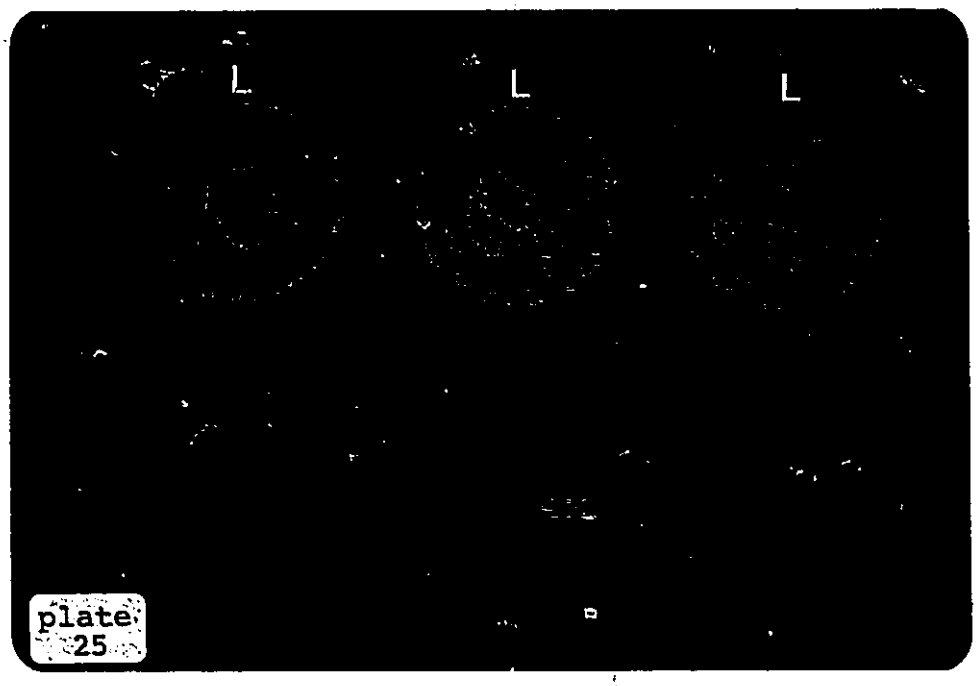
L
L
L
plate
25

PLATE 26 X, Y and Z axes preferred orientation patterns for barite from barite-sulphide-quartz schist sample B44EPL. (vertical line-foliation, L-lineation). Contouring based on Starkey, 1977.

PLATE 27 C-Axes preferred orientation patterns for quartz from barite-sulphide-quartz schist (samples Q44EPL and Q39). Sample Q23 is from quartz in deformed plagioclase-porphyritic intrusion. (vertical line-foliation, L-lineation). Contouring based on Starkey, 1977.

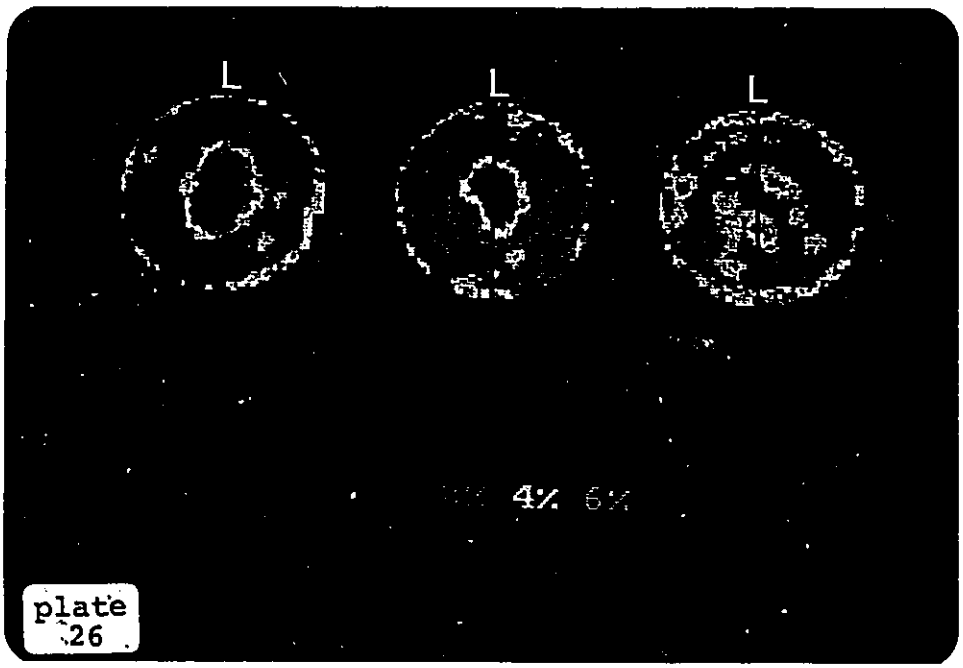
L
L
L
4% 6%
plate
26

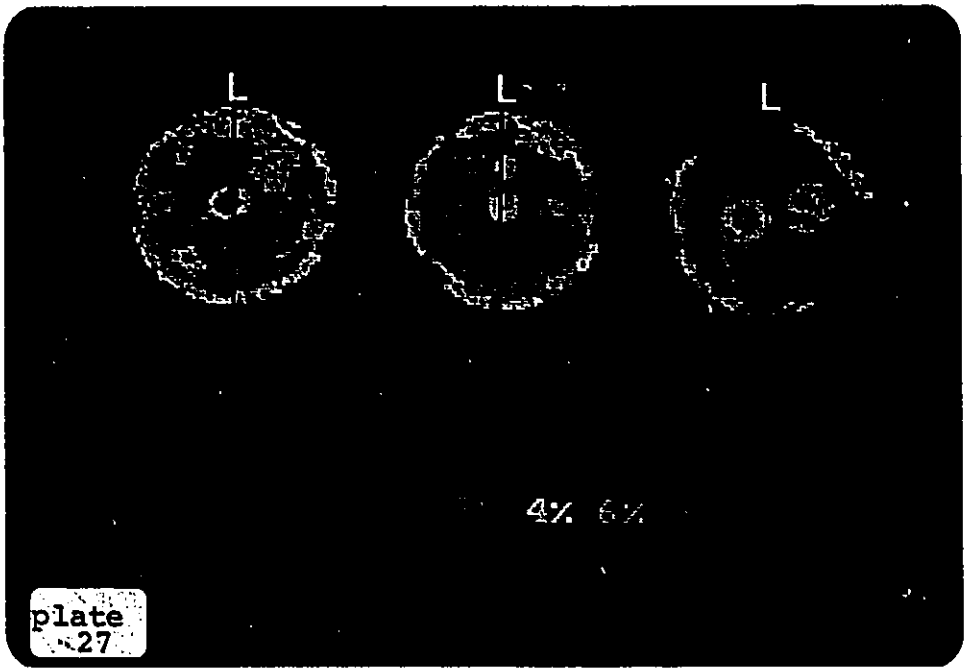
L
L
L
4% 6%
plate
27

PLATE 28 Photomicrograph of biotite (B) - ilmenite (I) foliation deflected around plagioclase phenocryst. Note the quartz (q) and ankerite (A) pressure shadows. Sample from plagioclase-porphyritic intrusion at Northern Eagle. (Single polarizer, width of photo is 3 mm).

PLATE 29 Photomicrograph of ilmenite (I) foliation deflected around plagioclase phenocryst. Sample from plagioclase-porphyritic intrusion at Northern Eagle. (Reflected light, width of photo is 3 mm).

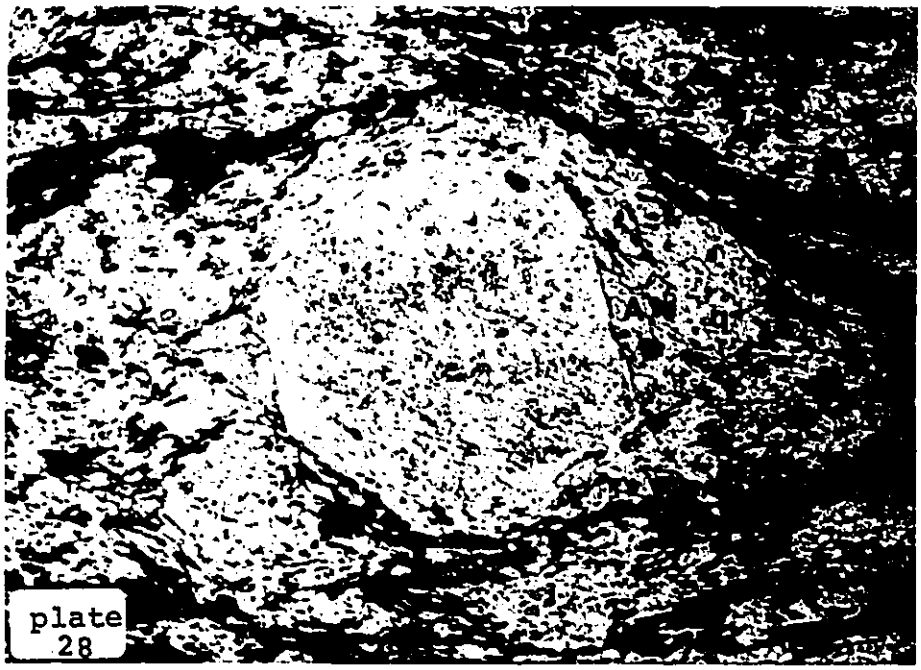
plate
28


plate
29

PLATE 30 Photomicrograph of euhedral plagioclase crystal displaying oscillatory zoning. Note the strongly-foliated matrix, and the recrystallized quartz (qp) and plagioclase (pp) phenocrysts. Sample from plagioclase-porphyrytic intrusion at Northern Eagle. (Crossed polars, width of photo is 6 mm).

PLATE 31 Photomicrograph of plagioclase phenocryst (pp) oriented with long-crystal faces parallel to foliation. Note the ankerite pressure shadow (a). (Sample from plagioclase-porphyritic intrusion at Northern Eagle). (Crossed polars, width of photo is 6 mm).

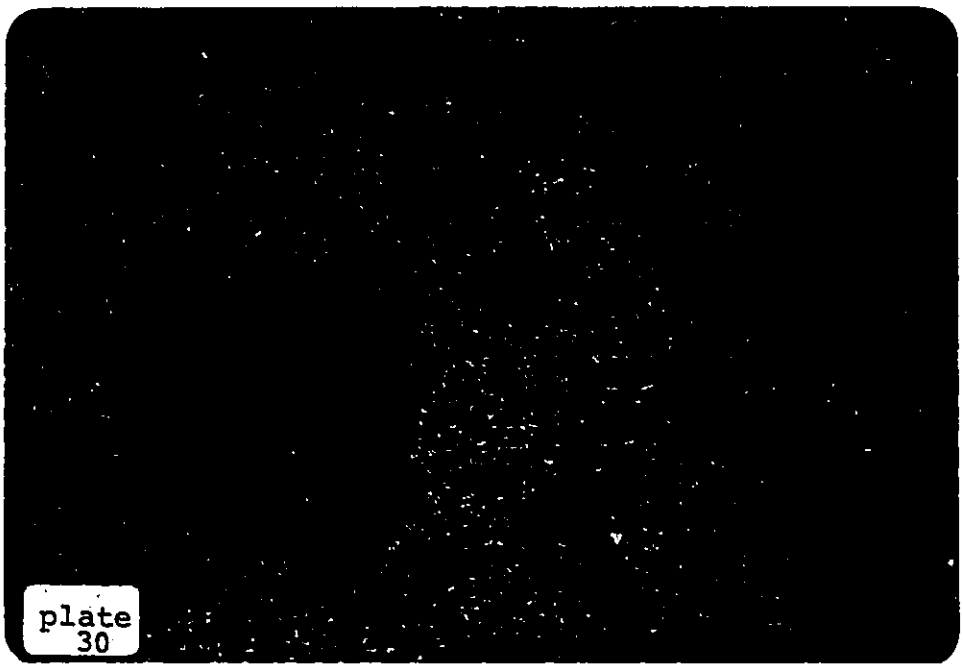
plate
30


plate
31

PLATE 32 Photomicrograph of ankerite (A) pressure shadow between 2 phenocrysts of plagioclase. Note how the edges of the plagioclase phenocryst fit together, possibly suggesting that this phenocryst was once a single grain. (Sample from plagioclase-porphyritic intrusion at Northern Eagle). (Crossed polars, width of photo is 6 mm).

PLATE 33 Photomicrograph of elongate quartz phenocryst, containing recrystallized grains. Note how the quartz aggregate anastomozes around the plagioclase phenocryst, as does the biotite foliation. (Sample from plagiocalse-porphyritic intrusion at Northern Eagle). (Crossed polars, width of photo is 6 mm).


plate
32

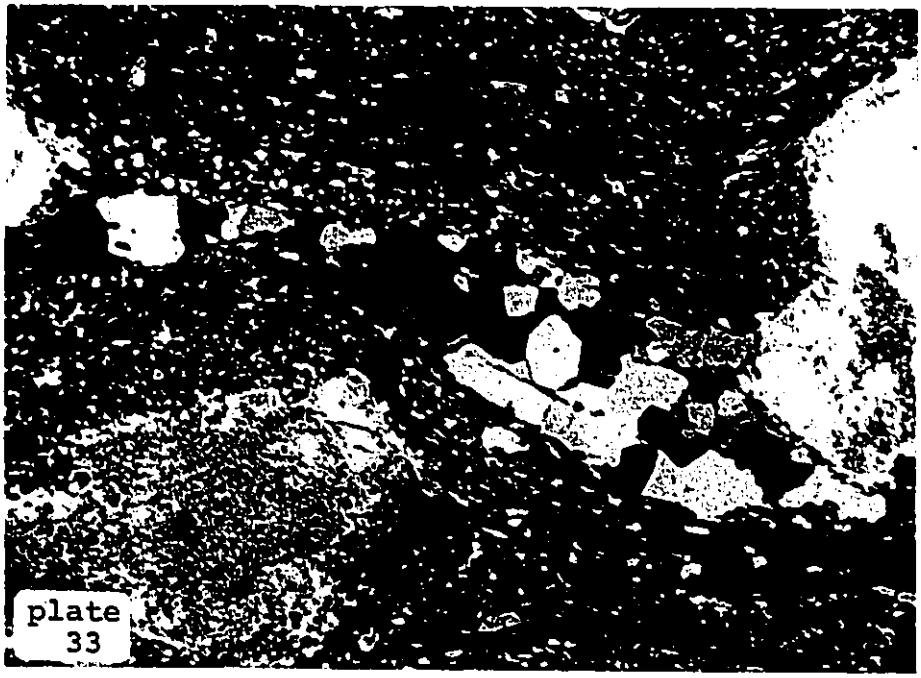
plate
33

PLATE 34 Photomicrograph of dynamically recrystallized plagioclase grains. Note the bulging, polygonal and serrated grain boundary. (Sample from plagioclase-porphyritic intrusion at Northern Eagle). (Crossed polars, width of photo is 3 mm).

PLATE 35 Photomicrograph of recrystallized plagioclase phenocryst. Note optical misorientation of newly recrystallized grains (rp). (Sample from plagiocalse-porphyritic intrusion at Northern Eagle). (Crossed polars, width of photo is 2 mm).

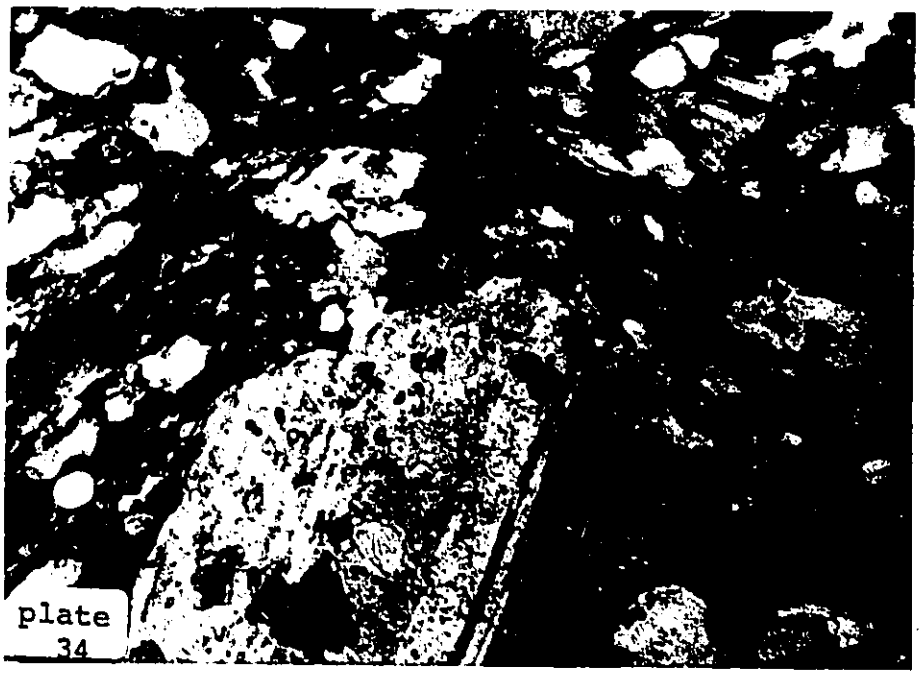

plate 34

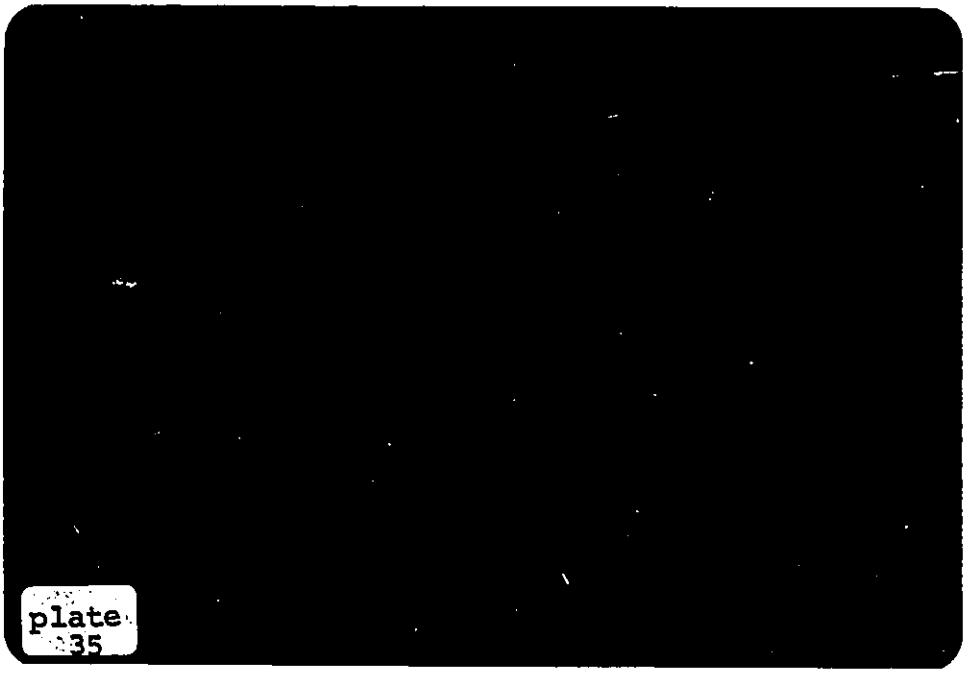

plate 35

PLATE 36 Photomicrograph of recrystallized plagioclase phenocryst (rp). Note the deflection of biotite foliation. (Sample from plagioclase-porphyritic intrusion at Northern Eagle). (Single polarizer, width of photo is 6 mm).

PLATE 37 Same as Plate 36- under crossed polars). Note how most of the phenocryst has been recrystallized.

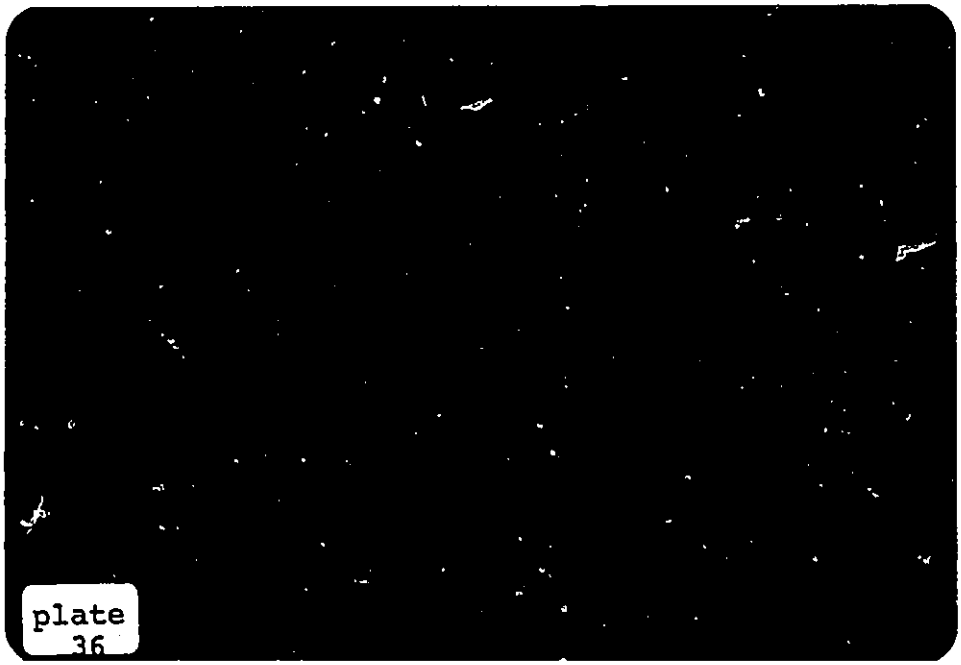
plate
36

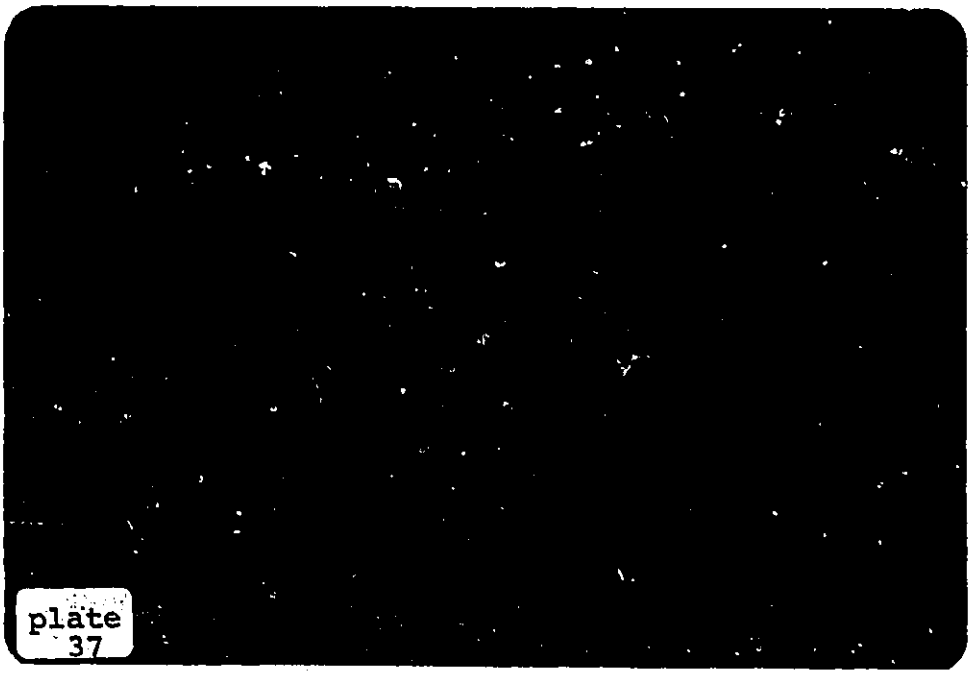
plate
37

PLATE 38 Photomicrograph of recrystallized quartz phenocryst (Q). Note the larger recrystallized grains in quartz, as compared to plagioclase (P). (Sample from plagioclase-porphyritic intrusion at Northern Eagle). (Crossed polars, width of photo is 6 mm).

PLATE 39 Photomicrograph of chromite (Cr) enveloped by a lens of chromium-muscovite (CM). Note the boundary between chromite and chromium-muscovite, which suggests the growth of chromium-muscovite at the expense of chromite. (Sample from chromium-muscovite schist at Padre). (Single polarizer, width of photo is 3 mm).

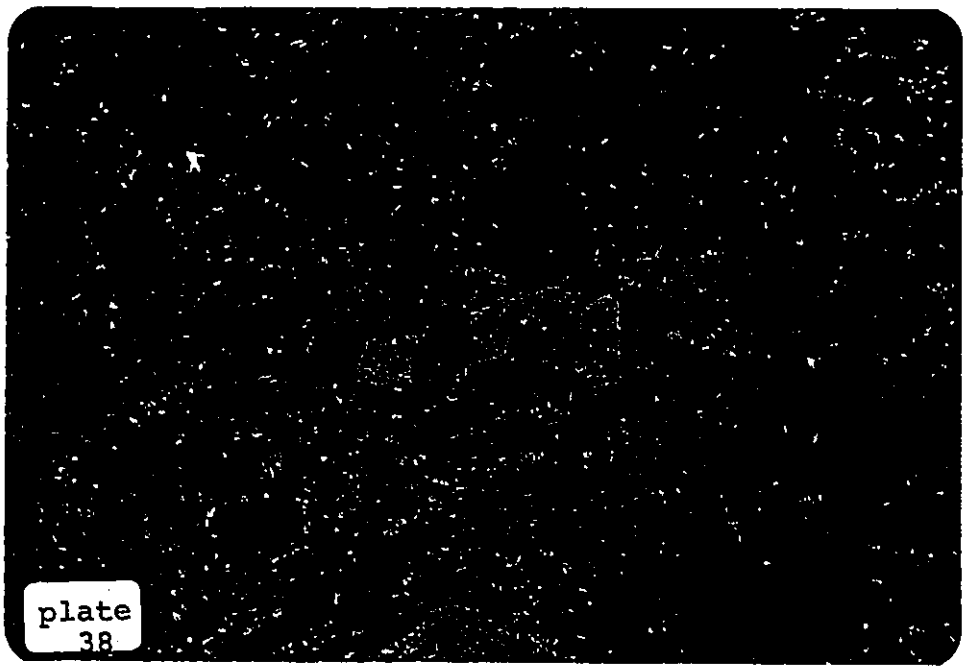
plate
38


Cr
plate
39

PLATE 40 Photomicrograph of lensoidal chromium-muscovite. Note the remnants of a former chromite grain. (Sample from chromium-muscovite schist at Padre). (Single polarizer, width of photo is 3 mm).


plate
40

APPENDIX A

MICROPROBE ANALYSIS

Microprobe analyses were carried out on optically indeterminate minerals. These include chromite, garnet, chromium-muscovite, and celsian. The analysis were conducted by D.C. Harris at the Geological Survey of Canada. The results of the microprobe analyses follow.

CONCENTRATION OF COMPONENT OXIDES IN MINERALS ANALIZED BY MICROPROBE

MINERAL ANALYZED IN WEIGHT % OXIDE

COMPOUND	CELSIAN	GARNET	CHROMITE	CHROMIUM MUSCOVITE
BaO	37.27	0.03	0.00	4.09
K_2O	0.34	0.00	0.00	8.82
Al_2O_3	29.46	21.00	16.36	31.88
V_2O_3	0.02	0.07	0.20	0.08
Na_2O	0.00	0.00	0.00	0.11
CaO	0.02	6.15	0.01	0.04
SiO_2	34.52	37.91	0.15	42.58
FeO	0.00	20.22	24.20	0.47
MgO	0.03	1.72	4.60	2.16
TiO_2	0.29	0.20	0.29	0.78
MnO	0.00	13.47	2.18	0.00
Cr_2O_3	0.00	0.32	49.41	3.69
TOTALS	101.94	101.08	99.89	94.95

APPENDIX B

SULPHUR ISOTOPIC ANALYSIS

Sulphur isotope analyses were carried out at stable isotope laboratory at the University of Ottawa. The physical nature of the sample, (ie. grain size, and mineralogy) dictated the methods used in sample preparation. The flow chart of Figure A.0 demonstrates the various methods used in sample preparation. Sulphur minerals were separated by physical and chemical techniques (for LAH extraction technique see Smith et al., 1964). Pure mineral separates were then combusted to yield SO_2 for mass spectrometric analysis.

The isotopic results are found in Fig. 12.

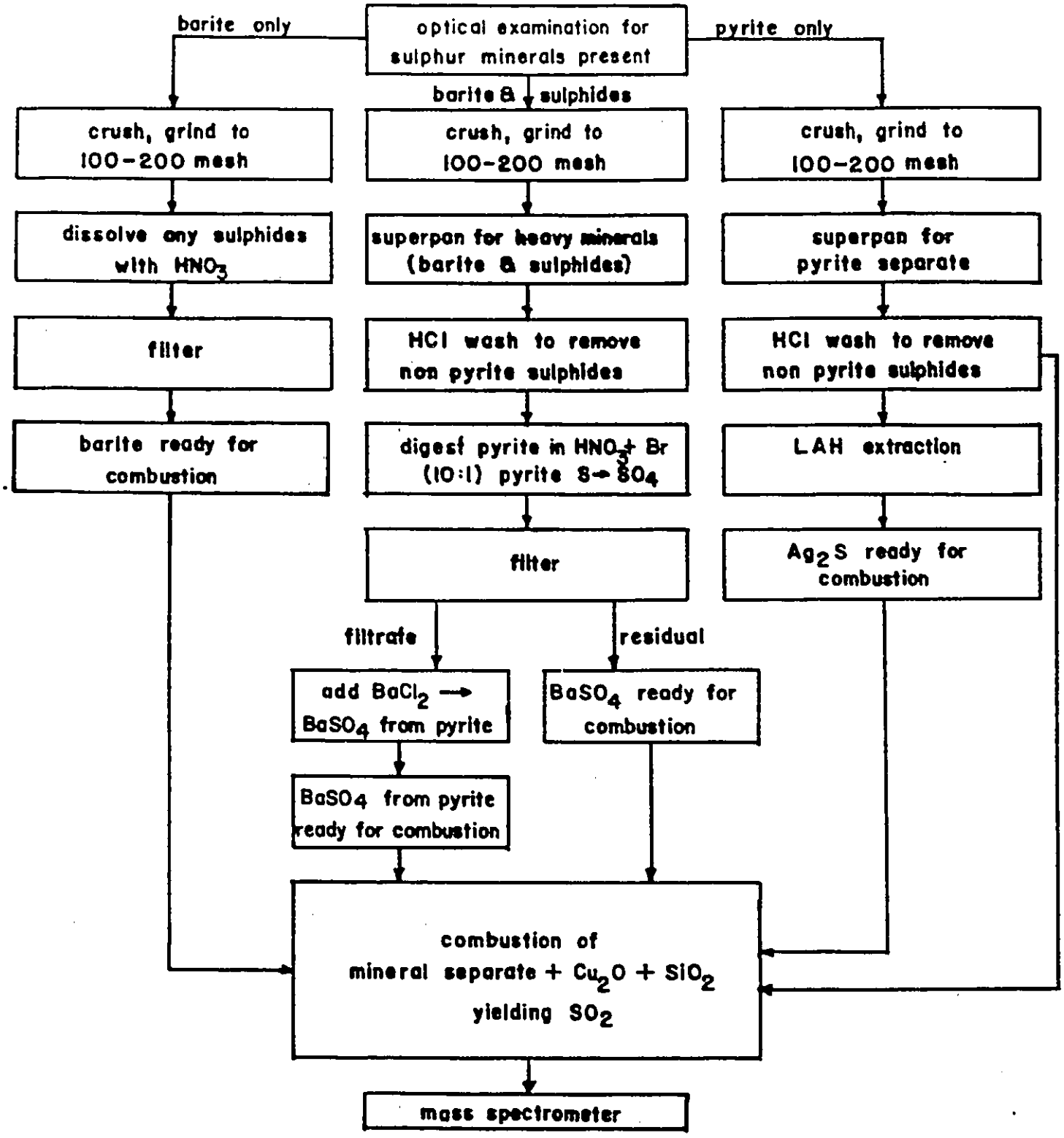

Figure A.0 Sample preparation.

APPENDICE C

CRYSTALLOGRAPHIC PREFERRED ORIENTATION STUDY

Data Aquisition

The orientation of vibration directions in barite were determined through optical methods described by Kerr (1977) for biaxial minerals. Only 2 optical directions were measured for each crystal. The third direction was determined by the CACPO (Computer Assisted Crystallographic Preferred Orientation) program, written by the author. During data entry, the CACPO program calculates the angle between the 2 measured axis. If this angle is + 4 from orthogonal, then the data are rejected (since barite is an orthorhombic mineral).

Quartz C-axis orientaions were determined by the method described by Kerr (1977).

Contouring Data

The CACPO contouring program does not contour a projection of points, as do manual contouring methods (see Hobbs, et al., 1976). Instead, the CACPO program contours data by counting the number of data points occurring within a cone around a known vector on the lower hemisphere. This

vector and its contoured value are then projected onto a 2 dimensional plane via equal-area projection.

Starkey, (1976) states that data sets of different sizes can be compared if the contouring area is equal to 100/n % (where n=number of samples). However, since the CACPO program contours the surface of the lower hemisphere, the contouring area is replaced by a contouring cone with semi-vertex angle equal to $\sqrt{100/n/pi}$. This allows for the comparison of data data sets of different sizes.

UNIVERSITÉ D'OTTAWA
UNIVERSITY OF OTTAWA